

Massive neutrinos and cosmic composition

Marilena Loverde^{1,*} and Zachary J. Weiner^{1,2,†}

¹*Department of Physics, University of Washington, Seattle, Washington, 98195, USA*

²*Perimeter Institute for Theoretical Physics, Waterloo, Ontario N2L 2Y5, Canada*

(Dated: December 18, 2024)

Cosmological data probe massive neutrinos via their effects on the geometry of the Universe and the growth of structure, both of which are degenerate with the late-time expansion history. We clarify the nature of these degeneracies and the individual roles of both probes in neutrino mass inference. Geometry is strongly sensitive to neutrino masses: within Λ CDM, the primary cosmic microwave background anisotropies alone impose that the matter fraction Ω_m must increase fivefold with increasing neutrino mass. Moreover, large-scale structure observables, like weak lensing of the CMB, are dimensionless and thus depend not on the matter density (as often quoted) but in fact the matter fraction. We explore the consequential impact of this distinction on the interplay between probes of structure, low-redshift distances, and CMB anisotropies. We derive constraints on the neutrino's masses independently from their suppression of structure and impact on geometry, showing that the latter is at least as important as the former. While the Dark Energy Spectroscopic Instrument's recent baryon acoustic oscillation data place stringent bounds largely deriving from their geometric incompatibility with massive neutrinos, all recent type Ia supernova datasets drive marginal preferences for nonzero neutrino masses because they prefer substantially larger matter fractions. Recent CMB lensing data, however, neither exclude neutrinos' suppression of structure nor constrain it strongly enough to discriminate between mass hierarchies. Current data thus evince not a need for modified dynamics of neutrino perturbations or structure growth but rather an inconsistent compatibility with massive neutrinos' impact on the expansion history. We identify two of DESI's measurements that strongly influence its constraints, and we also discuss neutrino mass measurements in models that alter the sound horizon.

CONTENTS

I. Introduction	2
II. Cosmology of massive neutrinos	5
A. Cosmological information independent of neutrino masses	6
B. Geometric signatures	7
C. Signatures in structure	12
III. Results	17
A. Geometric constraints and tensions	18
B. Impact of CMB lensing	26
IV. Discussion	31
A. Dataset tensions	31
B. Implications for cosmology	33
C. Implications for neutrino physics	36
V. Conclusions	37

* mloverde@uw.edu

† zweiner@perimeterinstitute.ca

Acknowledgments	39
A. Transverse BAO scale from CMB analyses	39
B. Supplementary results	40
1. Constraints on structure from lensing reconstruction and peak smearing	40
2. Consistency of low-redshift distance measurements	42
C. Impact of nonlinear evolution on neutrino mass inference	45
References	47

I. INTRODUCTION

On both theoretical and observational grounds, cosmology is no longer well described by the six-parameter Λ cold dark matter (Λ CDM) model. While current data from any single probe—cosmic microwave background (CMB) anisotropies, baryon acoustic oscillations (BAO), low-redshift distances from type Ia supernovae (SNe), and large-scale structure (LSS)—are *individually* well described by Λ CDM, many of these observables prefer mutually inconsistent parameter space. Moreover, laboratory experiments definitively establish that neutrinos are not massless, and cosmological datasets are already sensitive to the gravitational effects of their nonrelativistic dynamics. Neglecting the neutrinos’ masses or fixing them to some particular value imposes a strong prior that is neither theoretically nor experimentally justified. And while the critical issue remains corroborating whether discrepancies between datasets are cosmological or systematic in nature, their consistency must be assessed in the full parameter space that describes known physics—including neutrino masses.

On the one hand, the CMB [1–3] infers (within Λ CDM) an amplitude of matter clustering larger than that measured by some probes of LSS [4–9]. But massive neutrinos constitute hot dark matter—their thermal velocities permit them to stream in and out of CDM overdensities rather than cluster in tandem. The suppression of net structure growth by neutrinos, which accumulates over a large interval of expansion, is typically considered the most promising observable with which to measure their masses [10], motivating future surveys of CMB lensing [11–13], redshift-space distortions [14, 15], weak lensing of galaxies [16–19], cluster abundances [20], and other probes of the late time matter field [21–23]. The possibility that massive neutrinos could reconcile current determinations of clustering is complicated in part by a preference in *Planck*’s 2018 CMB data [1–3] for even greater smearing of the acoustic peaks induced by gravitational lensing than it predicts without massive neutrinos. Adding to the intrigue, a phenomenological analysis of peculiar velocity measurements and redshift-space distortions finds evidence that structure grows more slowly than Λ CDM predicts [24].

On the other hand, calibrating the local distance ladder with Cepheids [25–28] measures a present-day expansion rate H_0 severely larger than that inferred (again, within Λ CDM) by the distance to the last scattering surface via CMB data [1]. Alternative calibrations using the tip of the red giant branch [28–32] yield results that are less discrepant but still shifted toward larger H_0 . Massive neutrinos, however, increase the density (and so decrease the horizon) of the Universe in the matter-dominated era, requiring a compensatory decrease in density during the dark-energy epoch to preserve the distance to last scattering. Without additional physics, cosmologies with massive neutrinos thus only permit smaller Hubble constants than those without. Moreover, because dark energy domination began rather recently, fixing the distance to last scattering requires so disproportionate a decrease in the dark energy density that the matter fraction Ω_m must

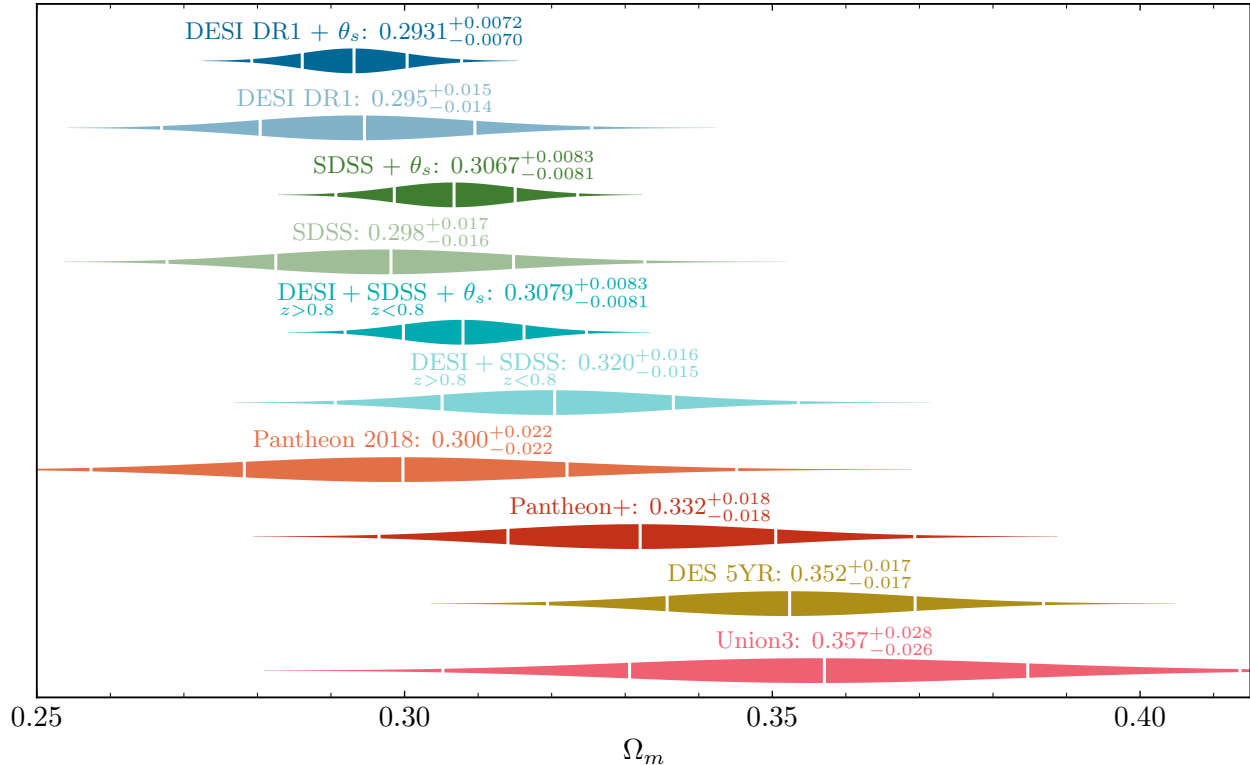


Figure 1. Recent measurements of the matter fraction Ω_m inferred within flat Λ CDM cosmology from various probes of late-time geometry (described in the text). White lines indicate the median and ± 1 and 2σ values, and each posterior is labeled by its median and $\pm 1\sigma$ deviations.

increase *fivefold* compared to the neutrinos’ relative contribution to the matter density.¹ Direct measurements of the late-time expansion history can break this degeneracy and stand to provide powerful, independent constraints on the neutrino masses. While both structure growth and geometric probes are sensitive to possible dynamics of dark energy, low-redshift distances can directly constrain the possibility. Furthermore, geometric probes suffer no degeneracy with the optical depth to reionization, a primary obstacle to uniquely inferring neutrino masses from the amplitude of structure [12, 33].

More recently, a number of datasets that directly measure the late-time expansion history with standardizable cosmological distances yield discrepant inference of the Universe’s composition. A great success of Λ CDM in the previous decade is its concordant inference of both H_0 and the present matter fraction Ω_m from CMB anisotropies and via the BAO feature measured in galaxy surveys at low redshift. But the most recent SNe datasets—Pantheon+ [34, 35], the five-year sample from the Dark Energy Survey (DES) [36], and Union3 [37]—all prefer a Universe comprising a greater fraction in matter than any BAO dataset (see Fig. 1). The sensitive increase of Ω_m with increasing neutrino mass (at fixed distance to last scattering) in principle provides a means to reconcile CMB and SNe data. But cosmological distances measured by SNe and BAO—even marginalizing over the calibration of their brightness and the sound horizon, respectively—directly trace the expansion history over the same interval of redshift, so it is unclear what cosmological (rather than systematic) effect could account for this apparent violation of the distance-duality relation [38].

The first BAO measurements released by the Dark Energy Spectroscopic Instrument (DESI) [39–41] yield neutrino mass bounds so stringent as to suggest incompatibility with the minimal ex-

¹ Extending late-time cosmology beyond the flat Λ CDM model we focus on introduces additional freedom that can break this relationship; such extensions may be tested directly by low-redshift distance measurements.

pectation from neutrino oscillation experiments [42, 43]. These tighter bounds derive not from improved precision—DESI’s data has not yet exceeded that of the Sloan Digital Sky Survey (SDSS) and its Extended Baryon Oscillation Spectroscopic Survey (eBOSS) measurements [44–47]—but rather from a preference for even smaller matter fractions than SDSS [39] that further preclude sizable neutrino masses when combined with CMB data. Data from luminous red galaxies that are discrepant with SDSS’s measurements at similar redshifts play an important role in this trend; Fig. 1 shows that exchanging DESI’s measurements for SDSS’s at low redshift yields inference of larger matter fractions more compatible with those from SNe (and also with heavier neutrinos). Moreover, when also including the analogous information from *Planck* (i.e., the angular extent of the photon sound horizon, θ_s), this combination agrees extremely well with SDSS’s, but both results are offset from DESI’s. If merely due to statistical fluctuations, subsequent data releases could counterintuitively produce weaker constraints on neutrino masses in spite of improved precision.

The advent of precision cosmology has thus yielded precision discrepancies with crucial implications for inferences of the neutrino mass scale. Identifying genuine signatures of massive neutrinos—or the absence of ones that are expected—requires a rigorous theoretical understanding of what cosmological observables measure, what degeneracies with Λ CDM parameters arise, and how those degeneracies are broken by combining datasets. In this work we clarify the manner in which the various effects of massive neutrinos are degenerate with the composition of the Universe. Emphasizing that (nearly) all cosmological observables measure dimensionless quantities, we demonstrate that the signatures of massive neutrinos—quantified by their nonrelativistic contribution to the matter density relative to that from baryons and cold dark matter—are degenerate with matter’s fractional contribution to the Universe’s energy density, not its absolute density. Section II shows how this degeneracy arises in neutrinos’ effects on both the geometry and the large-scale structure of the Universe. CMB data are crucial in breaking these degeneracies; Sec. II A reviews what information (and what dimensionless combinations of Λ CDM parameters) are robustly measured by CMB anisotropies independent of the neutrino masses.

In Sec. III we apply the theoretical description of Sec. II to interpret constraints on neutrino masses from current cosmological data. We identify combinations of datasets that yield constraints on both neutrinos’ geometric effects and their suppression of structure independently of the other; we specialize to CMB lensing as a probe of structure for concreteness and because of current observations’ important role in neutrino mass inference. Section III A studies the former—measurements of geometry from uncalibrated SNe data and from BAO data. We show how recent SNe datasets combine with geometric information from *Planck* to detect a nonzero neutrino mass sum with significance as high as 3σ , in striking contrast to the strong upper limits from DESI data. In Sec. III A 3 we investigate the origin of DESI’s constraints, exploring what subsets of DESI’s data and combinations with SDSS yield weaker constraints on the neutrino masses as well as inferences of the matter fraction consistent with SNe. Section III B then derives bounds purely on neutrinos’ suppression of structure using CMB lensing data from *Planck* and the Atacama Cosmology Telescope (ACT) [48, 49]. Prior bounds derived from recent CMB lensing data always include BAO data as well; the results we present that exclude this data better represent the independent constraining power provided by CMB lensing as a probe of structure. We then present constraints from various combinations of probes of geometry and structure, showing that a modest preference for neutrinos with mass sums ≈ 0.14 eV persists with DESI’s SNe data even when combined with all *Planck* data and the aforementioned CMB lensing data.

Finally, in Sec. IV we discuss the implications of our results in interpreting current datasets and on possible new physics. Section IV A surveys the implications of our results for the numerous tensions between cosmological datasets. We discuss cosmologies that alter the sound horizon in Sec. IV B: neutrino-mass bounds are largely robust in models that increase the density at recombination with new degrees of freedom, but early-recombination scenarios effectively remove

any geometric information about neutrino masses. In Sec. [IV C](#) we comment on the interpretation of current data as preferring neutrinos with “negative mass” and on new physics in the neutrino sector that might explain discrepant signatures in the Universe’s geometry and structure. We conclude in Sec. [V](#). A set of appendices describe the derivation of a geometric likelihood from *Planck* ([Appendix A](#)), present a number of supplementary figures ([Appendix B](#)), and demonstrate the importance of nonlinear structure growth on inference of neutrino masses from current CMB lensing data ([Appendix C](#)).

II. COSMOLOGY OF MASSIVE NEUTRINOS

We begin by reviewing the separate cosmological impact of massive neutrinos on the geometry ([Sec. II B](#)) and large-scale structure ([Sec. II C](#)) of the Universe. In each case we establish formalism and illustrate how relevant observables depend only on dimensionless quantities that characterize the composition of the Universe (namely, the matter fraction Ω_m in flat Λ CDM cosmologies). Within even the most conservative current limits, neutrinos become nonrelativistic only after recombination—otherwise, their transition from radiationlike to matterlike behavior hastens the onset of matter domination and alters the early integrated Sachs-Wolfe (ISW) effect to a unacceptable degree [[1](#), [50](#)]. In the regime in which their impact on the ISW effect is negligible, massive neutrinos affect cosmological observables only by altering distances (including that to last scattering) and suppressing the late-time growth of structure (which distorts the visible CMB via gravitational lensing). Before proceeding, we establish notation and (in [Sec. II A](#)) discuss what information the CMB robustly measures independently of the neutrino masses.

A single neutrino species with mass m_{ν_i} and temperature T_ν becomes semirelativistic (i.e., on average over phase space) at a redshift

$$z_{\nu_i} + 1 = \frac{m_{\nu_i}}{3.15T_\nu(a_0)} = 113 \frac{m_{\nu_i}}{0.06 \text{ eV}} \quad (2.1)$$

and has a present-day density² of

$$\omega_{\nu_i} = \frac{3\zeta(3)}{2\pi^2} \frac{m_{\nu_i} T_\nu(a_0)^3}{3H_{100}^2 M_{\text{pl}}^2} = \frac{m_{\nu_i}}{93.1 \text{ eV}}. \quad (2.2)$$

Equation [\(2.1\)](#) takes $3.15T_\nu$ as the average momentum for a Fermi-Dirac-distributed species, and the right-hand sides of Eqs. [\(2.1\)](#) and [\(2.2\)](#) account for phase space distortions generated when neutrinos decouple from the plasma [[51](#)]. Massive neutrinos therefore contribute to the matter density below a redshift and with an abundance both proportional to their mass. Neutrino oscillation experiments limit the sum of the neutrino masses to at least 0.0588 eV or 0.099 eV in the normal and inverted hierarchies, respectively [[42](#), [43](#)]. Since the visibility function peaks around a photon temperature of 0.26 eV (or redshift $z_\star \approx 1089$), the aforementioned requirement that neutrinos become nonrelativistic after recombination limits each species to be lighter than about 0.58 eV (barring any nonminimal neutrino dynamics). Unless otherwise stated, we approximate the mass hierarchy with three equal-mass neutrinos per standard practice [[52](#)], as their mass splittings only have a minor impact on their signatures and only for mass sums close to the minimum.

The early-time energy density of neutrinos is typically quantified in terms of the effective number of degrees of freedom N_{eff} as

$$\bar{\rho}_\nu(z \gg z_{\nu_i}) = \frac{7}{8} \left(\frac{4}{11} \right)^{4/3} N_{\text{eff}} \cdot \bar{\rho}_\gamma. \quad (2.3)$$

² The contributions of various species to the present-day energy density are parametrized by $\omega_X = \bar{\rho}_{X,0}/3H_{100}^2 M_{\text{pl}}^2$, i.e., $X = \gamma, b, c, \nu$, and Λ denoting photons, baryons, cold dark matter (CDM), neutrinos, and cosmological constant, respectively. We parametrize the Hubble constant by $H_0 = h \cdot 100 \text{ Mpc}^{-1} \text{ km/s} \equiv hH_{100}$.

Following convention, the total radiation density parameter denotes the sum of the relativistic neutrino and photon contributions, $\omega_r \equiv \omega_\gamma + \omega_\nu$, as if the neutrinos remained relativistic today. We denote the total matter density (i.e., at late times) as $\omega_m(z \ll z_{\nu_i}) = \omega_b + \omega_c + \omega_\nu$; ω_ν here denotes the density in nonrelativistic neutrinos, which comprise a fraction

$$f_\nu \equiv \frac{\omega_\nu}{\omega_m} = \frac{\omega_\nu}{\omega_b + \omega_c + \omega_\nu} \approx \frac{M_\nu}{13.2 \text{ eV}} \left(\frac{\omega_b + \omega_c}{0.142} \right)^{-1} \quad (2.4)$$

of the total matter density. Here $M_\nu = \sum_i m_{\nu_i}$ is the neutrino mass sum. When modeling \mathcal{N}_ν massive neutrino states, we fix the total early-time radiation density to correspond to $N_{\text{eff}} = 3.044$ [Eq. (2.3)] [53–55] by including an ultrarelativistic fluid with $N_{\text{eff}} - \mathcal{N}_\nu T_\nu^4 / (4/11)^{4/3}$ effective degrees of freedom.

A. Cosmological information independent of neutrino masses

The primary CMB anisotropies are generated by the dynamics of the photon-baryon plasma leading up to hydrogen recombination. Recombination happens to occur shortly after the radiation density drops below the total matter density, granting the primary anisotropies sensitivity to dark matter perturbations via their gravitational effects on the plasma. As established above, before recombination Standard Model neutrinos are still relativistic but are also collisionless; their free-streaming behavior while relativistic also has characteristic effects on, e.g., the location of the CMB acoustic peaks [56, 57], but these signatures are independent of their mass. To describe the physical effects constrained by the CMB, we follow the notation and arguments of Ref. [58], which took as time coordinate the scale factor relative to that at recombination, $x = a/a_\star$, and assumed the energy content of the early Universe is well described by photons, baryons, relativistic neutrinos, and cold dark matter.

The most robust observable in the CMB power spectrum is the structure and location of its peaks, which reflect the oscillations of acoustic waves traveling in the plasma at the time of recombination. The relative peak heights reflect the shift in the zero point of the density perturbations' oscillations due to the weight of the baryons relative to the photons' radiation pressure; with their precise measurements of the first several peaks, current datasets strongly constrain the baryon-to-photon ratio at recombination,

$$R_\star \equiv \frac{3\rho_{b,\star}}{4\rho_{\gamma,\star}} \propto \frac{3\omega_b a_\star}{4\omega_\gamma}. \quad (2.5)$$

Acoustic waves propagate a distance (the so-called sound horizon) determined by the sound speed of the tightly coupled photon-baryon plasma and the comoving horizon of the Universe. Because recombination occurs in the beginning of the matter era, the evolution of the sound horizon depends on when matter-radiation equality occurs relative to recombination,

$$x_{\text{eq}} \equiv \frac{a_{\text{eq}}}{a_\star} = \frac{\rho_{r,\star}}{\rho_{m,\star}} = \frac{\omega_r}{(\omega_b + \omega_c) a_\star}. \quad (2.6)$$

Cold dark matter makes gravitational potentials deeper during recombination to an extent that is also fully parametrized by x_{eq} , determining both of the so-called radiation driving and early ISW effects [59, 60]. When R_\star and x_{eq} are held fixed, the ratio of the sound horizon to the comoving horizon at equality $k_{\text{eq}} \equiv a_{\text{eq}} H_{\text{eq}}$ is invariant. The shape of the acoustic peaks therefore measures the abundances of both baryons and cold dark matter, but only at recombination and relative to the photon and radiation abundances, respectively.³

³ To be clear, the density ratios evaluated at recombination are fully sufficient to *parametrize* the impact of baryons and CDM on the CMB, assuming (as we are) that their evolution with redshift is unchanged. The primary CMB does depend on the conditions of the plasma over a finite duration in time about recombination (determined by the width of the visibility function) and on the evolution of metric potentials at all times (via the ISW effect).

Translating these dimensionless quantities to dimensionful, present-day baryon and CDM abundances requires knowledge of the photon and radiation densities and the scale factor at recombination. Since the baryon-to-photon ratio encodes the effect of their interactions, inferring the absolute density ω_b in this manner should be robust to any impact of massive neutrinos. Sufficiently heavy neutrinos could confound the inference of ω_c as $\omega_r/a_\star x_{\text{eq}} - \omega_b$ via their own transition to matterlike behavior, but only for masses that are safely excluded by current data. We emphasize that Eq. (2.6) depends only on whatever contributors to the matter density are present at recombination.

One of the few measured, dimensionful parameters relevant to the CMB is its present-day temperature, T_0 . The scale factor at recombination relative to today, of course, is given by the inverse ratio of the corresponding photon temperatures, $a_\star/a_0 = T_0/T_\star$. The temperature dependence of recombination largely arises relative to the ionization energy of hydrogen E_I , which of course is also measured. Assuming atomic parameters are unchanged at early times (i.e., no time variation of the fundamental constants) thus anchors the redshift of recombination.⁴ Finally, the (relativistic) neutrino abundance is predicted precisely in the Standard Model [51, 53–55, 61]; assuming no new physics again, measurements of T_0 and E_I calibrate a prediction for the *dimensionful* photon and radiation densities at recombination. The shape of the acoustic peaks then measures the dimensionful abundances of baryons and CDM.

Notably, calibrating ω_b and ω_c in Λ CDM does not hinge even on the angular scale of the acoustic peaks. The actual extent of these features on the sky instead measures the ratio of the sound horizon and the distance to last scattering. The former may be computed analytically in matter-radiation Universes [62] and is a function of the matter densities only via R_\star and x_{eq} :

$$r_s(a) = \frac{a}{\sqrt{\omega_r}} \frac{2\sqrt{x_{\text{eq}}/3R_\star}}{H_{100}/c} \ln \left(\frac{\sqrt{R_\star} \sqrt{x + x_{\text{eq}}} + \sqrt{1 + R_\star x}}{1 + \sqrt{R_\star x_{\text{eq}}}} \right) \quad (2.7)$$

where again $x = a/a_\star$. The distance to last scattering, on the other hand, depends on the expansion history in the matter and dark-energy eras; its dependence on the matter density is therefore not specified by the combination x_{eq} . Moreover, massive neutrinos become nonrelativistic during this period and alter the late-time expansion history in a mass-dependent manner, a geometric signature we discuss in Sec. II B.

Finally, we note several additional physical processes to which (primary) CMB polarization and small-scale anisotropies are uniquely sensitive. Small-scale power is suppressed by photon diffusion [63, 64] and is sensitive to the ratio of the photon and total radiation densities, for example. That recombination is not instantaneous—namely, that CMB photons visible today last scattered over a nonzero interval in time—both suppresses small-scale power [64, 65] and determines the amplitude of the polarization spectrum [64, 66]. Reference [58] discusses the parametrization of these effects and parameter degeneracies in extended models in detail. That current measurements of polarization and small-scale anisotropies are entirely consistent with Λ CDM (and the SM) without the need for additional parameter freedom is a definitive success of the model.

B. Geometric signatures

The classical cosmological probes of geometry use astrophysical measurements of a quantity that is dimensionful but supposed to be uniform (or at least predictively determined) across redshift. Any observed variability of these otherwise standard quantities is then associated to

⁴ Recombination is marginally sensitive to the expansion history, but T_\star varies at below the permille level within the limits of current CMB data if recombination is described by the SM.

a cosmological distance, and associating these observations with measured redshifts then traces out the expansion history [67]. Historically, the luminosities of supernovae (“standard candles”) provided the first probe of cosmic distances, but the spatial correlation of the matter and photon distributions due to acoustic oscillations also provides a standard distance scale (or “ruler”) [68–72]. Distance measurements thus constrain the geometry of the Universe—both spatial curvature and the evolution of the scale factor.

The fundamental distance measure is the transverse comoving distance [73],

$$D_M(a) \equiv \chi(a) \operatorname{sinc} \left[\sqrt{-\Omega_k} \frac{\chi(a)}{1/H_0} \right], \quad (2.8)$$

where Ω_k is the curvature parameter and the line-of-sight comoving distance is

$$\chi(a) = \int_a^{a_0} \frac{d\tilde{a}}{\tilde{a}} \frac{1}{\tilde{a}H(\tilde{a})}. \quad (2.9)$$

In flat Universes (with $\Omega_k = 0$), $D_M(a) = \chi(a)$. Specializing to Λ CDM, whose expansion history at late times is fully characterized by the scale factor at matter- Λ equality

$$a_{m-\Lambda} = \sqrt[3]{\frac{\omega_m}{\omega_\Lambda}} = \sqrt[3]{\frac{\Omega_m}{1 - \Omega_m}} \quad (2.10)$$

and the Hubble constant $h = \sqrt{\omega_m + \omega_\Lambda}$, the comoving distance Eq. (2.9) integrates to [74]

$$\chi(a) = \frac{2}{\sqrt{\omega_m} H_{100}/c} [F_M(1; a_{m-\Lambda}) - F_M(a; a_{m-\Lambda})], \quad (2.11)$$

where

$$F_M(a; a_{m-\Lambda}) \equiv \sqrt{a} \cdot {}_2F_1(1/6, 1/2; 7/6, -[a/a_{m-\Lambda}]^3) \quad (2.12)$$

and ${}_2F_1$ is a hypergeometric function. The hypergeometric function asymptotes to unity for $a \ll a_{m-\Lambda}$, i.e., it encodes the correction from Λ to the result for a pure matter Universe.

1. Baryon acoustic oscillations

The acoustic oscillations of the baryonic plasma also leave an oscillatory feature in the matter correlation function; the local maximum thereof (the “BAO scale”) effectively measures the comoving sound horizon when baryons decoupled, r_d [75, 76]. This so-called drag scale is slightly larger than $r_{s,\star}$ because baryons decouple slightly after recombination ($a_d > a_\star$) [62]. Galaxy surveys extract the BAO scale in various forms: the transverse scale (as an angular extent on the sky),

$$\theta_{\text{BAO},\perp}(a) \equiv \frac{r_d}{D_M(a)}, \quad (2.13a)$$

the line-of-sight scale,⁵

$$\theta_{\text{BAO},\parallel}(a) \equiv \frac{r_d}{cH(a)^{-1}}, \quad (2.13b)$$

⁵ Note that $\theta_{\text{BAO},\parallel}$ is written as a ratio of comoving and physical length scales following convention; the stray factor of a is irrelevant for BAO data because their redshifts are measured.

and a volume average of the two,

$$\theta_{\text{BAO}}(a) \equiv \sqrt[3]{\frac{\theta_{\text{BAO},\perp}(a)^2 \theta_{\text{BAO},\parallel}(a)}{(1/a - 1)}}. \quad (2.13c)$$

Substituting Eq. (2.11) for the comoving distance in Eq. (2.13a) and

$$H(a) = \sqrt{\omega_m} H_{100} \sqrt{a_{m-\Lambda}^{-3} + a^{-3}} \quad (2.14)$$

into Eq. (2.13b) shows that BAO distances depend on H_0 only through an overall scaling in the combination $r_d \sqrt{\omega_m} = r_d \sqrt{\Omega_m} H_0$:

$$\theta_{\text{BAO},\perp}(a) = \frac{r_d \sqrt{\omega_m}}{2c/H_{100}} [F_M(1; a_{m-\Lambda}) - F_M(a; a_{m-\Lambda})]^{-1} \quad (2.15a)$$

$$\theta_{\text{BAO},\parallel}(a) = \frac{r_d \sqrt{\omega_m}}{c/H_{100}} \sqrt{a_{m-\Lambda}^{-3} + a^{-3}}. \quad (2.15b)$$

Parametrizing the ‘‘amplitude’’ as $r_d \sqrt{\omega_m}$ rather than hr_d both yields simpler expressions and better facilitates interpreting the implications of BAO measurements for neutrino masses later on.

Equations (2.15a) and (2.15b) both depend on scale factor through a (nonlinear) function depending on cosmological parameters only via $a_{m-\Lambda}$ (or equivalently Ω_m). At very early times, the scaling of the BAO angles with the matter fraction asymptotes to $\theta_{\text{BAO},\perp}(a) \propto r_d \sqrt{\omega_m} \Omega_m^{-0.1}$ and $\theta_{\text{BAO},\parallel}(a) \propto r_d \sqrt{\omega_m} a^{-3/2}$. At very low redshift, both scale nearly with $r_d h$ (since they only depend on the very recent expansion history); combining measurements at moderate or high redshift with ones at very low redshift can therefore measure both $r_d \sqrt{\omega_m}$ and Ω_m individually. Measuring both $\theta_{\text{BAO},\perp}(a)$ and $\theta_{\text{BAO},\parallel}(a)$ at a single redshift also breaks the degeneracy, but only weakly because they scale with powers of Ω_m differing by no more than 0.15 to 0.2 in magnitude at any redshift (unless Ω_m is extremely small).

The BAO feature is measured by tracers from small redshift to redshifts of order a couple, well after the heaviest neutrinos become nonrelativistic.⁶ Taking ω_m to include all of the mass density in neutrinos at late times is thus an excellent approximation. BAO data on their own, however, cannot identify how the matter abundance is partitioned between baryons, CDM, and neutrinos; nor can they even infer the overall density without calibrating the drag horizon r_d (i.e., measuring a dimensionful scale). Using the information in the shape of the CMB power spectra (Sec. II A) to calibrate the absolute baryon and CDM densities (i.e., with assumptions about early-Universe physics), within flat Λ CDM cosmologies one can attribute to massive neutrinos any remaining matter density measured by BAO data.

2. Cosmic microwave background

The angular location of the acoustic peaks in the CMB is one of its most robust features, measuring the ratio of the sound horizon at recombination to the comoving distance to last scattering, $\theta_s \equiv r_s(a_*)/D_M(a_*)$. This geometric information is precisely analogous to the transverse BAO scale (and is largely robust to changes in the shape of the CMB power spectrum); in fact, though the CMB is most sensitive to the sound horizon at photon decoupling (being a measurement of the photon distribution), within Λ CDM and common extensions the evolution of the sound

⁶ The BAO scale is extracted by marginalizing over smooth features in the two-point function [see, e.g., 40, 41], and should therefore be estimated in a manner insensitive to the scale-dependent suppression of structure by massive neutrinos.

horizon between photon and baryon decoupling varies minimally with parameters [77]. The CMB therefore constrains the transverse BAO scale Eq. (2.13a) nearly as precisely as it does θ_s ; we describe this inference in more detail in Appendix A and, since they contain the same physical information, discuss the impact of massive neutrinos on θ_s next.

Again excluding neutrinos so heavy as to become nonrelativistic before recombination, the abundance of all matter relevant at late times is necessarily larger than that relevant at early times (i.e., $\omega_b + \omega_c$) by an amount determined by the neutrino's masses. In both the normal and inverted hierarchies, the neutrino species that comprise the majority of the neutrino mass density necessarily become nonrelativistic long before matter- Λ equality. The integral that defines the distance to last scattering $\chi_\star \equiv \chi(a_\star)$ [Eq. (2.9)] has most of its support around matter- Λ equality, since $1/aH$ increases in the matter era and decreases during dark-energy domination; for illustrative purposes, χ_\star may be approximated by simply taking ω_m to always include the full mass density of the neutrinos. For any mass hierarchy, the resulting error is comparable to the standard deviation of *Planck*'s measurement of θ_s [$\sim 4 \times 10^{-4}$; see Eq. (A1)] for the minimal mass sum and quadruples by $M_\nu = 1$ eV. *Planck* measures the angular drag scale so precisely, however, that this error (or even many multiples of it) is negligible compared to the precision of any other probe.

To understand the parametric dependence of the angle θ_s , note that $F_M(1; a_{m-\Lambda}) \approx 1.014 \Omega_m^{0.094}$ is accurate at the subpercent level for $\Omega_m > 0.1$ and the subpermille for $0.23 < \Omega_m < 0.39$.⁷ Then

$$\theta_s \approx \frac{r_s \sqrt{\omega_m} / (2c/H_{100})}{1.014 \Omega_m^{0.094} - \sqrt{a_\star}} \quad (2.16)$$

which, neglecting $F_M(a_\star, a_{m-\Lambda}) \approx \sqrt{a_\star} \sim 10^{-2}$ in the denominator and taking $r_s \propto r_d$ (see Appendix A), means the CMB's geometric degeneracy in flat Λ CDM cosmologies lies along

$$\Omega_m|_{\theta_s} \propto (\omega_m r_d^2)^{5.32}, \quad (2.17)$$

independent of early-time physics. To infer the implications of Eq. (2.17) for cosmological parameters (including neutrino masses), write the ratio of the late- and early-time matter densities in terms of the neutrino fraction Eq. (2.4):

$$\frac{\omega_b + \omega_c + \omega_\nu}{\omega_b + \omega_c} = \frac{1}{1 - f_\nu}. \quad (2.18)$$

Replacing ω_m in Eq. (2.11) with $\omega_r / (1 - f_\nu) a_\star x_{\text{eq}}$ and substituting the sound horizon Eq. (2.7) yields

$$\theta_s \approx \frac{1}{1.014 \Omega_m^{0.094} - \sqrt{a_\star}} \sqrt{\frac{a_\star}{1 - f_\nu}} \sqrt{\frac{1}{3R_\star}} \ln \left(\frac{\sqrt{R_\star} \sqrt{1 + x_{\text{eq}}} + \sqrt{1 + R_\star}}{1 + \sqrt{R_\star x_{\text{eq}}}} \right), \quad (2.19)$$

The terms in Eq. (2.19) that depend on R_\star and x_{eq} alone are measured no less precisely than $\sim 0.300 \pm 0.001$ in Λ CDM or any of the extended cosmologies discussed in Appendix A. The CMB thus tightly constrains the combination $\Omega_m^{1/5.32} (1 - f_\nu) / a_\star$. That is, fixing θ_s within flat Λ CDM cosmologies requires the late-time matter fraction to scale as

$$\Omega_m|_{\theta_s, x_{\text{eq}}, R_\star} \propto (a_\star [1 + f_\nu])^{5.32}. \quad (2.20)$$

⁷ Beware that these errors are larger than that with which *Planck* measures θ_s and, moreover, are smaller than that from neglecting the contribution of radiation to $\chi(a_\star)$. Avoiding these errors, which would clearly be overly pedantic for our present, illustrative purposes, is imperative for quantitative analyses (see Appendix A).

The resulting variation of the Hubble constant may be inferred by writing $\Omega_m = (\omega_b + \omega_c)/(1 - f_\nu)h^2 \approx (1 + f_\nu)\omega_r/h^2 a_\star x_{\text{eq}}$, such that [58]

$$h|_{\theta_s, x_{\text{eq}}, R_\star} \propto \frac{\sqrt{\omega_r}}{a_\star^{3.16} (1 + f_\nu)^{2.16}}. \quad (2.21)$$

Holding the angular extent of the sound horizon fixed thus requires not just a smaller Hubble constant but also a substantial distortion to the shape of the late-time expansion history when varying the neutrino mass sum (or the redshift of recombination).⁸ The scaling of Ω_m in Eq. (2.20) is especially steep compared to the trivial linear scaling from holding h fixed, $\Omega_m|_{h, \omega_b, \omega_c} \propto 1 + f_\nu$. But no quantification of the size of the Universe comes close to the CMB’s subper mille measurement of θ_s in precision or robustness; without invoking new physics to modify recombination (i.e., a_\star) or the dynamics of dark energy [such that Eq. (2.20) is invalid], the matter fraction necessarily increases steeply with neutrino mass. Geometric probes of late-time cosmology thus offer a substantial (and perhaps underappreciated) opportunity to measure the neutrino masses.

3. Type Ia supernovae

Type Ia supernovae (SNe Ia) are thought to occur at a characteristic mass that yields a standardizable luminosity suitable for inferring distances. The apparent magnitude of a SN Ia is parametrized as [34, 35, 67, 78]

$$m = 5 \log_{10} \left[\frac{a}{a_{\text{hel}}} \frac{D_L(a)}{10 \text{ pc}} \right] + M_B, \quad (2.22)$$

where M_B is the fiducial magnitude of an SN Ia and D_L the luminosity distance, $D_L(a) = D_M(a)/a$; the extra factor of a simply accounts for the diminishing luminosity of a distant source relative to its (more fundamental) comoving distance $D_M(a)$. In addition, the ratio of the CMB-frame (a) and heliocentric (a_{hel}) redshifts inside the logarithm corrects for peculiar velocities [79–81]; they are cosmology independent and may as well be absorbed into the apparent magnitude via the definition $\hat{m} \equiv m - 5 \log_{10}(a/a_{\text{hel}})$. Rearranging Eq. (2.22) into the apparent brightness yields a “luminosity angle” in analogy to the BAO angles Eq. (2.13):

$$\theta_L(a) \equiv \frac{10 \text{ pc} \cdot 10^{-M_B/5}}{D_L(a)} = 10^{-\hat{m}/5}. \quad (2.23)$$

The numerator of the middle expression is a standardized luminosity distance.

Like BAO distances, calibration is required to directly measure H_0 with SNe distances, i.e., calibration of the fiducial magnitude M_B using, e.g., Cepheids [25–28] or the tip of the red giant branch [28–32]. The “luminosity angle” [Eq. (2.23)] factorizes in the same manner as Eq. (2.15a):

$$\theta_L(a) = \frac{10^{\log_{10} \sqrt{\omega_m} - M_B/5}}{c \text{ s/m}} \frac{a}{2 [F_M(1; a_{m-\Lambda}) - F_M(a; a_{m-\Lambda})]}. \quad (2.24)$$

The Hubble constant is only constrained via the combination $\log_{10} h - M_B/5$ [which is linearly related to the normalization $\log_{10} \sqrt{\omega_m} - M_B/5$ in Eq. (2.24)]. To the extent that their luminosity is indeed standard, SNe distances can still robustly probe the shape of the expansion history independent of (i.e., marginalized over) its calibration. In particular, by measuring the matter fraction, SNe distances can break the CMB’s geometric degeneracy via Eq. (2.20).

⁸ Quantitatively, the scaling with $1 + f_\nu$ is slightly shallower than that reported in Eqs. (2.20) and (2.21) (about 5 rather than 5.32 for Ω_m), simply because these results assume the neutrinos are matterlike since last scattering; the interim period before they actually become nonrelativistic makes a small contribution to the distance to last scattering.

C. Signatures in structure

While geometric observables only probe background cosmology, large-scale structure is sensitive to the dynamics of neutrino perturbations because neutrinos do not cluster efficiently on scales shorter than their free-streaming length [10, 82]. When studying how external probes break the degeneracies of neutrino free streaming with other parameters, care must be taken to identify what geometric quantities are constrained; per Sec. II B, Λ CDM has the parameter freedom to hold only one of Ω_m , h , and θ_s fixed when varying the neutrino masses (and taking the baryon and CDM densities to be constrained by, e.g., the shape of the CMB anisotropies as described in Sec. II A). The interplay of lensing and geometric constraints can be especially subtle in extended models that modify the sound horizon. We next review the well-established formalism describing probes of weak gravitational lensing in order to elucidate these relationships and identify what parameter combinations are best constrained by probes of structure.

Weak lensing observables may be defined in terms of lensing potentials ϕ_X given by a weighted integral of the Weyl potential Ψ over the line of sight distance χ [83]:

$$\phi_X(\hat{n}) \equiv -2 \int_0^\infty d\chi W_X(\chi) \Psi(\eta(\chi), \chi \hat{n}) \quad (2.25)$$

where the dimensionless lensing kernel is

$$W_X(\chi) \equiv \int_\chi^\infty d\chi_1 n_X(\chi_1) \left(1 - \frac{\chi}{\chi_1}\right) \quad (2.26)$$

and $n_X(\chi_1)$ the (normalized) distribution of sources. The angular power spectrum for two such fields X and Y is likewise given by a weighted, line-of-sight integral over the dimensionless power spectrum of the Weyl potential,

$$\Delta_\Psi^2(\eta, k_1)(2\pi)^3 \delta^3(\mathbf{k}_1 + \mathbf{k}_2) \equiv \frac{k_1^3}{2\pi^2} \langle \Psi(\eta, \mathbf{k}_1) \Psi(\eta, \mathbf{k}_2) \rangle, \quad (2.27)$$

as

$$C_\ell^{XY} = \frac{2\pi^2}{L(\ell)^3} \int_0^\infty \frac{d\chi}{\chi} W_X(\chi) W_Y(\chi) \Delta_\Psi^2(\eta(\chi), L(\ell)/\chi). \quad (2.28)$$

Equation (2.28) takes the Limber approximation [84, 85], which sets $L(\ell) = \sqrt{\ell(\ell+1)}$ and is generally accurate at the permille level for multipoles $\ell \gtrsim 10$.⁹ Weak lensing probes are typically characterized by derivatives of ϕ_X with respect to angular displacements (i.e., orthogonal to the line of sight), like the lensing convergence $\kappa_X \equiv -\nabla^2 \phi_X / 2$.

The statistical properties of weak lensing observables [like Eq. (2.28)] are fundamentally quantified by the dimensionless angular correlations (and possibly the redshift) of dimensionless fields, such as angular deflections or density contrasts. As such, they can only constrain ratios of dimensionful quantities. In the remainder of this section we summarize the growth of structure in Λ CDM (Sec. II C 1) and its application to CMB lensing (Sec. II C 2), taking care to phrase results in terms of the most pertinent dimensionless ratios of densities and scales. We briefly comment on the secondary effects of massive neutrinos on the CMB temperature and polarization power spectra in Sec. II C 3.

⁹ CLASS and CAMB both use $L(\ell) \approx \ell + 1/2$, which approximates the CMB lensing spectrum with precision better than a part in 10^{-3} for $\ell \gtrsim 22$; using the full expression $L(\ell) = \sqrt{\ell(\ell+1)}$ instead achieves the same precision for $\ell \gtrsim 12$.

1. *Growth of structure with massive neutrinos*

The evolution of metric potentials is conventionally factored into a transfer function $T_\Psi(k)$ encoding dynamics of modes with wave number k from horizon crossing until the matter era and a growth factor $D_+(a)$ accounting for scale-independent growth during and after the matter era. We promote the growth factor to depend on k in order to schematically describe the additional scale dependence from freely streaming neutrinos on structure growth in that epoch. The power spectrum of the Weyl potential is thus related to that of the initial comoving curvature perturbation \mathcal{R} by

$$\Delta_\Psi^2(\eta, k) \equiv \left[\frac{6}{5} \frac{D_+(a(\eta), k)}{a} T_\Psi(k) \right]^2 \Delta_{\mathcal{R}}^2(k). \quad (2.29)$$

The early-time dynamics encoded by the transfer function $T_\Psi(k)$ largely depend on wave number only via k/k_{eq} [62, 86]. The effects of acoustic oscillations and anisotropic stress introduce additional scale dependence that, though crucial to the shape of CMB anisotropies, are relatively unimportant to weak lensing observables, which are projected over a range of scales. The transfer function thus deviates from unity at $k \gtrsim k_{\text{eq}}$, where it falls off $\sim (k/k_{\text{eq}})^{-2} \ln(k/k_{\text{eq}})$.

The late-time dynamics of observable modes (i.e., those that enter the horizon during or before the matter era) are stratified by the neutrino free-streaming scale [87],

$$k_{\text{fs}} \equiv \sqrt{\frac{3}{2}} \frac{aH}{c_{\nu_i}} = \frac{1.75 \times 10^{-2} \text{ Mpc}^{-1}}{\sqrt{1+z}} \frac{m_{\nu_i}}{0.06 \text{ eV}} \sqrt{\frac{\omega_m}{0.143}} \sqrt{1 + ([1+z]a_{m-\Lambda})^{-3}} \quad (2.30)$$

where $c_{\nu_i} = T_\nu(a)/m_{\nu_i}$ is a measure of the velocity of the i th neutrino species. In flat Λ CDM cosmologies, the linear growth factor for the fraction $1 - f_\nu$ of matter that does cluster is

$$D_\pm(a, k) \propto C_\pm a^{\gamma_\pm} \cdot {}_2F_1(\gamma_\pm/3, \gamma_\pm/3 + 2/3, 2\gamma_\pm/3 + 7/6, -[a/a_{m-\Lambda}]^3), \quad (2.31)$$

where γ_\pm are the growth rates in a matter-dominated Universe:

$$\gamma_\pm = -\frac{1}{4} \pm \frac{5}{4} \sqrt{1 - \frac{24}{25} f_\nu} = \begin{cases} 1 - \frac{3}{5} f_\nu & + \\ -\frac{3}{2} + \frac{3}{5} f_\nu & - \end{cases} + \mathcal{O}(f_\nu^2). \quad (2.32)$$

The k dependence of Eq. (2.31) is implicit in the interpretation of f_ν as a function of scale (and time). In application to massive neutrinos, Eq. (2.31) holds at $z < z_{\nu_i}$ [Eq. (2.1)] and on scales $k_{\text{fs}} \ll k \ll k_{\text{nl}}(a)$ [where $k_{\text{nl}}(a)$ is the scale at which nonlinear evolution becomes important]; at earlier times and/or on larger scales, the same result holds but with f_ν set to zero.¹⁰

In summary, at times well after matter-radiation equality and on linear scales that cross the horizon before the dark-energy era, the Weyl potential depends on cosmological parameters via

$$\Delta_\Psi^2(\eta, k) \approx \left[\frac{6}{5} \frac{D_+(a(\eta)/a_{m-\Lambda}, k/k_{\text{fs}}; f_\nu)}{a} T_\Psi(k/k_{\text{eq}}) \right]^2 A_s \left(\frac{k}{k_{\text{p}}} \right)^{n_s - 1}, \quad (2.33)$$

implicitly changing the arguments to D_+ and T_Ψ to reflect the dimensionless numbers (ratios of wave numbers and scale factors and the neutrino fraction) that by and large fully parametrize them. Recall that $a_{m-\Lambda}$ is specified by Ω_m [Eq. (2.10)]. Equation (2.33) also inserted the canonical parametrization of the primordial power spectrum in terms of a tilt n_s and the amplitude A_s at

¹⁰ None of these results account for the small, residual impact of radiation, whether from neutrinos while they remain relativistic or from photons.

an arbitrary pivot scale k_p , which is typically taken to be 0.05 Mpc^{-1} but may be freely redefined to, e.g., k_{eq} by redefining A_s . For sources with some fixed (i.e., externally measured) distribution n_X , Eq. (2.33) encodes nearly all of the cosmological dependence of weak lensing observables [Eq. (2.28)].¹¹ Before applying these results to a concrete example, we discuss pertinent numerical estimates for the dependence of the growth factor [and therefore Eq. (2.33)] on the parameters of late-time cosmology.

The hypergeometric function in the growth factor [Eq. (2.31)] approaches unity for $a \ll a_{m-\Lambda}$, i.e., it encodes the deviation from the matter-era result $\propto a^{\gamma_{\pm}}$ due to the onset of dark-energy domination. For $f_{\nu} = 0$, this growth deviation factor is 0.8725 at matter–dark-energy equality, while its present-day value is approximated reasonably well by $0.78 (\Omega_m/0.3)^{0.23}$ for $0.2 \lesssim \Omega_m \lesssim 0.6$. At fixed θ_s , increasing the neutrino mass sum increases the total matter fraction and thus delays the dark energy era; from Eq. (2.20), the present-day suppression factor in the growth factor scales as $\sim (1 + f_{\nu})^{1.15}$. The delayed onset of dark-energy domination thus offsets part of the suppression of structure accumulated while neutrinos do not cluster (as encoded by the factor a^{γ_+} in D_+), which itself may be approximated by

$$D_+(a)/a \approx 1 + (\gamma_+ - 1) \ln[(1 + z_{\nu_i})/(1 + z)] \approx 1 - \frac{3}{5} f_{\nu} \ln[(1 + z_{\nu_i})/(1 + z)] \quad (2.34)$$

in the matter era (with z_{ν_i} equal for all mass eigenstates for the degenerate hierarchy). For the minimum mass sum, the growth factor deviates from the $f_{\nu} = 0$ result by $-1.1f_{\nu}$ to $-2.2f_{\nu}$ between redshifts 5 and 0; the coefficients of f_{ν} increase to -2.4 and -3.4 , respectively, for $M_{\nu} = 0.5 \text{ eV}$.

While the individual components of Eq. (2.33)—the initial conditions, transfer function, and growth factor—are fairly straightforward to study (semi)analytically, the translation to the angular correlations of an observable [Eq. (2.28) in the Limber approximation] involves a weighted integral over Δ_{Ψ}^2 evaluated on scales and at times both specified by the line-of-sight distance. To concretely illustrate the true dependence of LSS observables on dimensionless cosmological parameters, we specialize to CMB lensing next.

2. CMB lensing

For CMB lensing the source distribution is the CMB visibility function, which peaks narrowly at recombination and may be approximated by a delta function at χ_* . The weight function is simply $W(\chi) = 1 - \chi/\chi_*$,¹² so

$$C_{\ell}^{\kappa\kappa} = \frac{2\pi^2 \ell^2 (\ell + 1)^2}{L(\ell)^3} \int_0^{\chi_*} \frac{d\chi}{\chi_*} \left(\sqrt{\chi_*/\chi} - \sqrt{\chi/\chi_*} \right)^2 \Delta_{\Psi}^2(\eta(\chi), L(\ell)/\chi). \quad (2.35)$$

The competition between the weight function (which diverges as $\chi/\chi_* \rightarrow 0$) and the shape of Δ_{Ψ}^2 (which falls off as four powers of $k/k_{\text{eq}} = L(\ell)/\chi k_{\text{eq}}$ at large k) places the bulk of the integral’s support roughly between redshifts 0 and 5 [83]. The CMB lensing spectrum thus retains mild sensitivity to the dark-energy era and thus can discern to at least some degree its delayed beginning in heavy-neutrino cosmologies (which entail a larger matter fraction Ω_m and equality scale factor $a_{m-\Lambda}$ when fixing θ_s , per Sec. IIB 2). Since the growth factor’s sensitivity to f_{ν} ranges between -2 and -4 over this redshift interval (for all but the smallest masses), the net suppression due to neutrino free streaming at large ℓ should asymptote to $1 - 6f_{\nu}$ or so (ignoring any changes to Ω_m).

¹¹ Typically the distribution of sources is measured over redshift; the conversion to line-of-sight distances χ in Eq. (2.26) does then depend on cosmology. For CMB lensing, which we specialize to in Sec. IIC 2, the line-of-sight distance to last scattering is essentially fixed by the precise constraint on θ_s in cosmologies that don’t alter the sound horizon.

¹² Technically, the lensing kernel averages the inverse comoving distance over the visibility function, which deviates from $1/\chi_*$ (i.e., evaluated at peak visibility) by about 0.1%. The use of χ_* in the kernel in both CLASS and CAMB incurs an error of the same order, growing to 0.3% at $\ell \geq 1000$.

Equation (2.35) shows that scale-dependent features in the Weyl scalar appear in the angular correlations of the CMB lensing potential at multipoles determined by the distance to last scattering. For instance, the horizon at matter-radiation equality k_{eq} , at which the transfer function turns over, corresponds to

$$\ell_{\text{eq}} \equiv \chi_{\star} k_{\text{eq}} \approx 2\sqrt{2} [F_M(1; a_{m-\Lambda}) - F_M(a_{\star}; a_{m-\Lambda})] \sqrt{\frac{1-f_{\nu}}{a_{\star} x_{\text{eq}}}}, \quad (2.36)$$

using Eq. (2.11) for χ_{\star} and approximating $k_{\text{eq}} = \omega_m H_{100} / \sqrt{\omega_r/2}$ as for Universes with only massless neutrinos. The neutrino free-streaming scale Eq. (2.30) imprints on sky multipoles of order

$$\ell_{\text{fs}}(a) \equiv \chi_{\star} k_{\text{fs}}(a) \sim 81 \frac{m_{\nu_i}}{0.02 \text{ eV}} \frac{2 [F_M(1; a_{m-\Lambda}) - F_M(a_{\star}; a_{m-\Lambda})]}{1.75\sqrt{1+z}} \sqrt{1 + ([1+z]a_{m-\Lambda})^{-3}}, \quad (2.37)$$

near $\ell_{\text{eq}} \approx 144$ in *Planck*'s best-fit, flat- Λ CDM cosmology [although $\ell_{\text{fs}}(a)$ is smaller at earlier times where Eq. (2.35) has most support]. Equation (2.37) is written relative to a fiducial $m_{\nu_i} = 0.02$ eV, i.e., as for degenerate neutrinos with the minimum mass sum of the normal hierarchy (for illustration). Since both k_{fs} and χ_{\star} are largely determined by the late-time expansion history, their product only depends on the Universe's late-time composition (Ω_m in flat Λ CDM cosmology) and the neutrinos' masses (relative to their average momentum, which we take as fixed by the SM prediction for neutrino decoupling). On the other hand, k_{eq} is a measure of the horizon at early times, and per Sec. II A, $\chi_{\star} k_{\text{eq}}$ is fixed when x_{eq} , R_{\star} , and θ_s also are (i.e., the same quantity is independently constrained by the shape of the primary CMB power spectra). Both scales mark where power begins to drop and happen to take on similar values, and anyway their corresponding features in wave number are blurred over multipole by the lensing kernel in the line-of-sight integral Eq. (2.35); CMB lensing data by itself thus cannot easily differentiate between the two angular scales for reasonable neutrino masses.

Figure 2 depicts the quantitative response of the CMB lensing spectrum to massive neutrinos. The fractional change of $C_{\ell}^{\kappa\kappa}$ divided by the neutrino fraction as depicted in Fig. 2 estimates the response exponent $\partial \ln C_{\ell}^{\kappa\kappa} / \partial \ln(1+f_{\nu})$. Figure 2 compares the response for a variety of neutrino mass sums when holding either θ_s or h fixed; consistent with expectations, the increase in the matter fraction $\Omega_m \propto (1+f_{\nu})^5$ incurred by the former indeed slightly mitigates the degree to which structure is suppressed (and also enhances structure on large scales where neutrinos do cluster [88]).¹³ The sensitivity of CMB lensing to neutrino masses near the minimum sum is yet weaker than commonly quoted because of the logarithmic dependence of Eq. (2.34) on z_{ν_i} : for the normal hierarchy's minimum mass sum, the sensitivity is only about two-thirds of that in the large-mass limit.

3. Peak smearing and the integrated Sachs-Wolfe effect

Structure at late times also distorts CMB temperature and polarization power spectra via weak lensing [89–91], the main effect of which is to smooth or smear the acoustic peaks. The degree of peak smearing inferred within a model thus probes massive neutrinos by effectively measuring the amplitude of gravitational potential fluctuations at late times [33, 92]. The impact of lensing on the primary anisotropies is partially degenerate with other physical effects whose spectral shape is smooth (e.g., the modulation of the evolution of gravitational potentials as the Universe transitions

¹³ The sensitivity of large-scale structure is also often phrased as that for the present-day matter power spectrum, which overestimates that of CMB lensing because most of the lensing integral's support is at redshifts of order a few (rather than zero). The matter power spectrum is also dimensionful, adding complexity in its translation to the CMB lensing spectrum compared to Eqs. (2.28) and (2.33).

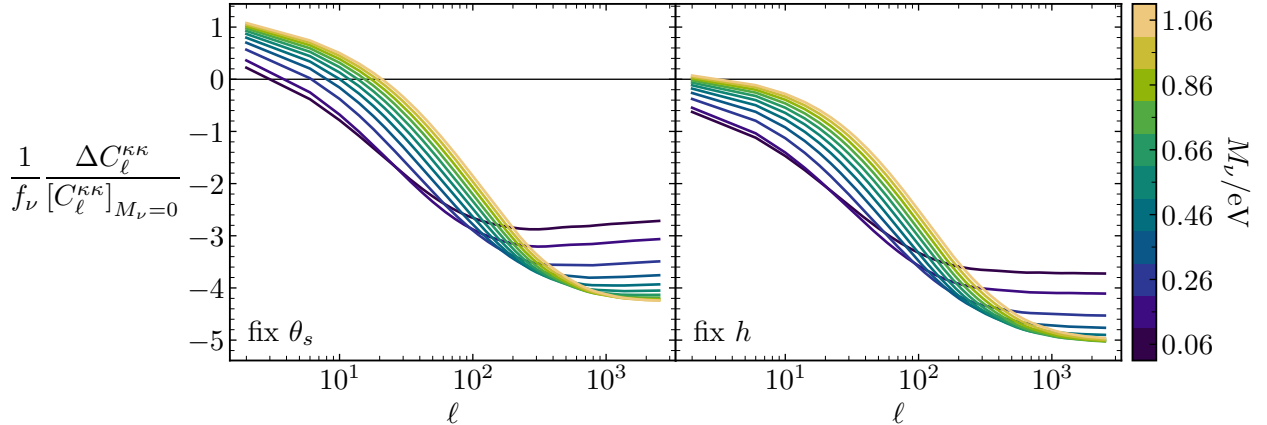


Figure 2. Residual of the CMB lensing spectrum for cosmologies varying the neutrino mass sum (by color) relative to a cosmology with massless neutrinos, measured in units of the neutrino fraction f_ν [Eq. (2.4)]. Results neglect nonlinear structure growth for illustration. Results also take the normal mass hierarchy because the equal-mass approximation underestimates the suppression for the minimum mass sum; for all other curves, the differences between the normal, inverted, and equal-mass hierarchies are negligible. The left and right panels respectively fix the angular extent of the photon sound horizon θ_s and the Hubble constant h . In the former case, the matter fraction increases as $\Omega_m \propto (1 + f_\nu)^5$, delaying the dark energy epoch; above the neutrino free-streaming scale [Eq. (2.30)] the lensing spectrum is thus enhanced by about one factor of $1 + f_\nu$, whereas on smaller scales the suppression is reduced to a similar degree compared to that if Ω_m were unchanged. In contrast, holding h fixed (as commonly taken) yields no large-scale enhancement and a greater degree of suppression at high ℓ .

to matter domination) or that yield oscillatory residuals (e.g., the amplitude of acoustic oscillations as controlled by the baryon density). Inferring the degree of lensing-induced peak smearing therefore depends partly on early-Universe physics.

The primary anisotropies independently constrain the six-parameter Λ CDM model via early-time effects well enough to tightly (but indirectly) constrain late-time cosmology and structure growth. The degree to which the observed acoustic peaks appear smeared relative to the (unlensed) Λ CDM prediction provides a consistency test, one that *Planck* data is known to not pass [1]. Introducing additional parameter freedom via a rescaling of the lensing potential A_L [93], *Planck* prefers excess peak smearing at the 2 to 3 σ level [1]. While the degree of this so-called lensing anomaly varies among recent *Planck* maps and likelihoods [94, 95] (e.g., the treatment of foregrounds), even direct reconstructions of the CMB lensing spectrum from four-point statistics prefer an amplitude of lensing larger than the Λ CDM prediction. This general lensing excess leaves little room for massive neutrinos to further suppress the amplitude of structure. Marginalizing over a parameter A_{smear} , which rescales the amplitude of the lensing spectrum insofar as it lenses the temperature and polarization anisotropies,¹⁴ effectively removes the information on late-time structure from the primary CMB.

Finally, massive neutrinos modify the time evolution of metric potentials as they become nonrelativistic, both by altering the expansion rate (compared to that for a pure-matter Universe, in which the potentials are constant) and the clustering of matter (compared to a Universe where all matter clusters) [50, 96, 97]. The incompatibility of measurements of the first acoustic peak (and lower multipoles) with these effects requires that neutrinos become nonrelativistic well after

¹⁴ Typically, the parameter referred to as A_L rescales the lensing spectrum consistently in its impact on temperature and polarization anisotropies as well as the predicted lensing spectrum itself (which is measured via the four-point function of CMB maps). Here by A_{smear} we denote only the former effect, which we use to derive constraints on structure from CMB lensing independent of the peak-smearing effect. Marginalizing over A_{smear} also yields CMB constraints on late-time cosmology that effectively only derive from geometry (i.e., θ_s), as employed in Sec. III A 2.

recombination. Since $T_\star \approx 0.3$ eV, upper limits on M_ν deriving only from this effect are of order 1 eV. In fact, by marginalizing over the amplitude of the lensing spectrum, the results in Fig. 4 using only *Planck* temperature and polarization power spectra are effectively driven only by the impact of an early-time nonrelativistic transition, consistent with analyses of large-scale CMB anisotropies alone (e.g., from the Wilkinson Microwave Anisotropy Probe [98, 99]). Because these effects have been excluded by multiple generations of CMB observations and are largely irrelevant in the mass regimes allowed by current data, we do not discuss them further. We note, however, that the 95% upper limit $M_\nu < 0.86$ eV (from Fig. 4 below) may be regarded as a cosmological bound largely independent of the lensing excess and of late-time dynamics, including in particular modifications to the dynamics of dark energy.

III. RESULTS

Using the physical understanding developed in Sec. II of neutrino cosmology and its degeneracies with the geometry of the late Universe, we next investigate the neutrino mass constraints derived from current data via geometry alone (Sec. III A) and in combination with probes of structure (Sec. III B). We study in detail the role of particular datasets, the sensitivity of results to potential statistical or systematic effects, and the manner in which dataset combinations break parameter degeneracies. Before proceeding, we describe our analysis methods and informative summary statistics for cosmological neutrino mass inference in light of the lower bounds imposed by neutrino oscillation data.

The posterior distributions over M_ν from (most) current cosmological data are not Gaussian, and on physical grounds the masses of SM neutrinos are positive *a priori*. Measuring the degree to which posteriors are consistent with nonzero M_ν is therefore nontrivial. For instance, the z score of $M_\nu = 0$ (i.e., quantifying the distance of the center from zero in units of the standard deviation) is not particularly meaningful when posteriors are nonnormal, let alone asymmetric. These subtleties motivate a more nuanced quantification of a “detection” of nonzero neutrino masses or the degree to which a particular cosmological model and set of data are compatible or not with massive neutrinos.

Since the only physical model of neutrinos we consider is the standard one—described by SM physics with mass terms for the neutrinos—we retain the physical prior that $M_\nu \geq 0$, under which “compatibility” with negative values (as explored by recent work [44, 100–104]) cannot be assessed. But current laboratory probes place precise, nonzero lower bounds on M_ν for the normal and inverted hierarchies. A more motivated metric for the compatibility of cosmological datasets with minimal, massive neutrinos is the fraction of the posterior below these lower bounds, i.e., the cumulative distribution function (CDF)

$$P(M_\nu < M_{\nu\text{min}}|\mathcal{D}) = \int_0^{M_{\nu\text{min}}} dM_\nu p(M_\nu|\mathcal{D}) \quad (3.1)$$

where $p(M_\nu|\mathcal{D})$ is the posterior density for dataset \mathcal{D} marginalized over all parameters but M_ν . (All probabilities here are implicitly conditional on the assumed model.) Equation (3.1) thus measures what fraction of the posterior is incompatible with a mass hierarchy whose minimum mass sum is $M_{\nu\text{min}}$. When $p(M_\nu|\mathcal{D})$ is nearly normal, Eq. (3.1) is of course equivalent to a z score (suitably translated to the CDF of a normal distribution).

In our analyses, we employ the 2018 *Planck* (PR3) likelihoods via the `Plik_lite` variants that are marginalized over the parameters of the foreground models [1, 2]; various combinations of BAO measurements from SDSS, including eBOSS DR12 and DR16 data [44–46] and the Main Galaxy Sample (MGS) from DR7 [47], and from DESI DR1 [39–41]; and supernova distance measurements from the Pantheon [78], Pantheon+ [34, 35], DES 5YR [36], and Union3 [37] results. Except where

noted, the SNe measurements are always marginalized over the fiducial magnitude rather than calibrated, i.e., by SH0ES [27]. We use CMB lensing data from the *Planck* PR3 release [3] and the ACT DR6 measurement [49] combined with *Planck* PR4 lensing data [105].¹⁵ Throughout we refer to the PR3 temperature and polarization likelihoods by “PR3 CMB” and explicitly state whether and what CMB lensing likelihood is included. We use CLASS [108, 109] and model nonlinear structure growth with HMCODE-2016 [110] (as used by CLASS, which has yet to update to the 2020 version [111]); we show in Appendix C that neglecting nonlinear effects biases neutrino mass constraints toward smaller values, even with current CMB lensing datasets.¹⁶

In parameter inference, we sample over the standard set of Λ CDM parameters with broad, uniform priors: the present baryon and CDM densities, $\omega_b \sim \mathcal{U}(0.005, 0.035)$ and $\omega_c \sim \mathcal{U}(0.01, 0.25)$; the Hubble rate $h \sim \mathcal{U}(0.25, 1.1)$; the tilt and amplitude of the scalar power spectrum, $n_s \sim \mathcal{U}(0.8, 1.2)$ and A_s via $\ln(10^{10} A_s) \sim \mathcal{U}(1.61, 3.91)$; the redshift of reionization $z_{\text{reion}} \sim \mathcal{U}(4, 12)$; and the neutrino mass sum $M_\nu/\text{eV} \equiv \sum_i m_{\nu_i}/\text{eV} \sim \mathcal{U}(0, 1.5)$. Here we use $\mathcal{U}(a, b)$ to denote a uniform prior between a and b . Some analyses also sample over a lensing amplitude $A_{\text{smear}} \sim \mathcal{U}(0, 2)$ that scales the impact of late-time structure on the primary temperature and polarization anisotropies (see Sec. II C 3). We employ parameter sampling methods (using *emcee* [112–114]) and likelihood implementations as described in Ref. [58].

A. Geometric constraints and tensions

Section II B established the critical role played by probes of the large-scale geometry of the Universe in neutrino mass inference. Uncalibrated distance measurements from BAO and type Ia SNe are intrinsically sensitive to the expansion history alone. CMB anisotropies, on the other hand, provide essential geometric information by precisely measuring the angular extent of the sound horizon, but they are simultaneously quite sensitive to the dynamics of spatial perturbations (as discussed in Sec. II C). In this section we explain how the CMB calibrates late-time geometry to constrain neutrino masses (Sec. III A 1) and present results deriving from current low-redshift distance datasets (Sec. III A 2). Motivated by discrepancies in these results, Sec. III A 3 investigates the origin of DESI’s putative incompatibility with massive neutrinos, comparing to results from SDSS.

Uncalibrated distance measurements via the BAO scale in flat Λ CDM are described by a two-parameter model (Ω_m and $r_d\sqrt{\omega_m}$); when deriving posteriors in these parameters we simply evaluate likelihoods on a grid rather than sampling (in Secs. III A 1 and III A 3 only). Similarly, when marginalizing over the overall amplitude of SNe distances $\log_{10} h - M_B/5$, we evaluate SNe likelihoods on a grid in Ω_m . To isolate the CMB’s geometric information in the $r_d\sqrt{\omega_m}$ - Ω_m plane, we derive from a complete analysis of *Planck* data a marginal posterior over the angular extent of the sound horizon to use in conjunction with low-redshift data; these results apply more generally scenarios featuring modified early-time dynamics to the extent that the sound/drag horizon remains a robust a predictor of the acoustic peak locations [115]. Appendix A describes the derivation of a likelihood over the transverse BAO scale from CMB data in more detail.

¹⁵ As noted by Ref. [106], version 1.2 of these likelihoods [107] has a moderate effect on results compared to prior versions (used, for instance, by Ref. [39]), depending on the likelihood configuration. We use the latest version (1.2).

¹⁶ Ref. [106] found that the variation in upper limits on M_ν varied negligibly between the 2016 and 2020 versions of HMCODE, but only for posteriors that include DESI DR1 data. As we discuss in Appendix C, DESI data have a much stronger impact on neutrino mass constraints than do lensing datasets; investigating the impact of nonlinear modeling for dataset combinations that do not exclude the regime in which they matter is a worthwhile task we leave to future work.

1. Neutrino masses from calibrated geometry

Constraining the Universe’s geometry—that is, dimensionless quantifiers of the background metric—is insufficient to measure the neutrino masses. Uncalibrated BAO and SNe distances directly constrain the late-time matter fraction Ω_m but are only sensitive to the absolute density ω_m relative to the drag horizon;¹⁷ either of these measurements may be calibrated to measure the dimensionful ω_m —with a prediction for r_d from early-Universe physics in the latter case or by calibrating the brightness of Ia SNe with Cepheids [25–28], the tip of the red giant branch [28–32], or other calibrators [28, 116, 117] in the former. Additional calibration is required because low-redshift distance measurements alone cannot determine the partitioning of the late-time matter density: they only probe the Universe’s geometry at times long after neutrinos become nonrelativistic, when they are indistinguishable from other forms of matter (at the background level). A CMB-derived constraint on the density of the matter components that are present at early times (baryons and CDM; see Sec. II A) thus isolates the neutrinos’ contribution to the total matter density at late times. While uncalibrated geometric information from CMB and BAO data provides constraints in the $r_d\sqrt{\omega_m}$ - Ω_m plane without appealing to a model of early-Universe physics [see Eq. (2.15)], the CMB’s calibration of the baryon and CDM densities derives from the shape of the power spectra and therefore is sensitive to modified early-Universe physics (e.g., in the manner captured by the parameters R_\star and x_{eq} per Sec. II A). The calibration of the drag horizon r_d also depends on early-Universe physics, of course, as does its relationship to the baryon and CDM densities.¹⁸

In sum, the difference in the densities of early- and late-time matter components, once each is calibrated, may be ascribed to massive neutrinos; ω_ν may then be translated directly to their summed masses via Eq. (2.2) if their number density n_ν is fixed, i.e., by the SM prediction for neutrino decoupling [Eq. (2.2)]:¹⁹

$$M_\nu = \frac{3H_{100}^2 M_{\text{pl}}^2}{n_\nu} (\omega_m - \omega_b - \omega_c) = 13.2 \text{ eV} \left(\frac{\omega_m}{\omega_b + \omega_c} - 1 \right) \frac{\omega_b + \omega_c}{0.142}. \quad (3.2)$$

If a combination of observations infers a late-time matter abundance *lower* than *Planck*’s early-time abundance, Eq. (3.2) would suggest the neutrinos have “negative mass”. Note, however, that the nonrelativistic energy density in neutrinos is truly $\rho_{\nu_i} \approx |m_{\nu_i}| n_{\nu_i}$, since the corresponding limit of each neutrino’s energy is $E(p) = \sqrt{p^2 + m_{\nu_i}^2} \approx |m_{\nu_i}| [1 + (p/m_{\nu_i})^2/2]$. Negative M_ν should thus be interpreted as a would-be decrement in the late-time matter abundance compared to the fiducial value of $\omega_b + \omega_c$ (which is itself measured with 1% precision), or as an incompatibility of standard neutrino physics with Λ CDM (or vice versa).

The CMB’s geometric information, despite being one dimensional, is so precise that it effectively selects a single line in the $r_d\sqrt{\omega_m}$ - Ω_m plane (within flat Λ CDM cosmologies)—one in which the shape of the expansion history (Ω_m) varies rapidly with the overall amplitude $r_d\sqrt{\omega_m}$ [per Eq. (2.17)]. Neutrino mass inference relies crucially on the interplay of this constraint with direct measurements in the plane from uncalibrated BAO data or with measurements of Ω_m from SNe distances, as depicted by Fig. 3. The discrepancy between SNe datasets and BAO datasets is immediately evident but is substantially more severe when considering each’s combination with *Planck*—much of the parameter space in which the BAO posteriors do overlap with DES’s measurement of Ω_m is entirely

¹⁷ The parameterization of the dimensionless “amplitude” of BAO angles [Eq. (2.13)] as $r_d\sqrt{\omega_m}$ is unhelpful—we drop the length unit c/H_{100} to instead report the drag horizon relative to a fiducial Λ CDM prediction.

¹⁸ Posteriors over θ_s or $\theta_{\text{CMB},\perp}(a_d)$ are moderately correlated with R_\star and x_{eq} , which only has a modest effect on inferring M_ν . When employing this reduced geometric information from *Planck*, we only use its calibration of $\omega_b + \omega_c$ (within Λ CDM) to illustrate how the $r_d\sqrt{\omega_m}$ - Ω_m parameter space translates to neutrino masses (i.e., on average) rather than to derive quantitative constraints (for which we use the full likelihoods).

¹⁹ *Planck*’s preferred baryon and CDM densities are slightly sensitive to the late-time effects of lensing—for instance, $\omega_b + \omega_c$ shifts lower by about 1σ when marginalized over A_{smear} (see Sec. II C 3 and Ref. [1]) without substantial degradation in precision. We take its central value of ≈ 0.142 from an analysis of Λ CDM (which holds with or without massive neutrinos) as a fiducial one in order to illustrate the impact of this calibration in standard analyses.

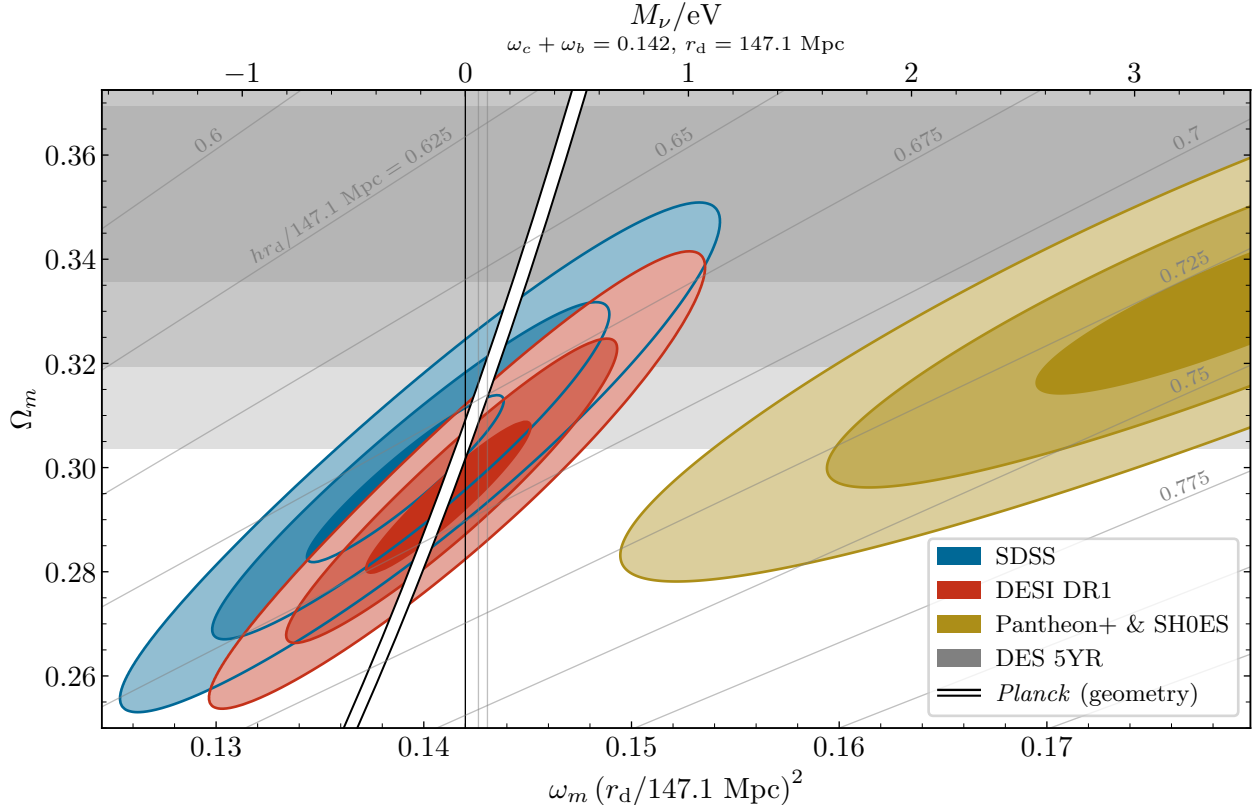


Figure 3. Geometric constraints on late-time Λ CDM cosmology, parametrized in terms of the matter fraction Ω_m and the late-time matter abundance relative to the sound horizon at baryon decoupling, $r_d\sqrt{\omega_m}$. The latter is reported relative to a fiducial drag horizon of 147.1 Mpc as predicted in Λ CDM. Colored regions depict 1, 2, and 3 σ contours of the two-dimensional joint posterior (i.e., the 39.3%, 86.5%, and 98.9% mass levels thereof) from SDSS [44–47] (blue), DESI [39–41] (red), and Pantheon+ [34, 35] using SH0ES calibrators [27] (gold). The white band outlined with black depicts the parameter space allowed by *Planck*’s geometric information [that is, the 3 σ level of its measurement of $\theta_{\text{CMB},\perp}$, Eq. (A1)]. The grey regions indicate the 1, 2, and 3 σ (68.3%, 95.4%, and 99.7%) intervals in Ω_m deriving from the calibration-marginalized DES 5YR supernova sample [36]. These geometric constraints make only minimal assumptions about physics before photon and baryon decoupling (see text for details); only the Pantheon+ & SH0ES posterior moves if the drag horizon differs from the fiducial value. The top axis depicts the neutrino mass sum [Eq. (3.2)] as attributed to the difference between ω_m and *Planck*’s preferred abundance of matter components at early times, $\omega_b + \omega_c \approx 0.142$, taking the same fiducial value for r_d . Both of these values are “calibrated” via the shape of the CMB power spectra within the Λ CDM model. Vertical grey lines indicate the minimum mass sums for the normal and inverted hierarchies. Diagonal grey lines mark constant $hr_d/147.1$ Mpc as labeled.

incompatible with *Planck*. Even ignoring the calibration information from SH0ES, the Pantheon+ SNe sample also measures larger matter fractions than either BAO dataset (as does Union3, per Fig. 1 but not displayed in Fig. 3); the Ω_m preferences from all SNe datasets combine with *Planck* to allow for relatively heavy neutrinos ($M_\nu \sim 0.2$ to 0.4 eV).

In contrast to any SNe result, BAO data from both DESI and SDSS favor *lower* matter densities than *Planck* infers in baryons and CDM, leading each to prefer that neutrinos have “negative” mass on average, purely on geometric grounds. This trend is compounded when combined with *Planck*’s geometric information (as illustrated by the marginal Ω_m posteriors in Fig. 1). Despite measuring slightly larger matter densities than SDSS on its own, and despite its measurements being of comparable precision to SDSS’s [39], DESI’s first data release exhibits an even stronger incompatibility with massive neutrinos when combined with *Planck*. Namely, because of its shift

toward smaller matter *fractions*, DESI’s 1σ mass level overlaps with *Planck*’s posterior fully where $\omega_m(r_d/147.1 \text{ Mpc})^2$ is smaller than *Planck*’s preferred abundance of baryons and CDM. Indeed, because of the relative orientation of the CMB and BAO posteriors, artificially shifting the latter to lower late-time matter densities $\omega_m r_d^2$ would yield a preference for heavier neutrinos!²⁰ Interpreting the combination of this geometric data instead in terms of hr_d (which, per Fig. 3, DESI prefers to be larger than does SDSS) obfuscates the actual causal relationship: per Sec. IIB 2 *Planck* cannot accommodate an increase in the matter abundance from massive neutrinos without steeply increasing the matter fraction, and BAO posteriors fall off rapidly in the parameter direction required to do so.

The SH0ES-derived calibration of the Pantheon+ distance ladder allows Hubble constants that, despite corresponding to larger matter densities on average (via larger h), are entirely inconsistent with both massive neutrinos and *Planck* simultaneously. A $\gtrsim 10\%$ miscalibration of h by SH0ES would be required for consistency with massive neutrinos (and the standard, Λ CDM-derived drag horizon). A comparable change in r_d is not in general equivalent, because scenarios that modify the sound horizon may also require different baryon and CDM densities (and therefore alter what remaining matter density may be attributed to neutrinos). Likewise, joint constraints from *Planck* and both BAO datasets cannot be reconciled with a neutrino mass sum larger than $\sim 0.1 \text{ eV}$ without modifying the sound horizon (discussed in Sec. IV B) or identifying an effect that would shift the relative positions of their posteriors in Fig. 3 (which we consider in Sec. III A 3).

2. Joint constraints from the CMB and low-redshift distances

To illustrate the quantitative impact of combining different low-redshift datasets with the CMB’s geometric information and its Λ CDM-based calibration of the baryon and CDM densities, Fig. 4 depicts the posteriors from each of DESI BAO, DES SNe, and *Planck* PR3 individually and combined. We now employ the full *Planck* temperature and polarization likelihoods (rather than a reduced geometric one as in Sec. III A 1). By marginalizing over the degree to which the primary CMB anisotropies are lensed (via the parameter A_{smear} ; see Sec. II C 3) and excluding four-point reconstructions of the lensing potential itself, the *Planck* results in Fig. 4 effectively remove neutrinos’ impact on structure at late times. (Reference [118] performed similar analyses using early BOSS data.)

Figure 4 shows that mass sums as large as an eV or so are allowed by *Planck* when marginalized over A_{smear} , beyond which the early-time impact of neutrinos’ transition to the nonrelativistic regime (via, for instance, the ISW effect; see Sec. II C 3) remains precluded. The *Planck*-only posterior in Fig. 4 thus follows the geometric degeneracy of Eq. (2.20) up to matter fractions as large as 0.41 in its 2σ mass level. [The Hubble constant h for cosmologies with neutrino masses and matter fractions so large is as low as 0.6 or so, consistent with Eq. (2.21).] The degeneracies with M_ν for BAO data are qualitatively similar but shallower because many DESI tracers reside at low redshift. SNe distances, by contrast, simply measure the matter fraction independently of h when marginalized over their calibration. As anticipated from Fig. 3, joint posteriors from *Planck* combined with either DESI or DES localize in completely distinct parameter space, with dramatic consequences for neutrino mass inference.

Figure 5 summarizes the neutrino mass constraints from combinations of *Planck* (still marginalized over A_{smear}) with all recent BAO and SNe datasets, reporting the hierarchy compatibility metric [Eq. (3.1)] and the 95th percentile of each posterior. As expected from Fig. 3, joint constraints with DESI DR1 localize close to zero (with 95% of the marginal posterior at $M_\nu \lesssim 0.2 \text{ eV}$). In sharp

²⁰ In such a counterfactual, the joint posterior, if shifted sufficiently, would localize in parameter space further from that which maximizes the BAO likelihood—that is, the joint inference of heavier neutrinos could degrade the fit to BAO observations.

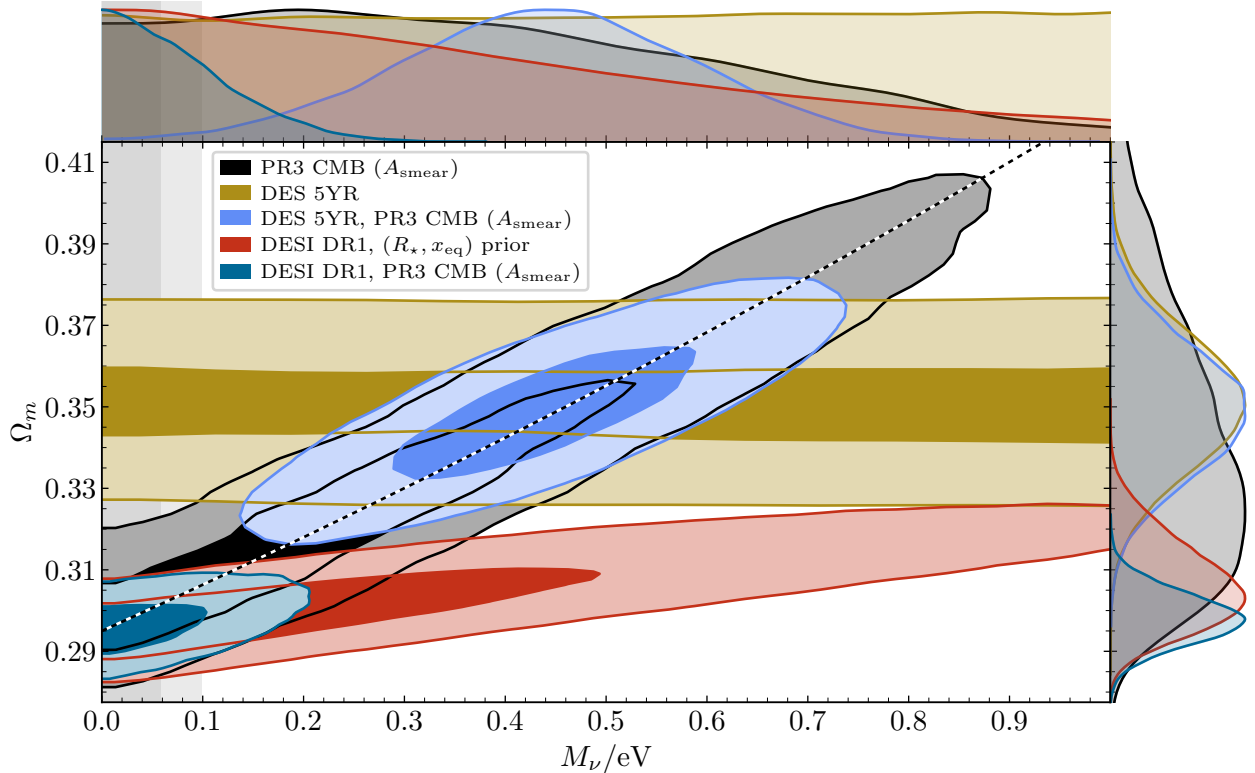


Figure 4. Geometric constraints on flat Λ CDM cosmologies with massive neutrinos, depicting posterior distributions using *Planck* PR3’s primary CMB data [1, 2] (grey), DESI DR1 BAO data [39–41] (red), DES 5YR SNe data [36] (gold), and *Planck* combined with each of DESI (dark blue) and DES (light blue). Results that employ *Planck* data include the A_{smeat} parameter in order to marginalize over the smearing of the primary CMB by gravitational lensing, while results that include only BAO data include a prior on the baryon and CDM densities derived from *Planck* data (Sec. II A). The lower left panel displays the 1 and 2σ contours (i.e., the 39.3% and 86.5% mass levels) of the two-dimensional marginal posterior density over the neutrino mass sum M_ν and the matter fraction Ω_m . Outer panels diagonal depict kernel density estimates of the one-dimensional marginal posteriors over each parameter normalized relative to the peak density. Vertical grey shading indicates neutrino mass sums incompatible with the normal and inverted hierarchies. The dashed black/white line indicates the expected degeneracy direction that fixes the distance to last scattering (Sec. II B 2), $\Omega_m \propto (1 + f_\nu)^5$ where the neutrino fraction f_ν is defined in Eq. (2.4). This figure quantitatively demonstrates how “calibrating” geometry with CMB data informs neutrino mass constraints, i.e., by marginalizing over r_d and $\omega_b + \omega_c$ within Λ CDM cosmologies (whereas Fig. 3 fixed values thereof for illustration). The two-dimensional posteriors demonstrate that the discordant geometric preferences of DESI BAO and DES SNe data combine with *Planck*’s measurement of the distance to last scattering to yield completely distinct inference of the neutrino mass sum (dark and light blue posteriors).

contrast, DES SNe’s preference for substantially larger Ω_m combines with *Planck* to *detect* nonzero $M_\nu/\text{eV} \approx 0.44 \pm 0.15$ (a Gaussian z score of nearly 3). While only 32% and 55% of the posterior for *Planck* combined with DESI are compatible with the inverted and normal hierarchies, respectively, only 1% and 0.4% of the DES & *Planck* posterior are *incompatible* with each. The recent Pantheon+ dataset (when uncalibrated) also yields a preference for nonzero masses, $M_\nu/\text{eV} \approx 0.30^{+0.16}_{-0.15}$; its spread is comparable to DES’s but centered at lower masses, which simply reflects the $\sim 1\sigma$ offset in their measurements of Ω_m (see Fig. 1). Both SNe posteriors are inconsistent with those from any BAO dataset in Fig. 5, but especially so for the full combination of DESI DR1 measurements. However, Fig. 5 also shows that replacing DESI’s low-redshift measurements with SDSS’s (which are of comparable precision) substantially weakens its limits on M_ν . In fact, SDSS data by itself yields

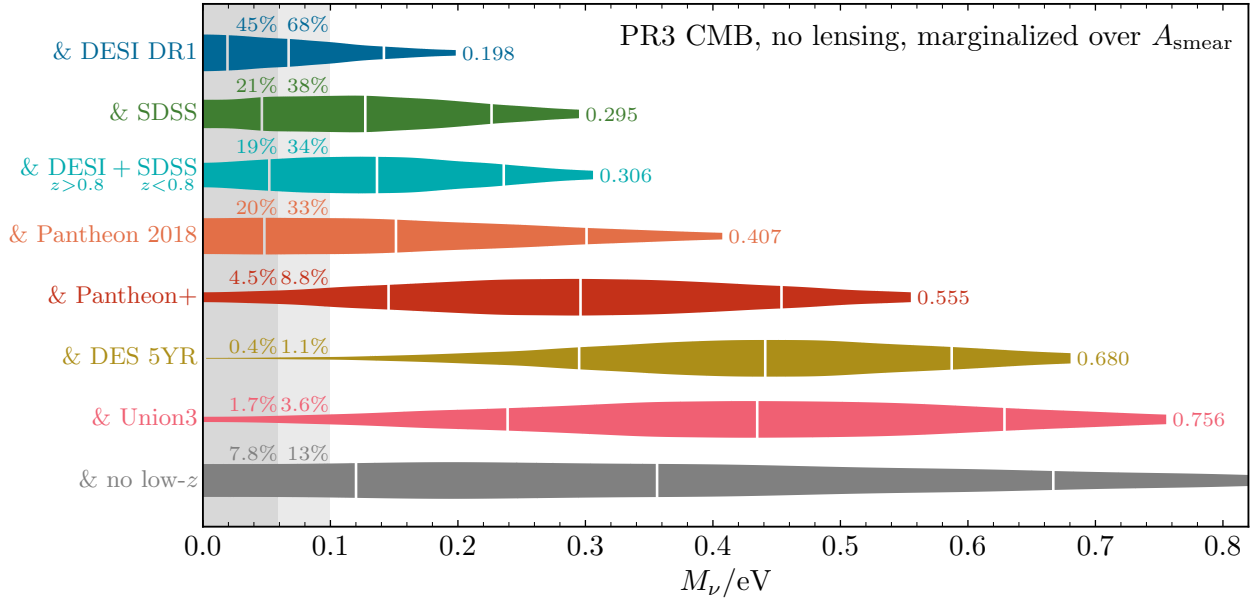


Figure 5. Marginal posterior distributions over the neutrino mass sum M_ν deriving largely from geometric information in *Planck* PR3 temperature and polarization power spectra [1, 2] combined individually with various BAO and (uncalibrated) SNe datasets as labeled. Results marginalize over the peak-smearing amplitude A_{smear} so that the CMB constraints are effectively independent of neutrinos’ effects on late-time structure (see Sec. II C 3). The shaded bands depict the range of masses that are incompatible with the normal and inverted hierarchies, and the fraction of each posterior within these ranges [Eq. (3.1)] is annotated on the figure. Posteriors are truncated at the 95th percentile (whose value is also labeled); vertical white lines indicate the median and $\pm 1\sigma$ quantiles. Note that the combination of DESI and SDSS data differs from that considered in Ref. [39]; see Sec. III A 3 for elaboration.

an extremely similar posterior that of this combination. We investigate what BAO measurements from individual tracers drive DESI’s strong preference for negligible neutrino masses next.

3. Impact of DESI luminous red galaxy measurements

Neutrino mass constraints are highly sensitive to any bias in low-redshift distance measurements because of the crucial role they play in breaking degeneracies in late-time cosmology, as well as the close proximity of current constraints to the prior boundary $M_\nu = 0$. Figure 3 shows that the tightened upper limit on M_ν from DESI compared to that from SDSS (each combined with *Planck*) derives only from a shift in their preferred matter fractions; both surveys at present constrain similar volumes in parameter space (i.e., at a given posterior mass level). While the DESI DR1 measurements pass numerous robustness tests [40, 41, 119], the difference between DESI and SDSS measurements for similar populations of tracers motivates scrutinizing the discrepancies carefully.

Figure 6 shows that, when interpreted in the flat Λ CDM model, DESI’s DR1 measurements from both LRG bins are nonnegligibly discrepant with all other tracers. In fact, just the line-of-sight measurement in the $z = 0.51$ bin (LRG1 $_{\parallel}$) and the transverse one in the $z = 0.706$ bin (LRG2 $_{\perp}$) are in tension; the posteriors from the other measurement in each bin coincide extremely well with the joint posterior from all other tracers (see Fig. 17).²¹ Moreover, these other tracers are far more compatible with the Ω_m measurements deriving from SNe datasets like DES 5YR and Pantheon+.

²¹ We obtain separate constraints from transverse and line-of-sight measurements simply by marginalizing over the other at the level of the likelihood; their correlation is accounted for in the joint likelihood as usual, but neglecting it only slightly distorts the shape of the resulting posterior.

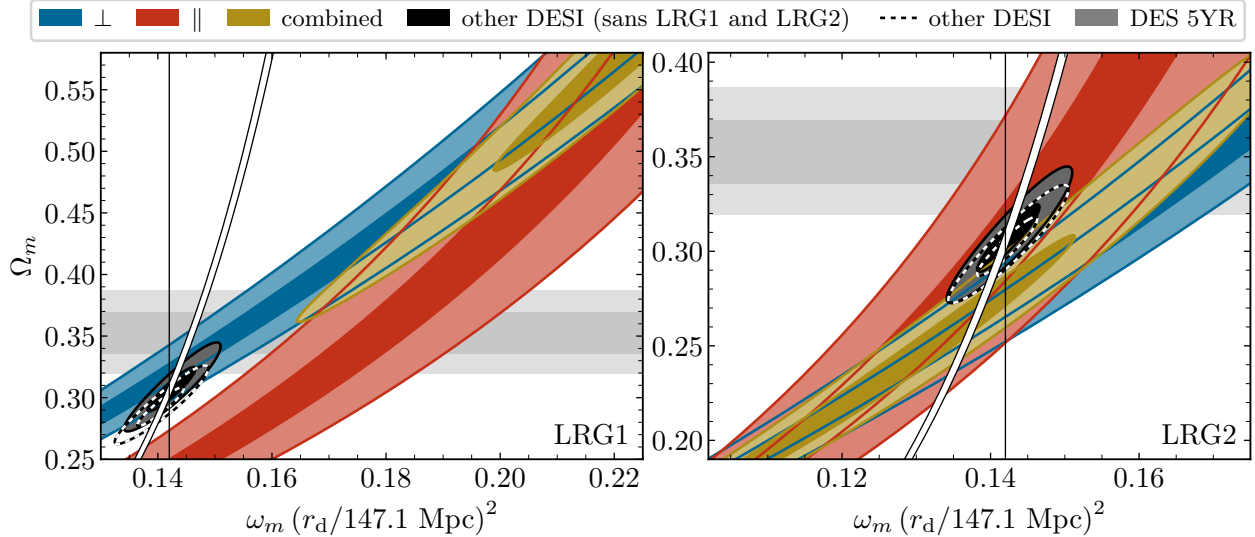


Figure 6. Comparison of Λ CDM parameter space compatible with DESI DR1’s BAO measurements [39–41] from luminous red galaxy samples at effective redshifts 0.51 (LRG1, left) and 0.706 (LRG2, right), displaying posteriors deriving from transverse (blue) and line-of-sight (red) measurements and their combination (gold). Appearing in addition are posteriors from all other DESI tracers (dashed black/white lines), from all other DESI tracers excluding both LRG bins (black), from the DES 5YR SNe sample [36] (grey), and from *Planck* (white band outlined in black with extent covering its 5σ interval; see Appendix A). Results are presented as in Fig. 3 but instead displaying only 1 and 2σ mass levels. While the LRG1 $_{\perp}$ and LRG2 $_{\parallel}$ measurements coincide quite well with the joint measurement from other tracers, the LRG1 $_{\parallel}$ and LRG2 $_{\perp}$ ones are each offset from this parameter space by several standard deviations. Comparing the filled black and unfilled dashed contours indicates the individual impact of the LRG2 (left) and LRG1 (right) measurements on joint constraints; both measurements truncate the joint posteriors at lower Ω_m , reducing the allowed contribution to the matter density from neutrinos (and increases the degree of tension with the range of Ω_m preferred by SNe datasets).

Observe that, though the joint LRG1 posterior itself localizes at substantially larger $\omega_m r_d^2$ and Ω_m than all other tracers, it only overlaps with the bulk of the posterior from all other tracers rather far in its tail, driving combined constraints toward lower matter fractions. This contrast in concordance is even more dramatic when considering their intersections with *Planck*’s geometric constraint (even without calibrating a value for the drag horizon). DESI’s other tracers, its LRG1 $_{\perp}$ and LRG2 $_{\parallel}$ measurements, and *Planck* all intersect in precisely the same region of parameter space, while LRG1 $_{\parallel}$ and LRG2 $_{\perp}$ ’s 2σ mass levels both intersect with the *Planck* constraint at much lower Ω_m and $r_d\sqrt{\omega_m}$.²²

Figure 7 illustrates the impact of these potential outliers on parameter inference by comparing various combinations of BAO measurements from DESI and SDSS. Reference [39] combined SDSS data below redshift 0.6 with DESI data above it, using a joint DESI+SDSS Ly- α measurement [40]. When combined with *Planck* data, the resulting neutrino mass constraints are slightly weaker than those from the DESI-only dataset in spite of the combination having slightly greater constraining power in the $r_d\sqrt{\omega_m}$ - Ω_m plane than the latter. Reference [39] identified the offset in hr_d preferred by each combination as the origin of this finding, but Fig. 3 and surrounding discussion show that this is only a happenstance consequence of the offset in Ω_m which, when projected along *Planck*’s constraint, produces a tighter constraint on M_{ν} . This particular combination, however,

²² See Fig. 16 in Appendix B2 for further illustration of this point and Fig. 17 for consistency tests analogous to Fig. 6 for all other tracers from DESI and eBOSS. Figure 17 in particular shows that eBOSS’s Ly- α measurements are slightly anomalous and also shift joint constraints toward parameter space that is less compatible with massive neutrinos.

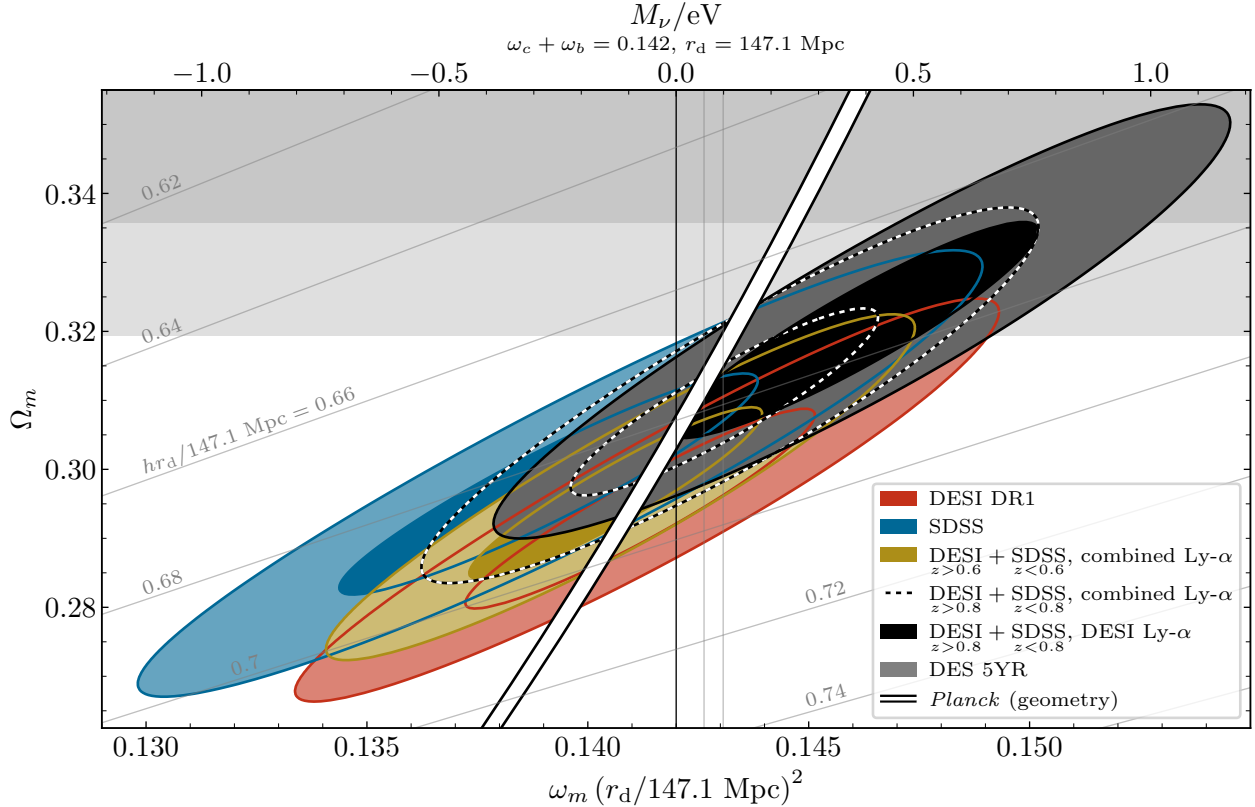


Figure 7. Geometric constraints on late-time Λ CDM cosmology from various combinations of SDSS [44–47] and DESI [39–41] data, presented as in Fig. 3 but instead displaying only 1 and 2σ mass levels (and the 2σ interval for *Planck*; see Appendix A). Results include all DESI tracers (red); all SDSS tracers, including both the DR7 MGS and eBOSS (blue); the “DESI+SDSS” combination from Ref. [39] which includes SDSS data at $z < 0.6$, DESI data at higher redshift, and the joint DESI+SDSS Ly- α dataset (gold); the same combination but instead split at $z = 0.8$ (dashed black/white); and the $z = 0.8$ split that only uses DESI’s Ly- α measurement rather than the joint DESI+SDSS analysis thereof. Note that the DESI/SDSS split at $z = 0.6$ (gold), as employed in Ref. [39], includes DESI’s LRG2 bin, which is replaced by eBOSS DR16’s measurement at a similar redshift in the other combinations split at $z = 0.8$; the latter combinations also exclude DESI’s LRG3+ELG bin (covering $0.8 < z < 1.1$) to be conservative about double counting information. Comparing these results shows that all BAO measurements from SDSS and DESI that could be interpreted as outliers within Λ CDM (LRG1 and LRG2 for DESI and Ly- α for SDSS) shift posteriors toward lower Ω_m and amplitude $r_d\sqrt{\omega_m}$, directions that each disfavor massive neutrinos.

includes both DESI’s LRG2 measurement and eBOSS’s Ly- α data. Figure 7 shows that splitting data from the surveys at $z = 0.8$ (i.e., using none of DESI’s LRG data) instead shifts posteriors toward higher Ω_m and $\omega_m r_d^2$. Swapping the combined Ly- α measurement for DESI’s alone further shifts the posteriors along this direction toward parameter space much more compatible with SNe data; however, these combinations prefer the same Ω_m at fixed amplitude $\sqrt{\omega_m} r_d$. Any dataset combination that uses SDSS’s LRG data rather than any of DESI’s—that is, both alternative combinations and the SDSS-only dataset—intersects with *Planck* at roughly the same point in parameter space (at 2σ), explaining the close agreement of posteriors over M_ν in Fig. 5.

In future data releases DESI’s apparent outliers could well shift back to concordant parameter space by pure statistical chance. To the extent that future data releases can be considered independent measurements with much higher precision (a decent approximation, given that the effective volume for LRGs will increase by about a factor of three [41]) and no systematic differences,

their central values may be considered a random draw from the DR1 likelihoods. The probability that the LRG1 line-of-sight measurement drops by more than 1σ while the transverse one shifts by no more than 1σ in either direction²³ is about 10%; a shift more than -2σ has 1% probability. The LRG1 and LRG2 bins (which are independent of each other) each have nearly the same correlation coefficient, so the same quantities apply to possible shifts in the LRG2 transverse measurement.

These likelihood-level metrics, however, ignore additional prior information from SDSS LRG measurements in a similar redshift range, which do prefer parameter space consistent with all other DESI tracers.²⁴ Reference [39] identified LRG2_⊥ as most discrepant from the most directly comparable SDSS measurement, though their line-of-sight measurements at $z \approx 0.51$ also do not agree well. And in contrast to Ref. [103], we find that one measurement from each redshift bin matters, not both in only the LRG2 bin: both outliers (LRG1_∥ and LRG2_⊥) have the same effect on joint posteriors (i.e., posteriors derived by excluding each are nearly identical). The measurements at lower redshift are especially important because the orientation of their posteriors in the $r_d\sqrt{\omega_m}-\Omega_m$ plane differs the most from those at high redshift (e.g., from the CMB), making them crucial for breaking degeneracies and determining the parameter values at which joint constraints localize.

Reference [41] found negligible shifts in results when applying DESI’s new analysis pipeline to the BOSS/eBOSS catalogs, suggesting that no presently known systematic can adjudicate these measurements. Reference [119] studies the sensitivity of DESI’s measurements to the fiducial cosmology employed in the analysis with mock data, finding in particular that a 14% reduction in Ω_m can lead to some of the largest scatter (up to 1 – 2%) among the alternative cosmologies tested. Given that the matter fraction preferred by DES SNe is 12% larger than the fiducial value used in DESI’s analysis, it would be interesting to further investigate the sensitivity thereof and test how the individual shifts in BAO measurements within each alternative cosmology jointly propagate to cosmological parameters. In addition, DESI’s likelihoods are specified by Gaussian approximations in $1/\theta_{\text{BAO},\perp}$ and $1/\theta_{\text{BAO},\parallel}$; it might also be worth checking this approximation, since the joint parameter space preferred by all DESI data lie rather far in the tail of, e.g., the LRG1_∥ measurement [see Fig. 6].

B. Impact of CMB lensing

We now explore the impact of CMB lensing data on neutrino mass inference. In Sec. III B 1 we study constraints that effectively remove the CMB’s geometric information, seeking to illustrate how low-redshift distance datasets break the degeneracy between M_ν and the matter fraction Ω_m that derives purely from the growth of structure. Section III B 2 then presents results from the full combination of CMB temperature and polarization spectra, CMB lensing, and low-redshift distance datasets, sans any nonstandard modifications.

1. CMB lensing without CMB geometry

Large-scale structure observations alone are sensitive to the combined effect of the expansion history and clustering of matter components, but direct probes of late-time geometry can break this degeneracy. As an approximate means to remove geometric information from CMB likelihoods, we construct a multivariate normal approximation to posteriors derived using uniform priors over

²³ The reported probabilities increase by a factor of 1.5 to 2 if allowing the transverse measurement to instead shift by as much as $\pm 2\sigma$. The transverse and line-of-sight measurements would have to be much more correlated (than their ~ -0.4 coefficient) for this marginalization to have a more substantive effect. Measurements in other bins are independent; the additional penalty in probability incurred by requiring they not become apparent outliers is likewise independent of any shift in the particular bins we call out.

²⁴ As discussed in Ref. [39], the two surveys overlap, making a quantitative comparison nontrivial; our discussion is meant only to be illustrative.

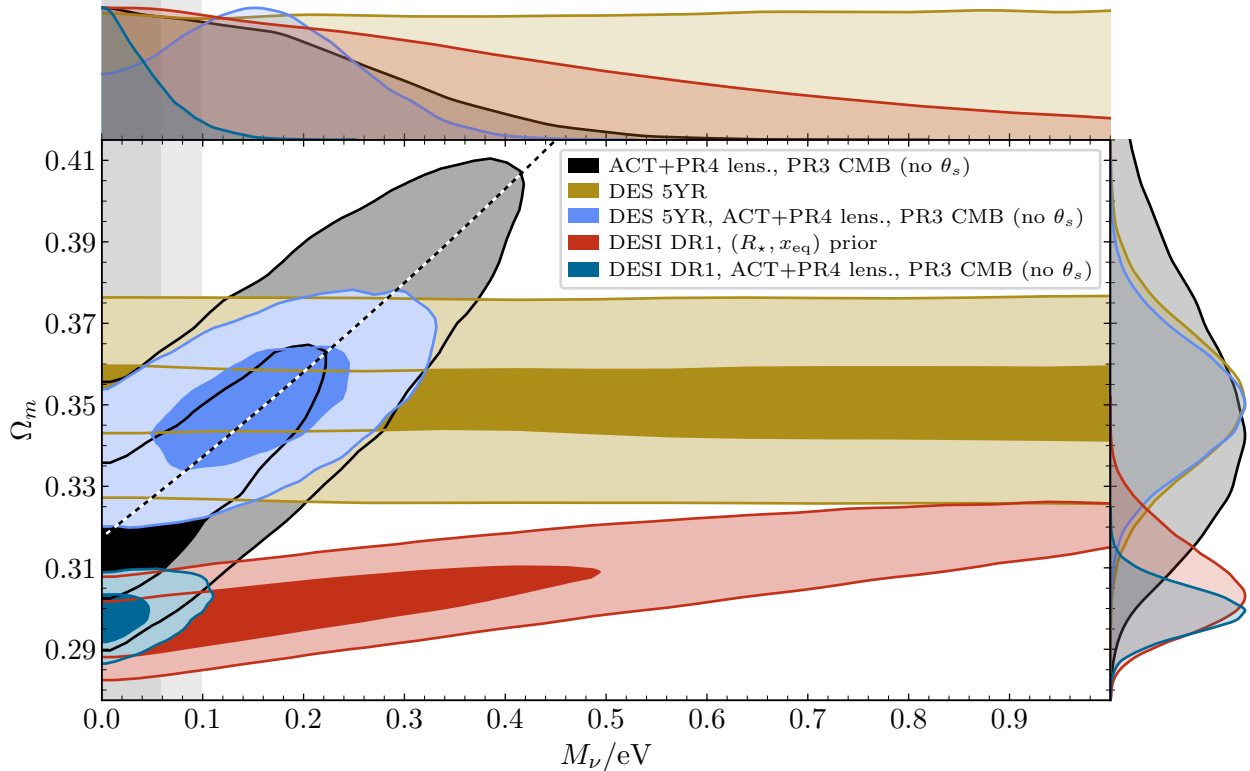


Figure 8. Posterior distribution over the neutrino mass sum M_ν and the matter fraction Ω_m , ACT + *Planck* PR4 lensing data [49, 105] (grey), DESI DR1 BAO data [39–41] (red), DES 5YR SNe data [36] (gold), and the lensing dataset combined with each of DESI (dark blue) and DES (light blue). Results that include lensing data impose a prior on all Λ CDM parameters except θ_s , deriving from the posterior using *Planck* PR3 CMB data [1, 2] (also marginalized over A_{smear}), while results that exclude *Planck* data instead include a prior on the baryon and CDM densities derived from *Planck* data (Sec. II A). The dashed black/white line indicates the parameter direction $\Omega_m \propto (1 + f_\nu)^8$ (chosen to match by eye the orientation of the posterior using only CMB and lensing data). Results are otherwise presented as in Fig. 4.

Λ CDM parameters and *Planck* temperature and polarization data (by computing the mean and covariance of a sample thereof) and marginalize over θ_s (i.e., by removing that dimension from the approximate posterior). While this procedure is rather *ad hoc*, it simply serves as a means to take *Planck*’s information on the shape of the CMB anisotropy spectra as a prior for CMB lensing likelihoods. To showcase the constraining power of CMB lensing maps in probing structure, we also marginalize the *Planck* posteriors over A_{smear} .

We take this posterior approximation as a “geometry-free” *Planck* prior over ω_b , ω_c , τ_{reio} , n_s , and A_s in combination with measurements of the CMB lensing power spectrum from ACT and *Planck* PR4 in Fig. 8. Without *Planck*’s geometric information to pin the dark energy density and fix the distance to last scattering, the matter fraction is only constrained with $\sim 5\%$ precision (at any particular value of M_ν , increasing to $\sim 9\%$ when marginalized). The suppression of structure by massive neutrinos can thus be partly compensated for by delaying the dark energy era, leading to a degeneracy direction $\Omega_m \propto (1 + f_\nu)^8$ or so. The posterior for lensing data alone falls off at a 95th percentile of $M_\nu \approx 0.4$ eV, at which point neutrinos suppress the amplitude of structure to an extent intolerable to the ACT+PR4 lensing dataset.

The step correlation between the neutrino mass sum and the matter fraction again poises low-redshift distances to contribute substantially to neutrino mass constraints. Figure 8 also displays the same posteriors using DESI DR1 BAO and DES 5YR SNe from Fig. 4 and the combination of

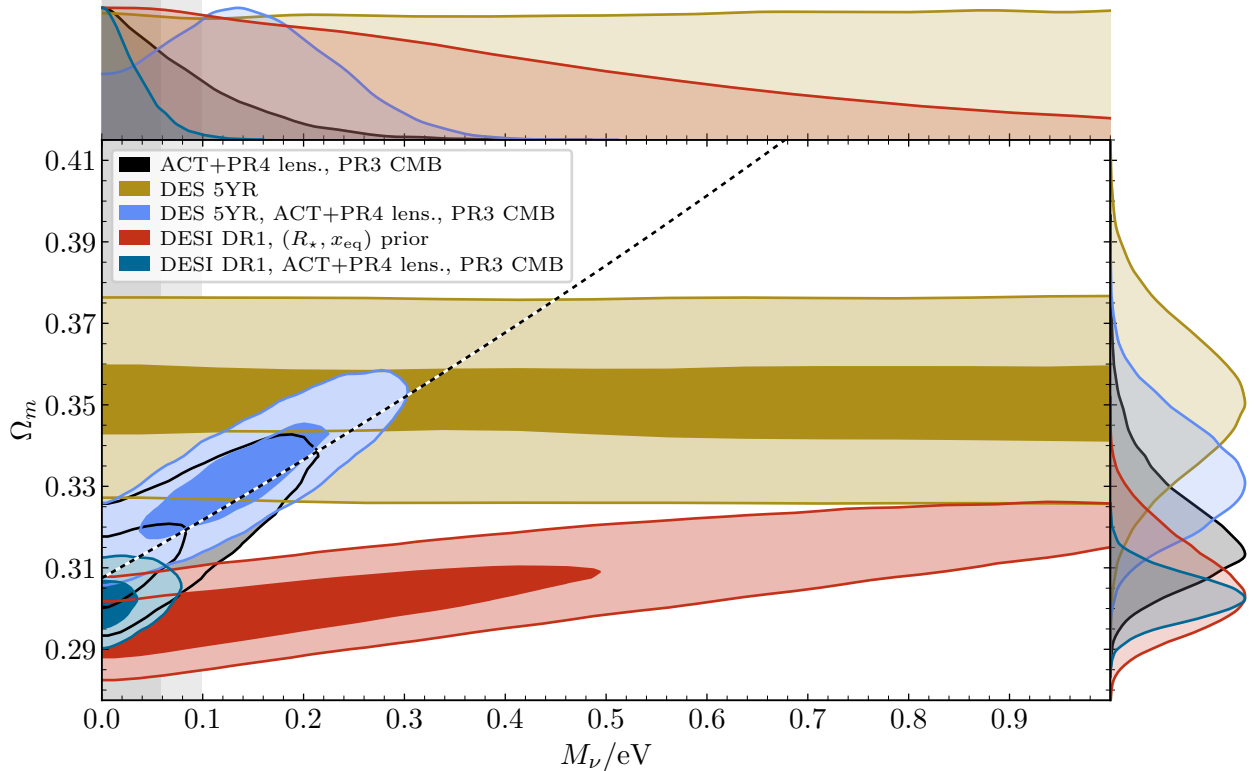


Figure 9. Constraints on flat Λ CDM cosmology with massive neutrinos using information from both geometry and structure, displaying posterior distributions over the neutrino mass sum M_ν and the matter fraction Ω_m using *Planck* PR3 CMB [1, 2] and ACT + *Planck* PR4 lensing data [49, 105] (grey), DESI DR1 BAO data [39–41] (red), DES 5YR SNe data [36] (gold), and the CMB and lensing datasets combined with each of DESI (dark blue) and DES (light blue). The dashed black/white line indicates the parameter direction $\Omega_m \propto (1 + f_\nu)^6$ (chosen to match by eye the orientation of the posteriors using only CMB and lensing data). Results are otherwise presented as in Figs. 4 and 8.

these data with ACT+PR4 lensing and the geometry-free *Planck* prior. Once again, the inconsistent geometric preferences of these two distance datasets yield strikingly different inference of neutrino masses—a tight upper limit from DESI compared to a marginal preference for $M_\nu \approx 0.15$ eV from DES SNe. The latter dataset requires so late an onset of dark-energy domination that massive neutrinos are in fact required to fit the amplitude of structure measured directly by the CMB lensing power spectrum. In contrast, DESI infers a matter fraction substantially lower than the CMB lensing dataset even without massive neutrinos; this apparent tension drives their combination to hardly allow for massive neutrinos at all.

2. Joint constraints

Having established that low-redshift distances also impact neutrino mass inference via the amplitude of structure, we now study constraints deriving jointly from low-redshift distances and CMB lensing data (as well as primary CMB data). Figure 9 displays the analog of Fig. 8 including the full *Planck* likelihoods (rather than artificially removing *Planck*'s geometric information). Clearly, DESI BAO and DES SNe's distinct preferences for Ω_m still lead to discrepant neutrino mass inference, even when consistently accounting for all of their effects. However, though both geometry and structure yield a positive correlation between the neutrino mass sum and the matter

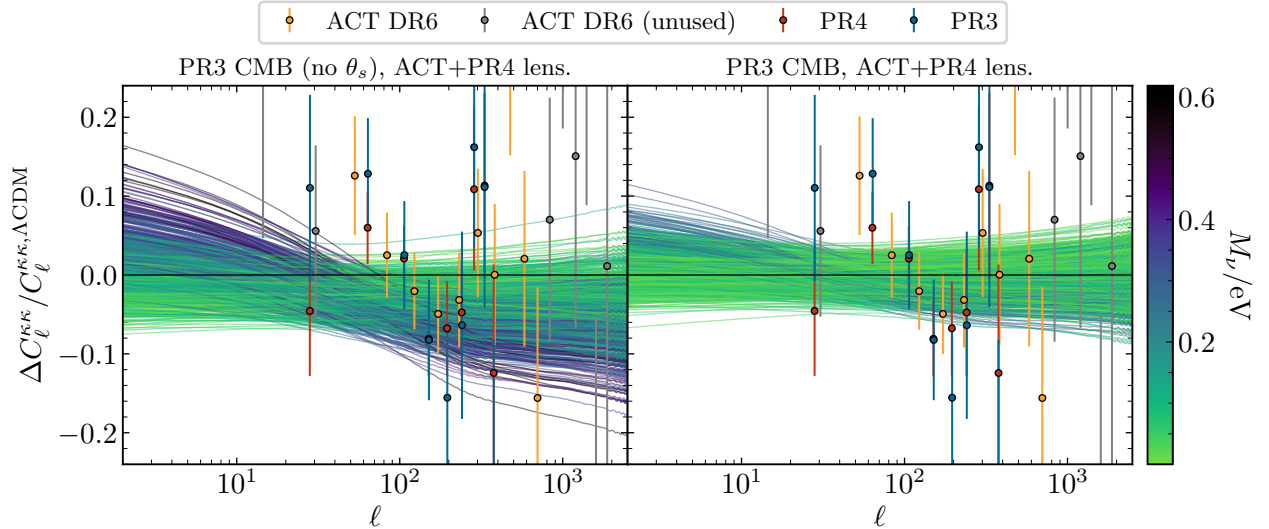


Figure 10. Residuals of the CMB lensing convergence relative to the Λ CDM best fit (using *Planck* PR3 CMB and ACT+PR4 lensing data) for samples from posteriors that use the full *Planck* likelihoods (right) and that artificially remove its geometric information (left), as described in Sec. III B 1. Note that the reference result includes no massive neutrinos. Curves are colored by their value of M_ν and data from various observations are also depicted as labeled in the legend; note that the data included for the posteriors depicted here are labeled ACT DR6 (yellow) and PR4 (red).

fraction, the degree to which these combinations disagree is less severe than when constraining geometry (Fig. 4) or structure (Fig. 8) separately. Neutrino mass bounds are also tighter for *Planck* CMB data combined with ACT+PR4 lensing without any low-redshift data, signaling that *Planck*'s geometric preferences alone prefer smaller matter fractions than CMB lensing data does by itself. Nevertheless, whereas the combination with DESI data yields posteriors that are largely incompatible with either mass hierarchy, the posterior using DES SNe data peaks not just at nonzero M_ν but at $M_\nu \approx 0.14$ eV, greater than the minimum mass for either hierarchy.

The apparent tension between structure and geometry evident in the comparison of the CMB-only posteriors in Figs. 4 and 8 could be interpreted as a manifestation of the lensing excess. Note however that Fig. 15 shows that marginalizing over the amplitude of lensing that smears the acoustic peaks (A_{smear}) only marginally weakens neutrino mass bounds. In particular, the direct reconstruction of the CMB lensing spectrum from ACT and *Planck* PR4 yields nearly identical posteriors, indicating that its information on late-time structure dominates that inferred from the smearing of the acoustic peaks. These results should therefore be robust to any systematic explanation for the lensing anomaly from *Planck*'s PR3 power spectra, but they still suggest that four-point reconstructions of CMB lensing prefer more structure growth than *Planck* data would otherwise predict. A preference for lensing amplitudes larger than predicted in Λ CDM also persists in the South Pole Telescope's newest reconstructed lensing spectrum [120].

To illustrate the impact of *Planck*'s geometric information on predictions for the CMB lensing spectra, Fig. 10 depicts residuals of posterior samples relative to the Λ CDM best-fit cosmology (with massless neutrinos only) for results using all CMB and CMB lensing data (as depicted in Fig. 9) and that with *Planck*'s geometric information artificially removed (Fig. 8). Figure 10 also superimposes CMB lensing measurements from various *Planck* and ACT datasets, also relative to the best-fit cosmology with massless neutrinos. Intriguingly, the data skew above this best-fit prediction at $\ell \lesssim 100$ and below at $100 \lesssim \ell \lesssim 300$ —a feature Fig. 2 suggests could possibly be accounted for by massive neutrinos, given the correlated increase in Ω_m (at fixed θ_s) that enhances structure

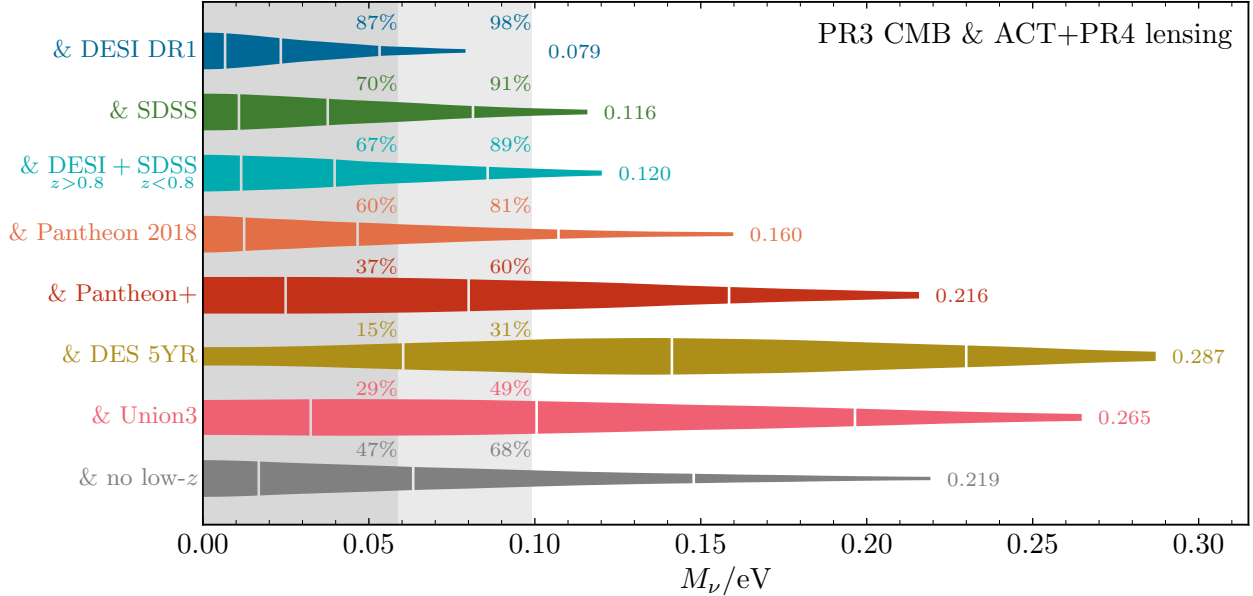


Figure 11. Marginal posterior distribution over the neutrino mass sum M_ν for *Planck* PR3 CMB [1, 2] and ACT+PR4 CMB lensing data [49, 105] combined with various BAO and uncalibrated SNe datasets as labeled. Results thus consistently derive from massive neutrinos’ effects on both geometry and structure (in contrast to Fig. 5, which effectively derives only from geometry). The shaded bands depict the range of masses that are incompatible with the normal and inverted hierarchies, and the fraction of each posteriors within these ranges [Eq. (3.1)] is annotated on the figure. Posteriors are truncated at the 95th percentile (whose value is also labeled); vertical white lines indicate the median and $\pm 1\sigma$ quantiles.

on large scales. This scale-dependent trend indeed appears to partially drive the geometry-free result in Fig. 10: the correlated increase of M_ν and Ω_m in Fig. 8 roughly fixes power at moderate scales (near $\ell \sim 100$) while enhancing it above the neutrino free-streaming scale and suppressing it below. When employing the full primary CMB likelihood, however, heavier neutrinos can only partially explain the shape of the data’s residuals because *Planck*’s geometric information (Fig. 4) requires smaller matter fractions at a given M_ν . Note that Λ CDM without massive neutrinos has no freedom to explain such scale-dependent features—samples of the model’s posterior, subjected to the same datasets, only yield residuals that are effectively flat across ℓ .

Given the close coincidence of ℓ_{fs} [Eq. (2.37), below which neutrino free-streaming imprints] and ℓ_{eq} [Eq. (2.36), the multipole at which the turnover in the transfer function imprints, per Sec. II C 1], it is unclear what this trend may be attributed to. Since primary CMB data is also strongly sensitive to ℓ_{eq} , it could arise due to an internal tension in the scale of matter-radiation equality preferred by each observable. On the other hand, neutrino free streaming provides a plausible explanation for such a mismatch. Regardless, Fig. 10 shows that standard cosmology with standard massive neutrinos cannot explain this feature in lensing data sufficiently well to actually detect nonzero neutrino masses. We comment on what hypothetical new physics could improve massive neutrino’s capacity to better improve upon Λ CDM’s fit to these data in Sec. IV C. Finally, we note that, because lensing data no longer systematically skew below the best-fit Λ CDM prediction at $\ell \gtrsim 300$, modeling of nonlinear structure growth (or neglecting it) has a nonnegligible impact on neutrino mass inference, a point elaborated on in Appendix C.

To close, in Fig. 11 we present final constraints on the neutrino mass sum deriving from the full *Planck* CMB and ACT+PR4 CMB lensing datasets when combined with the same set of low-redshift datasets displayed in Fig. 5. Beyond the near-incompatibility of DESI with massive neutrinos and

DES SNe’s measurement of $M_\nu/eV = 0.141^{+0.089}_{-0.081}$, Fig. 11 demonstrates again how varied neutrino mass bounds are between BAO and SNe datasets. The differences between these posteriors in M_ν correlate strongly to the dispersion in Ω_m measurements displayed in Fig. 1, corroborating the unique importance of late-time geometry to neutrino mass inference explained in Sec. II. Likewise, the influence of outliers in DESI’s DR1 data as identified in Sec. III A 3 carries over to analyses including structure as well as geometric information: the SDSS/DESI combination that excludes these outliers again yields a posterior nearly identical to that from SDSS alone. Finally, we note that the neutrino mass bounds originally derived from ACT’s DR6 lensing data included BAO data [48]; given the disparate inference among various late-time probes in Fig. 11, the results presented in this section that combine with *Planck*’s primary CMB data alone (and no late-time dataset) perhaps represent a more conservative bound on neutrino masses from CMB lensing as a probe of structure. Figure 15 in Appendix B 1 includes results derived from other CMB lensing datasets combined with *Planck*.

IV. DISCUSSION

In this section we discuss the broader implications of the discordance in neutrino mass inference established by Sec. III. We first comment on the discrepant inference of the low-redshift expansion history from distance datasets and other longer-standing dataset tensions in Sec. IV A. These tensions may well signal a need for extending standard cosmology, which we consider in Sec. IV B. Neutrino mass constraints in cosmologies with modified late-time dynamics are well studied, but new physics at early times yields qualitatively distinct possibilities that have received less attention [58]. Finally, the apparent incompatibility of DESI’s BAO data (combined with CMB data) with massive neutrinos has prompted consideration of new neutrino physics. In Sec. IV C we comment on the ramifications of our findings for interpreting evidence for nonminimal neutrino dynamics in current data.

A. Dataset tensions

The qualitatively distinct preferences for massive neutrinos between current BAO and SNe distance datasets underscores the growing tension in their inference of the Universe’s composition, even independent of its overall scale (i.e., of the Hubble tension). Within the flat Λ CDM model with massive neutrinos, both observables are individually consistent with the CMB’s geometric information, but in highly separated regions of parameter space (as evident in Fig. 3). The most recent BAO dataset from DESI, combined with CMB and CMB lensing data, is nominally almost completely incompatible with the inverted mass hierarchy and perhaps even the minimum mass sum required by either hierarchy. Figures 6 and 7, however, show that inference within Λ CDM using BAO data from DESI and SDSS is strongly influenced by data points that appear to be outliers compared to most other data within each survey—measurements that moreover are inconsistent with comparable ones from the other survey. Figure 6 (and extended discussion in Appendix B 2) indicates that all BAO measurements that could be interpreted as outliers turn out to drive constraints away from parameter space that is both consistent with SNe data and with massive neutrinos. Notably, the SDSS/DESI split at $z = 0.8$ described in Sec. III A 3, which excludes these outliers (and differs from the combined dataset considered in Ref. [39]) measures $\Omega_m = 0.320^{+0.016}_{-0.015}$ (see Fig. 1); the Gaussian tension of this combination with DES 5YR drops from 2.6 to 1.4 σ compared to DESI DR1 alone (and from 1.6 to 0.5 σ with Pantheon+).

The tension between SNe and BAO distances, regardless of their calibration, cannot be reconciled by massive neutrinos, nor by any modification of physics at early times. Understanding why direct

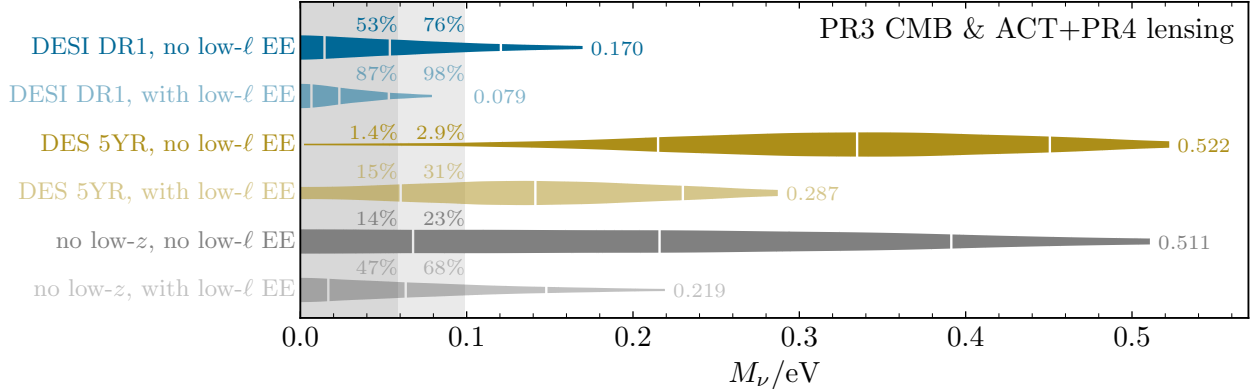


Figure 12. Impact of direct measurements from large-scale CMB polarization of the optical depth to reionization τ_{reio} on neutrino mass inference, displaying marginal posteriors over the neutrino mass sum M_ν for *Planck* PR3 CMB data [1, 2] combined with various BAO and SNe datasets as labeled either including (transparent) or excluding (opaque) *Planck*’s low- ℓ polarization data. The shaded bands depict the range of masses that are incompatible with the normal and inverted hierarchies, and the fraction of each posteriors within these ranges [Eq. (3.1)] is annotated on the figure. Posteriors are truncated at the 95th percentile (whose value is also labeled); vertical white lines indicate the median and $\pm 1\sigma$ quantiles.

probes of distances over a similar range of redshifts infer different matter fractions is thus of paramount importance to arbitrate between their respective implications for neutrino masses. (See Fig. 18 in Appendix B 2 for a comparison of transverse distance measurements from SNe and BAO surveys across redshift.) While recent combined analyses of these SNe, BAO, and CMB datasets suggest a preference for nonstandard dark energy [36, 39], it is unclear whether it is driven by genuine physical features evinced by individual datasets or simply by the model’s expanded freedom to superficially improve the consistency of BAO and SNe distances. Indeed, the preference for evolving dark energy is stronger the more the combined datasets are in tension (within Λ CDM).

Beyond dimensionless measures of geometry, the longer-standing tension between CMB- and distance-ladder-based inference of the Hubble constant is only worsened by massive neutrinos: the CMB’s geometric degeneracy requires $h \propto (1 + f_\nu)^{-2}$ [Eq. (2.21)], all else equal. Among attempts to resolve the tension with new early-time physics, modified recombination exhibits a unique interplay with massive neutrinos [58], which we discuss in Sec. IV B. The (milder) tension in the amplitude of structure, however, could more plausibly relate to massive neutrinos. References [121, 122] suggest that this tension may arise from mismodeling of nonlinear structure (to which weak galaxy lensing surveys are sensitive), i.e., if dynamical effects suppress structure to a greater degree than assumed. Sufficiently heavy neutrinos could provide a natural realization of this hypothesis.

The amplitude of structure inferred by the CMB, whether through lensing reconstruction or its impact on the power spectra, is inextricably tied to the optical depth to reionization; indeed the optical depth has long been recognized as a main source of uncertainty in neutrino mass constraints based purely on the growth of structure [12, 33]. Figure 10 suggests that CMB lensing data prefer a greater amplitude of structure than predicted by Λ CDM on length scales larger than the neutrino free-streaming scale and smaller than the nonlinear scale,²⁵ which could be explained if *Planck*’s measurement of τ_{reio} [1] were biased low. Namely, the small-scale anisotropies precisely measure the amplitude $A_s e^{-2\tau_{\text{reio}}}$, whereas late-time structure depends only on A_s . Inference of the lensing

²⁵ As mentioned previously, the lensing amplitude as inferred from the two-point statistics of the temperature and polarization spectra [1, 3] is even larger than that inferred from lensing spectra reconstructed via four-point statistics. The analysis of Fig. 15 in Appendix B 1, however, shows that current CMB lensing datasets yield independent neutrino mass constraints that are consistent with (if not more constraining than) that inferred from the smearing of the acoustic peaks alone, confirming their robustness to a possible lensing anomaly inferred from peak smearing [101].

amplitude parameter A_L different from unity could be explained if *Planck*'s measurement were biased by $\Delta\tau_{\text{reio}} = -(A_L - 1)/2$.

Figure 12 displays the impact of large-scale polarization data from *Planck*, which directly measure τ_{reio} , on neutrino mass inference. Excluding these data has a similar effect to marginalizing over the lensing amplitude A_L and illustrates the extent to which the lensing excess is alleviated in the absence of direct constraints on τ_{reio} via the resulting impact on neutrino mass inference. Large enough τ_{reio} does have directly observable impacts on other CMB data, which limits the extent to which the lensing excess could be explained by a biased inference of τ_{reio} from large-scale polarization data; without this data, *Planck* (combined with ACT+PR4 lensing data) measures $\tau_{\text{reio}} = 0.094 \pm 0.023$, nearly twice as large as the measurement $\tau_{\text{reio}} = 0.0542_{-0.0072}^{+0.0075}$ inferred in combination with low- ℓ polarization.²⁶ This difference of 0.04 is quite consistent with the preferences for $A_L \sim 1.08$ in most recent CMB dataset [120], but would amount to more than a 5σ offset from the measurement from *Planck*'s low- ℓ polarization data.

Figure 12 shows that neutrino mass bounds become substantially weaker without large-scale polarization data (by about a factor of two), no matter what low-redshift dataset is used. In particular, while the combination with DESI data still exhibits no preference for nonzero M_ν because of its geometric incompatibility with massive neutrinos, the combination with DES SNe instead demonstrates a detection thereof comparable to its pure-geometry measurement [Fig. 5]. Figure 12 thus illustrates the significant sensitivity of neutrino mass bounds deriving from CMB lensing to possible biases in the optical depth.

Finally, identifying the implications of individual datasets for the physical signatures of massive neutrinos (or lack thereof) requires a judicious combination of datasets and comparative analysis thereof, not simply combining as many as possible in the name of breaking degeneracies. The previous era of cosmological data may have only evinced a consistent cosmological model because of the granularity afforded by the data's precision; the choice of data is as much of an assumption in Bayesian analyses as the choice of a model and therefore necessitates scrutiny, even if only to recognize that parameter constraints may be artificially strong because of unexplained incompatibilities in the data. Determining whether joint parameter constraints derive from genuine physical predictions of a model is only possible through comparisons in the space of the data—that is, by comparing the posterior predictive distribution (not just a single best-fit prediction) to the data itself.²⁷ For instance, the analysis of Fig. 10 reveals that current CMB lensing data *do* exhibit trends that evoke the scale-dependent suppression characteristic to massive neutrinos; that the posterior predictive distribution does not reproduce these features may suggest some degree of model tension (whether or not it is a genuine signal of massive neutrinos), as discussed in Sec. III B 2.

B. Implications for cosmology

Because the observable signatures of massive neutrinos are (individually) largely degenerate with other cosmological parameters, inference of their masses is sensitive to modifications to the baseline cosmological model. Nonminimal physics relevant at late times—e.g., nonzero spatial curvature or dark energy beyond a cosmological constant—introduces additional freedom that in principle relaxes the close relationship between massive neutrinos and the matter fraction, both geometrically and within the growth of structure. Such scenarios have been studied extensively [106, 123–129]. We leave a comparison of geometry- and growth-of-structure-based constraints on neutrinos (and the individual role of current datasets) in modified late-time cosmologies to future work.

²⁶ The lensing anomaly has a nonnegligible effect on the latter measurement—the full set of *Planck* CMB data excluding lensing and marginalized over A_{smear} yields $\tau_{\text{reio}} = 0.0486_{-0.0080}^{+0.0077}$.

²⁷ A possible exception is models of sufficiently low dimensionality whose predictions are fully encoded by an easy-to-visualize parameter space—e.g., the two-dimensional plane $(r_d\sqrt{\omega_m}, \Omega_m)$ that fully specifies the flat- Λ CDM predictions for the BAO scale (and the CMB's geometric information), as displayed in Figs. 3, 6, 7, and 17.

The implications of modified early-time physics, on the other hand, are qualitatively different because such scenarios can alter the CMB’s calibration of both the sound horizon and the density of early-time matter (that in baryons and CDM) [58]. To study the cosmology dependence of neutrino mass inference more generally, rewrite Eq. (3.2) in terms of $\omega_b + \omega_c = \omega_r/a_*x_{\text{eq}}$ [see Eq. (2.6)] and $\omega_m r_{s,*}^2$,²⁸ and express $r_{s,*} \equiv a_*/(\sqrt{\omega_r}H_{100}/c) \cdot F_{r_s}(R_*, x_{\text{eq}})$ [see Eq. (2.7)]:

$$M_\nu = \frac{3H_{100}^2 M_{\text{pl}}^2}{n_\nu} \frac{\omega_r}{a_* x_{\text{eq}}} \left(\frac{\omega_m r_{s,*}^2}{a_*} \frac{(H_{100}/c)^2}{F_{r_s}(R_*, x_{\text{eq}})^2/x_{\text{eq}}} - 1 \right). \quad (4.1)$$

The neutrino mass sum is thus inferred via three factors encoding the number density of neutrinos n_ν contributing to their net density ω_ν , the overall density of matter components present during recombination, and the relative increase in the matter abundance afterward. The neutrino number density is largely fixed within the SM and is also probed via their contribution to the relativistic energy density at early times; we comment on physics that modify this prediction in Sec. IV C. The density in radiation (or equivalently N_{eff}) at early times could also be increased by modifying the physics of neutrino decoupling, but such effects would presumably also impact their number density; a simpler possibility is that new, light degrees of freedom increase the radiation density [130]. These scenarios are strongly constrained by CMB anisotropies on small scales via their effect on diffusion damping [1]. Early recombination—mechanized for instance by supposing the electron mass varies in time [131, 132]—also increases this factor, since fixing x_{eq} requires increasing density of baryons and CDM (so that matter-radiation equality occurs at the same moment relative to recombination).

The final factor in Eq. (4.1) shows that, at fixed $\omega_m r_{s,*}^2$, early recombination incurs an additional increase in M_ν not present when varying N_{eff} . What distinguishes early-recombination and extra-radiation scenarios in this term is that, at fixed θ_s , varying the radiation density itself does not traverse the CMB’s geometric degeneracy, Eqs. (2.17) and (2.20).²⁹ As shown in Ref. [58] (and reviewed in Sec. II B), varying the electron mass and the neutrino mass sum (or, more generally, the ratio of the late- and early-time matter abundances) and other Λ CDM parameters yields a novel geometric degeneracy.³⁰ Namely, proportional increases of the Hubble constant h , the neutrino fraction $1 + f_\nu$, $1/a_*$, ω_b , and ω_c leave BAO distances and the primary CMB anisotropies invariant—that is, the matter fraction, the product hr_d or $r_d\sqrt{\omega_m}$, θ_s , R_* , and x_{eq} all remain unchanged. This degeneracy is notable in contrast to Λ CDM, in which neutrino masses and h are anticorrelated at fixed θ_s .

The potential of early recombination with massive neutrinos to solve the Hubble tension, however, is ultimately limited by the impact of neutrino free-streaming on the growth of structure allowed by *Planck* (i.e., via secondary effects at late times) [58]. Following the discussion in Sec. II C 2, the angular scale of the horizon at matter-radiation equality [Eq. (2.36)] is unchanged along the degeneracy. The neutrino free-streaming scale [Eq. (2.30)], on the other hand, scales with $M_\nu\sqrt{\omega_m} \propto M_\nu/r_d$, meaning $\ell_{\text{fs}} \propto M_\nu\chi_*/r_d \propto M_\nu/\theta_{\text{CMB},\perp}(a_d)$ scales simply with M_ν . The neutrino mass sum increases superlinearly with $1/a_*$ [Eq. (4.1)], however, and the redshift at which they become nonrelativistic is unchanged, so their suppression of structure increases relatively rapidly along the degeneracy.

Reference [58] studied this scenario in detail in application to a hyperlight scalar field (in this case postulated to mechanize the time variation of fundamental constants) and showed that the

²⁸ We write Eq. (4.1) in terms of the sound horizon at photon rather than baryon decoupling for simplicity, which makes no material difference because a_*/a_d and $r_{s,*}/r_d$ are precisely measured and insensitive to modified physics [77, see also Appendix A].

²⁹ The partitioning of the energy density in this case is unchanged because fixing x_{eq} requires $\omega_b + \omega_c \propto \omega_r$, i.e., leaves $(\omega_b + \omega_c)r_d^2$ invariant; the same matter fraction is then required to fix θ_s [Eq. (2.19)]. The geometric degeneracy between Ω_m and $1 + f_\nu$, however, holds regardless of the overall density of the Universe.

³⁰ Varying the present-day CMB temperature T_0 [133] (i.e., ignoring precise measurements thereof [134, 135]) also mechanizes early recombination (or rather, “late present”), but with different consequences for the present-day matter density and neutrino number density. Both n_ν and $\omega_b + \omega_c$ drop with T_0^3 simply due to redshifting; larger M_ν are thus enabled only via the third factor in Eq. (4.1), which varies even while compensatory changes to a_* and $1 + f_\nu$ keep the matter fraction fixed.

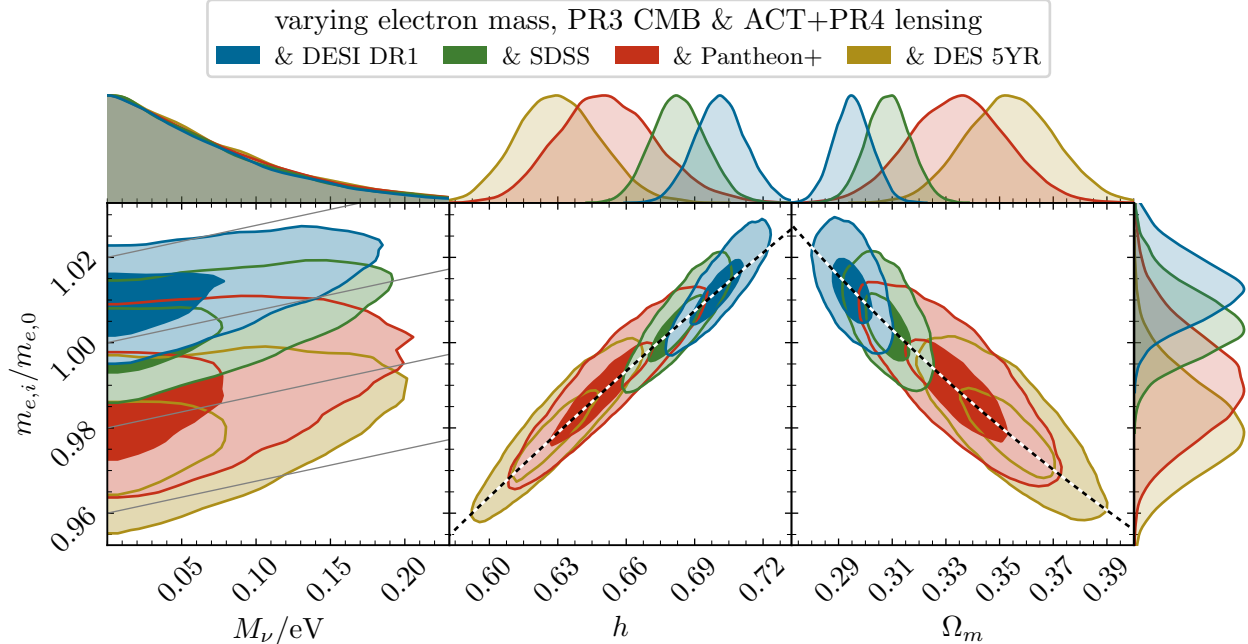


Figure 13. Constraints on early-recombination cosmologies via a varying electron mass including massive neutrinos, displaying joint posteriors over the early-time electron mass $m_{e,i}$ with the neutrino mass sum M_ν , the Hubble constant h , and the matter fraction Ω_m (presented as in Fig. 4). All results use *Planck* PR3 CMB [1, 2] and ACT + *Planck* PR4 lensing data [49, 105], combined with either BAO data from DESI DR1 (blue) or SDSS [44–47] (green) or uncalibrated SNe data from Pantheon+ [34, 35] (red) or DES [36] (gold). Dashed black/white lines indicate the parameter directions $h \propto m_{e,i}^{3.16}$ and $\Omega_m \propto m_{e,i}^{-5.32}$ expected from the CMB’s geometric degeneracy at fixed neutrino fraction [Eqs. (2.20) and (2.21)]. The grey lines in the leftmost panel lie along $m_{e,i} \propto 1 + f_\nu$, the degeneracy between early recombination and late dark matter presented by Ref. [58] that would fix Ω_m [see Eq. (2.20)]. For these results (and any of the other low-redshift datasets presented in Fig. 11), the marginal posteriors over M_ν all have 95th percentiles at ≈ 0.2 eV, and about 50% and 75% of the posteriors are incompatible with the normal and inverted hierarchies, respectively.

results are qualitatively similar with massive neutrinos instead. The resulting posteriors, displayed in Fig. 13 for the latter case, therefore predominantly exhibit the degeneracy $h \propto a_\star^{-3.16}$ evident in Eq. (2.21) at fixed neutrino fraction. Moreover, the matter fraction is as sensitive to the scale factor of recombination as to neutrino masses [Eq. (2.20)], making parameter inference thereof just as sensitive to the geometric tensions in low-redshift distance datasets [58]. Despite the discordance in preferred low-redshift expansion histories, bounds on the neutrino mass sum are robust across dataset combinations. The geometric degeneracy between a_\star and the neutrino fraction is still at play, as evident in Fig. 13—just not to an extent that qualitatively alters the marginal posteriors over other parameters. The scenario effectively marginalizes out geometric sensitivity to neutrino masses by adjusting a_\star as needed to match a given dataset’s preferred Ω_m ; in analogy to the A_{smear} -marginalized results of Figs. 4 and 5, the posteriors in Fig. 13 over M_ν effectively derive only from the impact of neutrinos on the growth of structure (as constrained by *Planck* CMB data and the ACT+PR4 lensing dataset).³¹

While the treatment of Ref. [58] (and Sec. IIB) applies to a number of extended cosmologies (namely, those whose additional free parameters are nominally fixed by SM predictions, like the fundamental constants and N_{eff}), it does not precisely capture cases that introduce new degrees of freedom featuring qualitatively distinct dynamics. One such example is early dark energy [136, 137].

³¹ Marginalizing over lensing amplitude parameters (A_L or A_{smear}) as well therefore completely relaxes constraints on neutrino masses, up to the point that they become nonrelativistic during recombination (Sec. IIC3).

The parameter relations found in models with extra radiation, however, may extend to this case to the extent that its effects on the background cosmology reduce to an increase in the density at recombination. Indeed, Ref. [138] found that varying the neutrino masses had little impact on the preferred parameter space for axionlike early dark energy (and vice versa). Early recombination thus appears unique in its consequences for massive neutrinos (a finding observed but not explained in Ref. [139]).

C. Implications for neutrino physics

Establishing whether cosmological data truly call for new physics ultimately requires testing concrete models—not just to ensure analyses capture the full set of predicted physical effects, but also to place results in the context of theoretical priors and external constraints. In this paper we treat neutrinos consistently within the predictions of the Standard Model, in which they both contribute to the matter density and also resist gravitational clustering. A number of recent articles, on the other hand, explored the putative preference for “negative” neutrino mass deriving from DESI data, taking alternative approaches that seek to emulate different new-physics scenarios. For example, Refs. [100, 101] did so solely via the A_L parameter (i.e., by attributing a rescaling of the lensing spectrum to neutrino masses, positive or negative); this analysis, however, neglects the contribution of neutrinos to the matter density in the cosmological background, which our results show is critical to both geometry and structure. Namely, neglecting the neutrino’s background effect overestimates their net impact on structure because they also require substantially larger matter fractions (at fixed θ_s). The identified preference for $A_L > 1$ bears no impact on DESI’s geometric incompatibility with massive neutrinos (as illustrated by Figs. 3 and 4), though it may mimic the outcome of a scenario in which new physics solely affects the growth of structure. Of course, the preference for excess lensing in CMB data has long been appreciated [1, 3, 140]; the only substantive difference made by recent data is DESI’s nominally stronger preference for even lower matter fractions than *Planck* would itself prefer.

Reference [100] also surveys a number of new-physics scenarios that might modify the dynamics of neutrinos and their inferred masses as a result. In one category, the neutrino abundance is depleted via decays or annihilations into radiation after recombination but before neutrinos would become nonrelativistic; while the possibility would remove the prolonged period over which standard neutrinos suppress structure growth, it would also eliminate their impact on the cosmological background. The late-time matter density would then be just that from baryons and CDM; to the extent that the expansion history reproduces that in Λ CDM with massless neutrinos, the matter fraction inferred from the CMB’s geometric information would then agree with that measured directly via BAO or SNe distances. Models with time-varying neutrino masses could yield similar phenomenology, although the scalar field responsible for the variations would have its own gravitational effects [58].

Another category attempts to modify the scale on which neutrinos freely stream, e.g., by reducing their phase-space-averaged momentum after recombination [to reduce c_{ν_i} in Eq. (2.30)] without affecting their number density. In this case, geometry would play a larger role in neutrino mass inference as discussed in Secs. II B and III A; Fig. 5 suggests that such neutrinos could still have masses compatible with either hierarchy or that mass sums $M_\nu \sim 0.3$ to 0.5 eV would be preferred, depending on the low-redshift distance dataset. Mechanizing a smaller free-streaming scale, moreover could also enable massive neutrinos to better fit features in current CMB lensing data that Λ CDM cannot explain (see Fig. 10 and surrounding discussion). Finally, Ref. [100] considered modified physics outside of the neutrino sector that could explain the lensing excess, which would also leave neutrino masses to be probed via geometry. One example—new long-range forces between

dark matter particles—would again entail additional dynamics from the mediator; Refs. [141–143], however, show that this scenario does not ultimately affect the amplitude of structure due to an effective cancellation between the clustering rate and the modified redshifting of dark matter.

Other authors extrapolated to negative masses by simply fitting a normal distribution to posteriors inferred using the physical prior that $M_\nu > 0$ [44, 102, 103] or extrapolated at the level of the theoretical model by subtracting the residual of a positive- M_ν cosmology relative to that with $M_\nu = 0$ [104]. We emphasize that a posterior peaked at the boundary of a parameter’s prior is entirely expected if a given dataset is unable to resolve the impact of its deviation from that boundary (i.e., if the true value of the parameter is close to the boundary compared to the spread of the posterior). For example, posterior distributions for the tensor-to-scalar ratio r from current data take the same form for the same reason: both M_ν and r are nonnegative *a priori* on grounds of theoretical consistency (the latter because an autopower spectrum cannot be negative). The more curious feature of neutrino mass constraints that include BAO data is not that their marginal posteriors appear as if they would peak at unphysical, negative values, but rather that they peak below the minimum mass sum for either hierarchy and with substantially higher density than at $M_{\nu\text{min}}$. (Figure 11 demonstrates that this feature is not universal across dataset combinations, however, since it derives from offsets in Ω_m measurements.) Assessing whether such a distribution indicates a systematic inconsistency or tension within the data or calls for a different physical model requires both testing viable candidate models and carefully examining what in the data drives such preferences.

V. CONCLUSIONS

Cosmological observations definitively confirm the role of relativistic neutrinos predicted by the Standard Model. The current interpretation of cosmological evidence for or against their masses, however, is nebulous, if not entirely inconsistent. The signatures of massive neutrinos in both the Universe’s geometry and its large-scale structure are partially degenerate with the composition of the Universe at late times, positioning direct probes of the late-time expansion history as crucial in pinpointing the neutrino mass scale. By carefully considering what relevant quantities are actually constrained by observations—in particular, the angular extent of the photon-baryon sound horizon θ_s , and therefore the comoving distance to last scattering in standard cosmology—we showed that heavier neutrinos imply an increase in the present-day *fraction* of energy in all matter (Ω_m) that is five times the neutrino’s relative contribution to the matter *density*. In other words, the well-known geometric degeneracy between the neutrino mass sum and the Hubble constant entails a surprisingly large modification to the composition of the Universe.

Dimensionless quantifiers such as Ω_m are not just those that directly control the late-time growth of structure (independent of neutrinos’ resistance to clustering) but are also what low-redshift distance datasets directly measure, even without calibration. Geometric probes, moreover, are immune to the physical effects that challenge the detection of neutrinos’ suppression of large-scale structure growth (e.g., the optical depth τ_{reio} , which is difficult to measure independently with sufficient precision) [12]. Section II shows that indeed, contrary to common thought, measurements of the matter fraction via cosmological distances are more sensitive to neutrino masses than equally precise measurements of the amplitude of structure below the free-streaming scale via CMB lensing.

The same opportunity afforded by geometric probes to inform neutrino mass measurements also presents a vulnerability to unknown systematics and inconsistencies between datasets. A growing number of cosmological observations yield inconsistent parameter inference within the standard cosmological model; we showed that the strikingly discrepant preferences in late-time geometries (i.e., matter fractions Ω_m) between the most recent BAO and (uncalibrated) SNe datasets beget a

starkly divergent compatibility with massive neutrinos, both on purely geometric grounds (Fig. 5) and in combination with observations of structure (Fig. 11). Resolving this geometric tension, even independently of the tension in calibration (i.e., H_0), is thus paramount to place robust constraints on all of massive neutrinos’ cosmological effects. Ultimately, a genuine measurement of neutrino masses from CMB data and low-redshift distances derives from concordant inference of their independent effects on geometry and structure in the Ω_m - M_ν plane—only their combination can break their respective degeneracies $\Omega_m \propto (1 + f_\nu)^5$ (Fig. 4, deriving from θ_s) and $\Omega_m \propto (1 + f_\nu)^8$ (Fig. 8, independent of θ_s).

Because posteriors over the neutrino mass sum from numerous contemporary datasets peak near the lower boundary of the prior ($M_\nu = 0$), upper limits on M_ν —measures of the tail of its one-sided distribution—can be exponentially sensitive even to small shifts in central values from data, whatever their origin. In Sec. III A 3, we identified two individual data points among DESI’s measurements that strongly influence its apparent preference for “negative neutrino mass” and its discrepancy with SNe datasets. The thorough analyses of systematics and robustness in Refs. [40, 41, 119] make it challenging to interpret the impact of these measurements and their inconsistency with those made previously by SDSS. Nevertheless, when a small subset of the data drive strong conclusions about models, a Bayesian must weigh the possibility of statistical effects (as discussed in Sec. III A 3) and unknown systematics (which are more challenging to naïvely quantify) against their theoretical prior. Neutrinos are indisputably massive today, though their mass mechanism is yet unknown; the theoretical plausibility and cosmological viability of nonminimal neutrino physics can only be fairly assessed in the context of concrete microphysical models with a consistent implementation of their predicted phenomenology. Of course, too strong a prior defeats the purpose of taking data in the first place, but open mindedness to hints of new physics must be tempered by careful scrutiny of the data that might drive them. In Sec. IV B we studied the impact of modified early-Universe physics on neutrino mass inference, of which early recombination provides a particularly intriguing example (see also Ref. [58]). We leave dedicated analyses of possible nonminimal neutrino physics, like those commented upon in Sec. IV C, to future work.

Our findings likely generalize to other scenarios featuring light relics [130], whether hyperlight scalars [58, 144–148] or thermal relics like hot axions [149–153], since such scenarios can also increase the matter abundance after recombination and entail qualitatively similar effects on structure growth. Trends in recent data also motivate revisiting the growth versus geometry analyses of Refs. [154–160]. The implications of modified late-time cosmologies (such as evolving dark energy) for neutrino mass inference may well also be sensitive to the choice of low-redshift dataset (if studied individually rather than combined).

Despite the contemporary ambiguity in their implications, the advantage of geometric probes is that they more or less directly measure the late-time expansion history. Future data with increased sample size and redshift coverage, like BAO data from Euclid [19, 161], Roman [162], and subsequent DESI releases [163] and SNe data from the Zwicky Transient Facility [164] and the Vera Rubin Observatory [165], can definitively test the significance of the trends in current data. These datasets themselves provide the means to constrain late-time expansion histories beyond Λ CDM that can confound neutrino mass inference from both geometry and structure. Moreover, it is fortuitous to have multiple independent methods of measuring late-time geometry in the first place. An abundance of future surveys will also probe the suppression of structure characteristic to neutrinos, including not just DESI, Euclid, Roman, and Rubin but also CMB-S4 [12] and Simons Observatory [13]. Synergy—and concordance—between these distinct observables will ultimately be imperative to conclusively measure the neutrino mass scale with cosmological data.

ACKNOWLEDGMENTS

We thank Masha Baryakhtar, Stephen Chen, Marco Costa, Jessie Muir, Caio Nascimento, Murali Saravanan, and Olivier Simon for helpful discussions. M.L. and Z.J.W. are supported by the Department of Physics and College of Arts and Science at the University of Washington and the Dr. Ann Nelson Endowed Professorship. M.L. is also supported by the Department of Energy grants DE-SC0023183 and DE-SC0011637. M.L. is grateful for the hospitality of Perimeter Institute where part of this work was carried out. Research at Perimeter Institute is supported in part by the Government of Canada through the Department of Innovation, Science and Economic Development and by the Province of Ontario through the Ministry of Colleges and Universities. This research was also supported in part by the Simons Foundation through the Simons Foundation Emmy Noether Fellows Program at Perimeter Institute. This work made use of the software packages `emcee` [112–114], `corner.py` [166], `NumPy` [167], `SciPy` [168], `matplotlib` [169], `xarray` [170], `ArviZ` [171], `SymPy` [172], and `CMasher` [173].

Appendix A: Transverse BAO scale from CMB analyses

In this appendix we describe the construction of likelihoods for the CMB-derived transverse BAO scale, $\theta_{\text{CMB},\perp}(a_d)$, used in Sec. III A. The angular scale θ_s measured by the CMB is the transverse BAO scale, except that it measures the sound horizon when photons decoupled rather than when baryons decoupled (i.e., because it quantifies the angular correlation of the photon distribution). The two epochs are separated by a rather narrow interval of expansion, $a_\star/a_d \approx 1.0268 \pm 6 \times 10^{-4}$, that is determined by the baryon-to-photon ratio R_\star (i.e., the ratio of their number densities), which itself is well constrained by the shape of the acoustic peaks (Sec. II A). As such, θ_s and $\theta_{\text{CMB},\perp}(a_d)$ are closely related [77]—namely, $\theta_{\text{CMB},\perp}(a_d)$ should be a derived quantity as model independent as θ_s itself. Phrasing the CMB’s geometric information in terms of $\theta_{\text{CMB},\perp}(a_d)$ enables a direct comparison to BAO measurements without assumptions on the magnitude of the sound/drag horizon, i.e., in the common parameter space $(r_d\sqrt{\omega_m}, \Omega_m)$.

Reference [77] inferred geometric constraints on hr_d and Ω_m from CMB experiments by marginalizing over the uncertainty in a_\star/a_d and $r_{s,d} - r_{s,\star}$ to translate a measurement of θ_s to one of $\theta_{\text{CMB},\perp}(a_d)$. We take an approach that is more direct and precise by simply calculating $\theta_{\text{CMB},\perp}(a_d)$ itself from posterior samples. The posterior over θ_d deriving from *Planck* PR3 data (excluding lensing and marginalizing over M_ν and A_{smeas}) is well approximated by

$$100\theta_{\text{CMB},\perp}(a_d) \sim \mathcal{N}(1.06061, 4.2 \times 10^{-4}), \quad (\text{A1})$$

where $\mathcal{N}(\mu, \sigma)$ denotes a normal distribution with mean μ and standard deviation σ . For comparison, $100\theta_s \sim \mathcal{N}(1.04198, 3.1 \times 10^{-4})$ from the same posterior, a measurement only marginally more precise.

To demonstrate the robustness of Eq. (A1) to early-Universe physics, Appendix A tabulates results for a number of additional models and dataset combinations. Notably, the measurement is identical in Λ CDM and cosmologies that vary the electron mass; since early recombination by varying the electron mass (or the present-day CMB temperature [133]) is the only (known) model that completely opens a geometric degeneracy in the distance to last scattering without modifying the flat Λ CDM model at late times, this finding corroborates the robustness of the angular drag scale even if the absolute length scale is substantially different from the Λ CDM prediction. The result is also robust to varying the neutrino mass sum, A_{smeas} , or both. As another test, the precision of Eq. (A1) degrades to the same degree as the measurement of θ_s itself does (by a factor of 3) when varying both N_{eff} and the helium yield Y_{He} . In this case, the free-streaming fraction

μ	$10^3\sigma$	additional parameters	data
1.06081	0.39		<i>Planck</i> PR3
1.06077	0.38		<i>Planck</i> PR3 (with lensing)
1.06051	0.42	A_{smear}	<i>Planck</i> PR3
1.06083	0.39	M_ν	<i>Planck</i> PR3
1.06080	0.40	M_ν	<i>Planck</i> PR3 (with lensing)
1.06061	0.42	M_ν, A_{smear}	<i>Planck</i> PR3
1.06090	0.39	$m_{e,i}$	<i>Planck</i> PR3 (with lensing)
1.06167	1.2	$N_{\text{eff}}, Y_{\text{He}}$	<i>Planck</i> PR3 (with lensing)

Table I. Mean and standard deviation of $100\theta_{\text{CMB},\perp}(a_d)$ inferred from Λ CDM and a number of extensions (whose additional free parameters are enumerated), including *Planck* PR3 CMB data and PR3 lensing data where indicated.

varies, which induces a phase shift in the acoustic peaks [56, 57], while the helium yield is free to compensate for the effect of additional radiation on the damping tail. In spite of this, the mean $\theta_{\text{CMB},\perp}(a_d)$ hardly moves, and permille precision is still superior by an order of magnitude to any single BAO measurement.

The precise redshift of baryon drag (or of peak photon visibility, for that matter) is constrained with high (but not infinite) precision by *Planck* data (in cosmologies that do *not* vary the fundamental constants). For the same posterior from which Eq. (A1) is derived, $1 + z_d \approx 1061.13 \pm 0.33$ (similar precision to that for z_*). Because decoupling occurs so early, the relative uncertainty propagated to the comoving distance $\chi(a_d)$ is $\lesssim 10^{-4}$ —small compared to the precision of Eq. (A1). Decoupling occurs so early, however, that the impact of radiation on expansion leads to $\sim 0.5\%$ corrections to $F_M(a_*, a_{m-\Lambda})$ evaluated with Eq. (2.11). The comoving distance in a Universe with radiation as well as matter and cosmological constant does, however, have an analytic form in terms of elliptic integrals [174] which are often available as special functions in numerical software. These functions provide an efficient means to calculate $\theta_{\text{CMB},\perp}(a_d)/r_d\sqrt{\omega_m}$, and simply evaluating the comoving distance at fixed $a_d = 1/1061.1$ provides sufficient precision for measurements as precise as Eq. (A1).

Appendix B: Supplementary results

1. Constraints on structure from lensing reconstruction and peak smearing

Figure 14 displays posterior distributions over the neutrino mass sum M_ν analogous to Figs. 5 and 11 for additional analysis variants. In particular, Fig. 14 includes results combining various low-redshift distance datasets with *Planck* CMB data alone, combined with ACT+PR4 lensing data (the same results as Fig. 11), and combined with the same lensing data but marginalized over A_{smear} . These results thus compare the amount of information added by the ACT+PR4 reconstructed lensing map both with and without the influence of *Planck*'s own inference of lensing via its temperature and polarization power spectra.

Figure 15 again displays posteriors over M_ν deriving from *Planck* CMB data, various lensing datasets, and either no low-redshift distances, DESI's BAO data, or DES's SNe data. Each panel compares results marginalized or not over A_{smear} as a test of the sensitivity of M_ν bounds to the *Planck* lensing anomaly. Figure 15 includes results using not just the ACT+PR4 lensing dataset but also an extended variant thereof (including multipoles up to 1250) as well as the *Planck* lensing data from 2018 (i.e., PR3). Comparing pairs that do and do not marginalize over A_{smear} shows that the information content in PR3 temperature and polarization power spectra only marginally tightens neutrino mass bounds from PR3 lensing data and has an even more negligible effect on

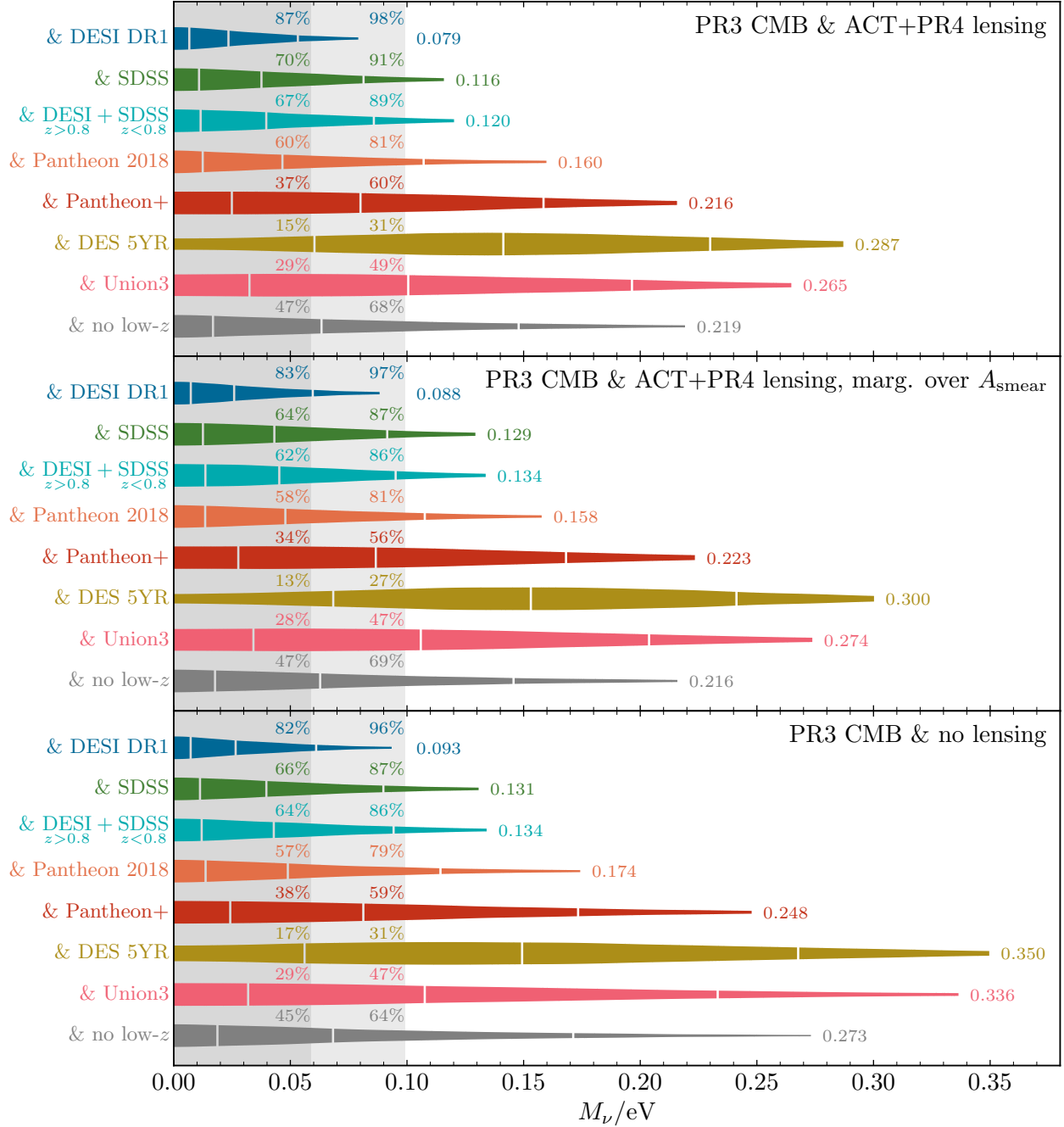


Figure 14. Marginal posterior distribution over the neutrino mass sum M_ν for *Planck* PR3 CMB combined with various BAO and uncalibrated SNe datasets (by color) and no lensing data (bottom panel) and ACT+PR4 lensing data excluding (top) and including (middle) the parameter A_{smear} . The shaded bands depict the range of masses that are incompatible with the normal and inverted hierarchies, and the fraction of each posterior within these ranges [Eq. (3.1)] is annotated on the figure. Posteriors are truncated at the 95th percentile (whose value is also labeled); vertical white lines indicate the median and $\pm 1\sigma$ quantiles.

inferences using ACT DR6 + *Planck* PR4 lensing; neutrino mass constraints from LSS are thus largely robust to any potential systematic lensing anomaly in *Planck*'s primary CMB data. In addition, comparing to results with no lensing dataset (grey) shows that the peak-smearing effect by itself yields similar constraints to the PR3 lensing reconstruction. Figure 15 also shows that this

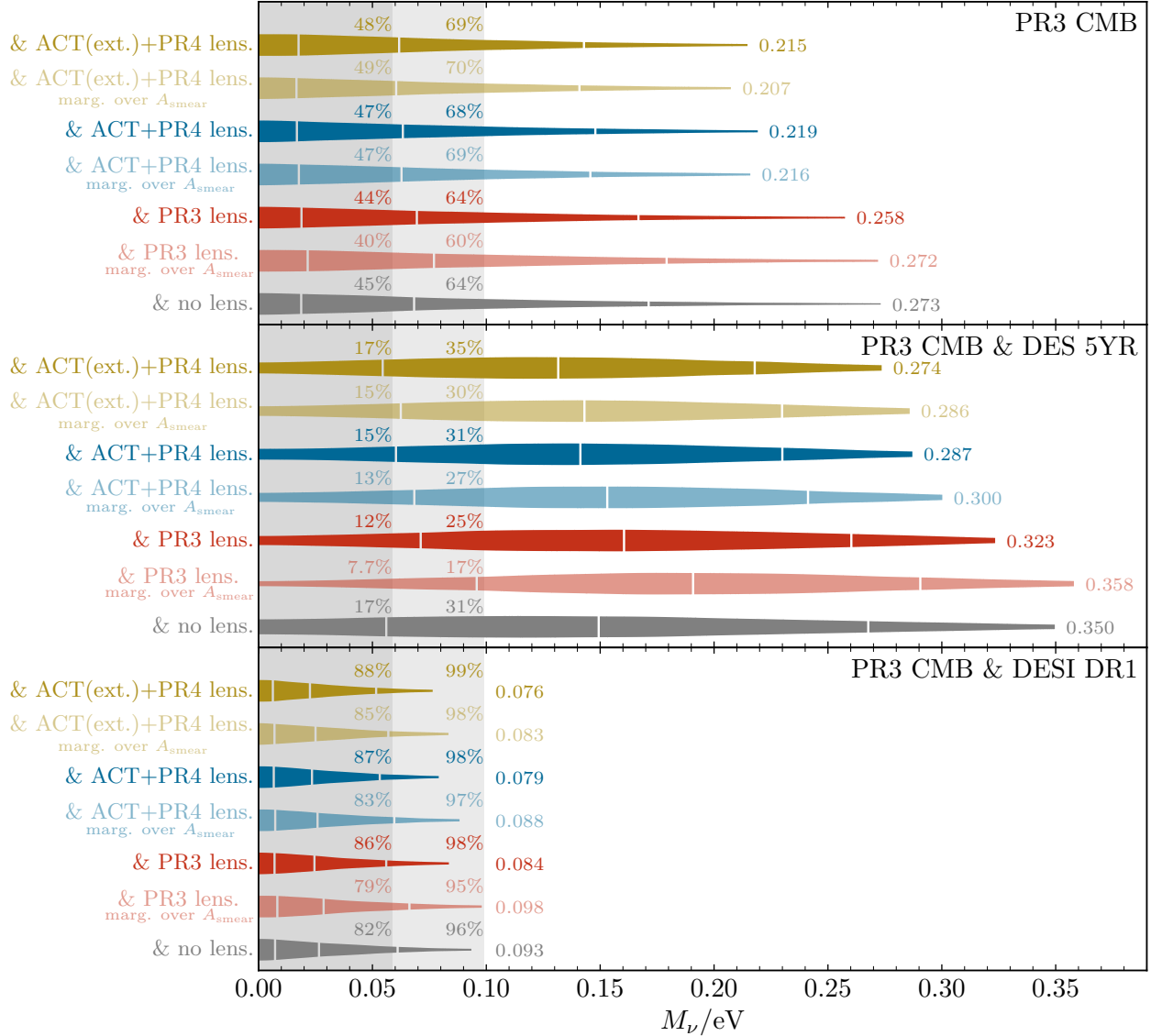


Figure 15. Marginal posterior distribution over the neutrino mass sum M_ν for *Planck* PR3 CMB data combined with various lensing datasets (by color), each marginalized over A_{smeared} (transparent, lighter colors) or not (opaque, darker colors). Results are presented as in Fig. 14. Here ACT(ext.)+PR4 denotes the ACT+*Planck* lensing combination that includes ACT data up to a larger maximum multipole (1250). The middle and bottom panels respectively include DES 5YR SNe data and DESI DR1 BAO data.

conclusion holds regardless of what (if any) low-redshift data are included.

2. Consistency of low-redshift distance measurements

Figure 16 displays joint posteriors from DESI BAO data that include and exclude the outliers identified in Fig. 6. The 2σ mass level of their combination does not overlap with that from other tracers or even that from the concordant LRG1 $_{\perp}$ and LRG2 $_{\parallel}$ measurements. Taking *Planck*'s shape-based calibration of $\omega_b + \omega_c \approx 0.142$ in standard cosmology, Figs. 6 and 16 shows that these outliers clearly bear most of the responsibility for favoring Λ CDM parameter space that is incompatible with the effect of massive neutrinos on geometry and structure. Excluding these

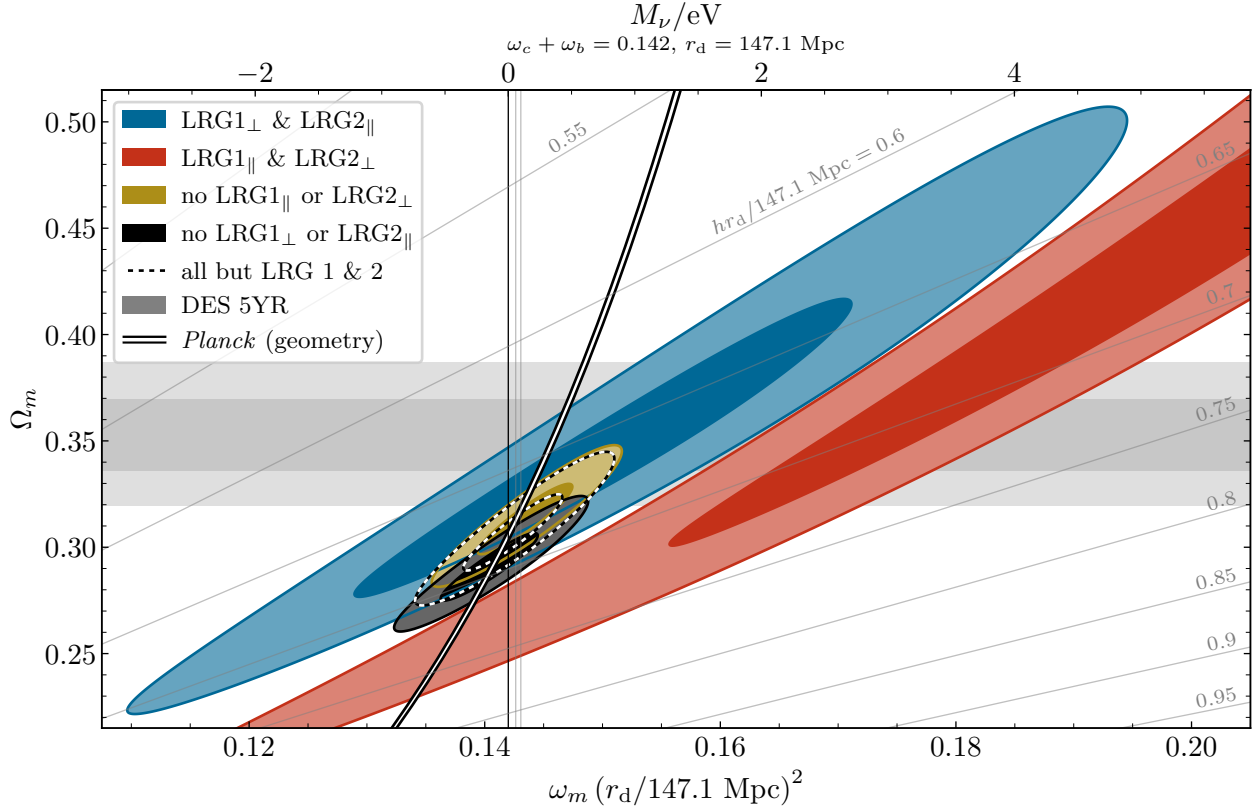


Figure 16. Geometric constraints on late-time Λ CDM cosmology from various subsets of DESI data, presented as in Fig. 3 but instead displaying only 1 and 2σ mass levels (and just *Planck*'s 2σ interval). Posteriors from the line-of-sight measurement in the $z = 0.51$ LRG bin (LRG1 $_{\parallel}$) combined with transverse one in the $z = 0.706$ LRG bin (LRG2 $_{\perp}$) appears in red and the combination of all DESI data except these two points in gold. Constraints from the other measurements in the LRG bins (LRG1 $_{\perp}$ and LRG2 $_{\parallel}$) appear in blue and that from all measurements except these two in black. The posteriors from DESI excluding the LRG1 and LRG2 bins entirely appear as unfilled, dashed black/white lines. While the LRG1 $_{\perp}$ and LRG2 $_{\parallel}$ combination (in blue) is quite consistent with all other tracers and only marginally shrinks the posterior when combined with them (comparing the black/white dashed lines to the gold contours), the apparent outliers (red) are in clear tension with all other measurements and shift the combined posterior (black) substantially in the direction that disfavors massive neutrinos.

outliers yields a constraint that agrees better with recent SNe datasets (that all prefer larger matter fractions) and allows for substantially larger neutrino masses.

Figure 17 displays the same internal consistency test (within flat Λ CDM cosmologies) from Fig. 6 for all other DESI and eBOSS tracers that include separate transverse and line-of-sight measurements. These results demonstrate the internal consistency of all other tracers from DESI DR1 (i.e., except for the LRG1 and LRG2 measurements displayed in Fig. 6), as well as most eBOSS tracers. The eBOSS results that include Ly- α measurements (LYAUTO and LYXQSO), however, are moderately discrepant with the joint result from other tracers, and, like DESI's LRG measurements, prefer parameter space that is largely incompatible with massive neutrinos. (The LRG measurements from SDSS DR16 [at $z = 0.698$] are also slightly offset from all other tracers, but in the opposite direction in parameter space.) Figure 17 thus demonstrates the sensitivity of neutrino mass constraints to potential outliers (again, when interpreted in flat Λ CDM cosmologies) from individual tracers and explains our combination of SDSS data below and DESI data above redshift 0.8 (using DESI-only Ly- α) as an illustrative example.

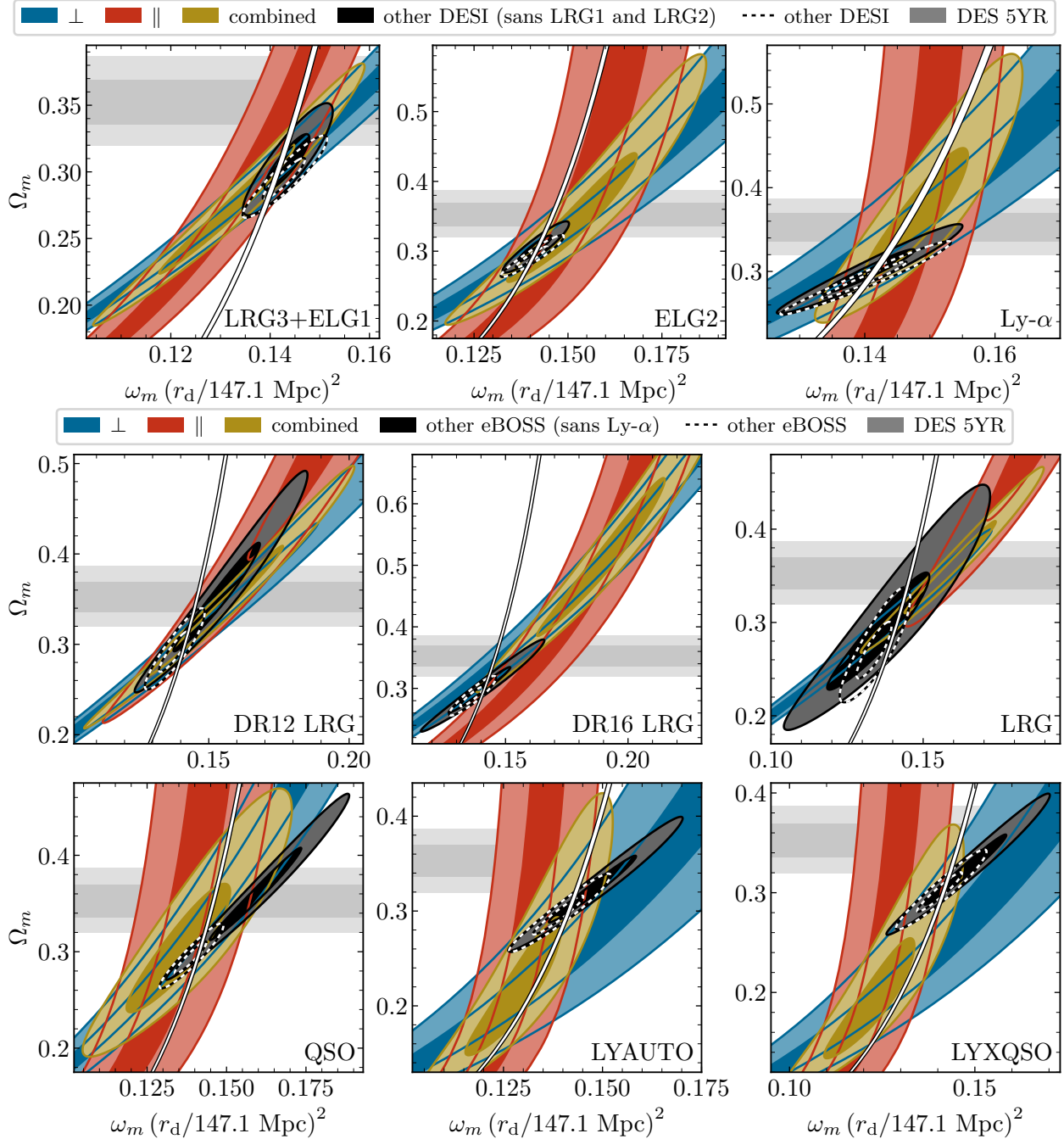


Figure 17. Comparison of Λ CDM parameter space compatible with BAO measurements from individual tracers (by panel), displaying posteriors deriving from transverse (blue) and line-of-sight (red) measurements and their combination (gold), presented as in Fig. 6. The top figure display results from DESI DR1, including posteriors from all other DESI tracers (dashed black/white lines), from all other DESI tracers excluding both LRG bins (black), from the DES 5YR SNe sample (grey), and from *Planck* (white band with extent covering its 5σ interval for visibility). The bottom figure displays analogous results for the final eBOSS BAO dataset, including results from all other eBOSS tracers (dashed black/white lines) and all other eBOSS tracers excluding both Ly- α bins as well (black).

Finally, Fig. 18 compares transverse distance measurements from SNe (i.e., translated from their luminosity distances) to those from BAO as a function of redshift, displayed relative to a

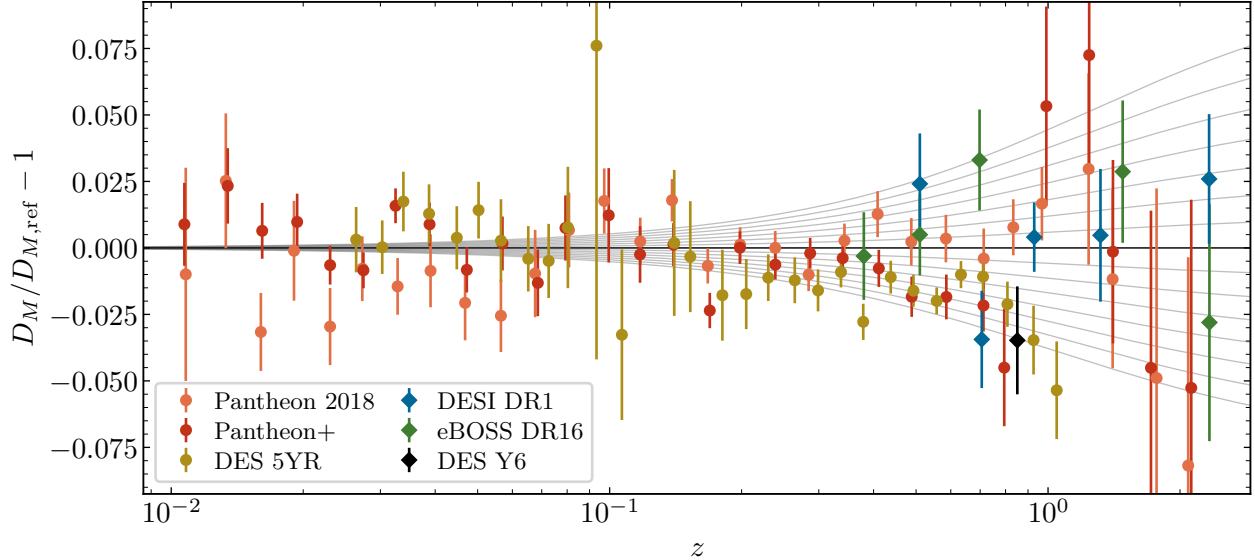


Figure 18. Comparison of transverse distance measurements D_M versus redshift from various SNe (circles) and BAO (diamonds) surveys, normalized to a fiducial cosmology with $\Omega_m = 0.31$ and $h = 0.685$. Results take *Planck*'s best-fit $r_d = 147.1$ Mpc and fix the fiducial magnitude M_B to the best fit for each individual SNe survey (to remove any calibration difference—e.g., datasets differ in their conventions for normalizing magnitudes). The SNe data are binned as described in the text. Grey lines indicate the residuals for cosmologies with different Ω_m , spaced by increments of 0.01. Note that, on a bin-by-bin basis, these comparisons do depend on the fiducial calibration taken, but different calibrations only have a uniform impact across redshifts.

fiducial cosmology with $\Omega_m = 0.31$. To facilitate visualization, the SNe data are binned into 30 logarithmically spaced intervals between the minimum and maximum redshift of each survey in a manner similar to Ref. [175], computing inverse-variance-weighted redshifts and magnitudes using the sub-block of the covariance matrix within each bin. That is, the measurements i within a bin with subcovariance C have weights $w_i = [C^{-1}]_{ii}$ and combine into a magnitude $\sum_i w_i \hat{m}_i / \sum_i w_i$ at redshift $\sum_i w_i z_i / \sum_i w_i$ with variance $1 / \sum_i w_i$. These binned magnitudes are then translated to transverse distances and their errors propagated accordingly. Cross-bin covariance is neglected, but it cannot be depicted in Fig. 18 anyway. At $z \gtrsim z_{m-\Lambda} \approx 0.3$, measurements from the most recent SNe datasets (Pantheon+ and DES 5YR) in Fig. 18 systematically trend low, indicative of their preference for higher matter fractions Ω_m , i.e., lower $z_{m-\Lambda}$; most of those from eBOSS and DESI, on the other hand, are consistent or skew slightly higher than the fiducial cosmology (since each prefers Ω_m near but slightly below 0.31).

Appendix C: Impact of nonlinear evolution on neutrino mass inference

In this appendix we demonstrate the impact of nonlinear structure growth on neutrino mass inference with current datasets. Figure 19 compares the one-dimensional posteriors over M_ν for various dataset combinations when including and excluding nonlinear effects (modeled with HMCODE-2016 [110]). Neglecting nonlinear evolution clearly biases neutrino mass constraints, artificially shifting posteriors to lower values to a modest degree. The bias varies between 0.03 eV (for PR3 lensing data) and 0.05 eV (for ACT+PR4) except when combining with DESI data. In that case, DESI's constraints on the expansion history (combined with *Planck*'s primary CMB data) disfavor the larger matter fractions that are required to accommodate massive neutrino's geometric

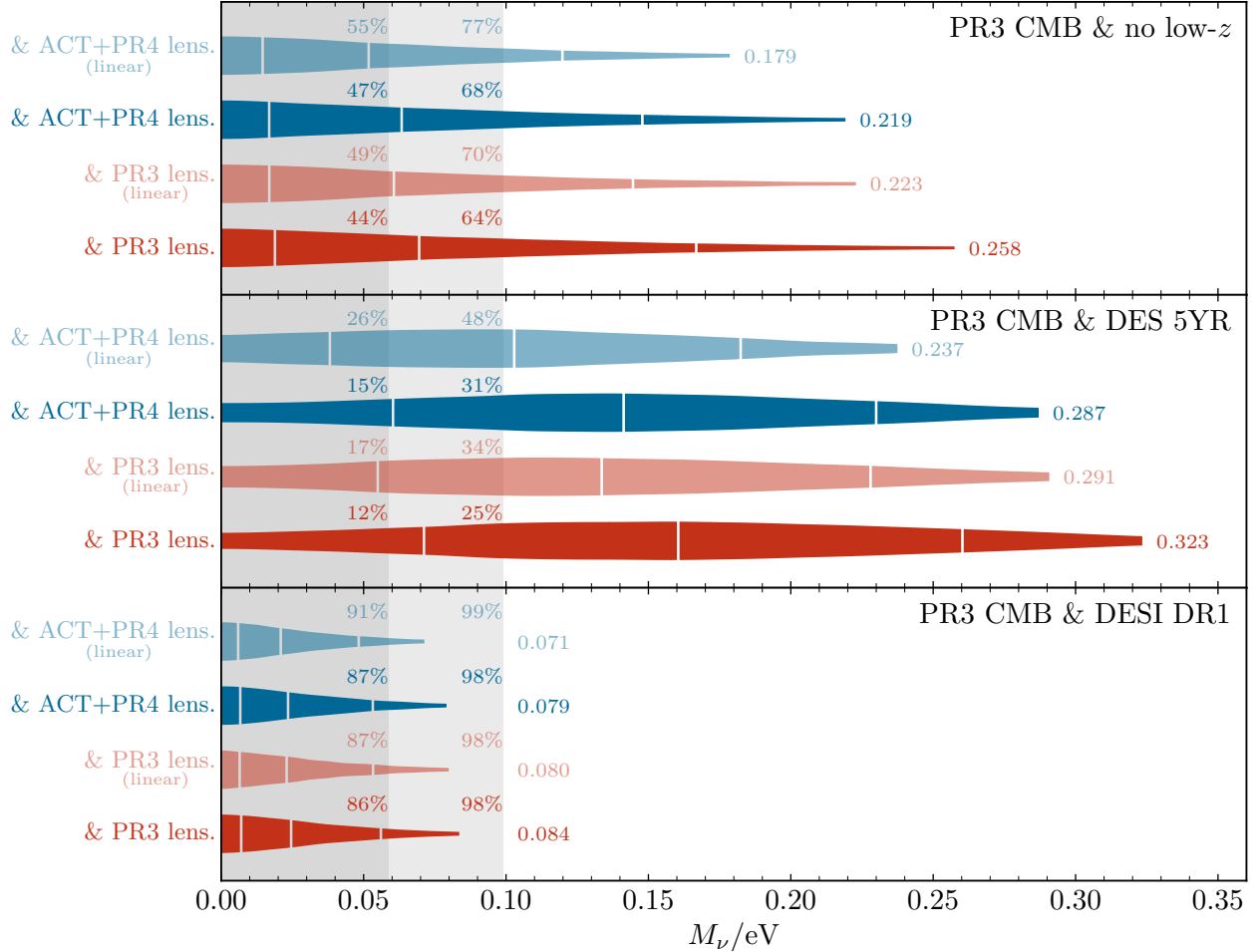


Figure 19. Marginal posterior distribution over the neutrino mass sum M_ν when including (opaque) and excluding (transparent) nonlinear contributions to the growth of structure. Each posterior uses *Planck* PR3 CMB data combined with various BAO and SNe datasets (labeled on each panel) and PR3 lensing (red) or ACT+PR4 lensing (blue). Results are presented as in Fig. 14.

effects and that would give more room for neutrinos to suppress structure growth, independent of whether nonlinear effects are included. Though the posteriors do shift marginally, accounting for nonlinear evolution does not alter any qualitative conclusions for dataset combinations that include DESI DR1 (like, for instance, their incompatibility with the inverted hierarchy).

To illustrate what in the lensing data allows for heavier neutrinos when nonlinear effects are accounted for, Fig. 20 displays the residuals of posterior samples relative to the Λ CDM best-fit cosmology (with massless neutrinos only) with current lensing data superimposed. Though nonlinear effects play no role at the multipoles $30 \lesssim L \lesssim 200$ where the data exhibit a clear downward trend relative to the Λ CDM best-fit, they have a significant impact at higher multipoles where the data skew back toward positive residuals. Though the measurements at $L \gtrsim 300$ are noisy and do not incontrovertibly demonstrate a systematic upward trend, the majority of the data points do indeed skew upward. In this range, the posterior samples for fully linear predictions drop precipitously and are unable to accommodate these data points, especially for heavier neutrino masses. Because nonlinear evolution enhances small-scale structure, one can only expect this trend to become more important as future observations improve the accuracy of measurements at high multipoles, underscoring the importance of nonlinear modeling to unbiased neutrino mass constraints using

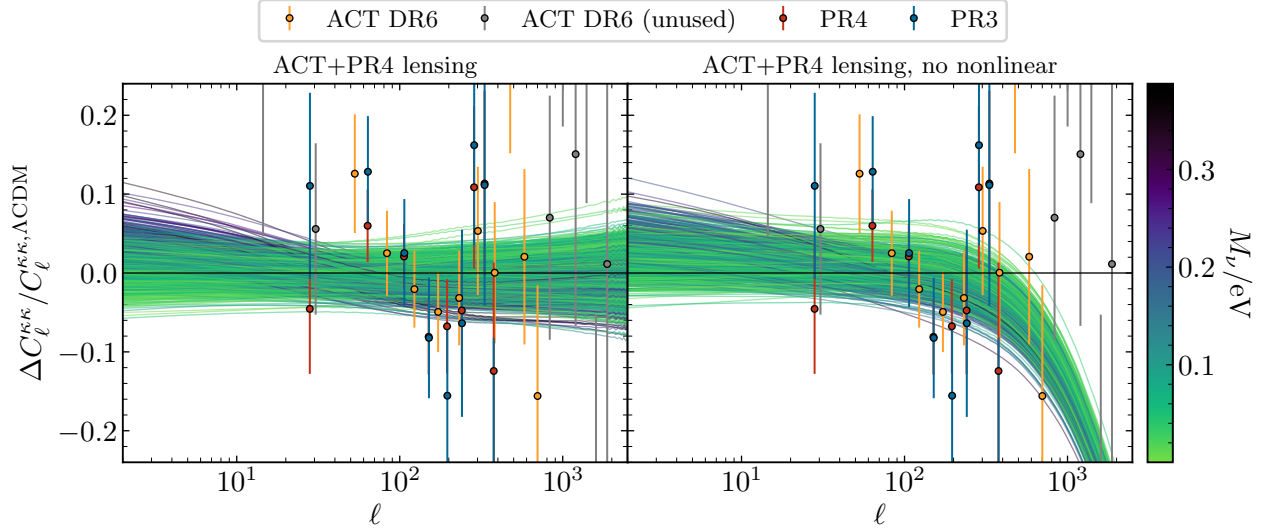


Figure 20. Residuals of the CMB lensing convergence relative to the Λ CDM best fit (using *Planck* PR3 CMB and ACT+PR4 lensing data) for samples from various posteriors that include (left) and exclude (right) nonlinear corrections to the growth of structure. Note that the reference result includes no massive neutrinos but does account for nonlinear evolution. Curves are colored by their value of M_ν and data from various observations are also depicted as labeled in the legend; note that the data included for the posteriors depicted here are labeled ACT DR6 (yellow) and PR4 (red).

such data.

-
- [1] N. Aghanim *et al.* (Planck), Planck 2018 results. VI. Cosmological parameters, *Astron. Astrophys.* **641**, A6 (2020), [Erratum: *Astron. Astrophys.* 652, C4 (2021)], [arXiv:1807.06209](https://arxiv.org/abs/1807.06209) [astro-ph.CO].
 - [2] N. Aghanim *et al.* (Planck), Planck 2018 results. V. CMB power spectra and likelihoods, *Astron. Astrophys.* **641**, A5 (2020), [arXiv:1907.12875](https://arxiv.org/abs/1907.12875) [astro-ph.CO].
 - [3] N. Aghanim *et al.* (Planck), Planck 2018 results. VIII. Gravitational lensing, *Astron. Astrophys.* **641**, A8 (2020), [arXiv:1807.06210](https://arxiv.org/abs/1807.06210) [astro-ph.CO].
 - [4] M. M. Ivanov, M. Simonović, and M. Zaldarriaga, Cosmological Parameters from the BOSS Galaxy Power Spectrum, *JCAP* **05**, 042, [arXiv:1909.05277](https://arxiv.org/abs/1909.05277) [astro-ph.CO].
 - [5] M. Asgari *et al.* (KiDS), KiDS-1000 Cosmology: Cosmic shear constraints and comparison between two point statistics, *Astron. Astrophys.* **645**, A104 (2021), [arXiv:2007.15633](https://arxiv.org/abs/2007.15633) [astro-ph.CO].
 - [6] C. Doux *et al.* (DES), Dark energy survey year 3 results: cosmological constraints from the analysis of cosmic shear in harmonic space, *Mon. Not. Roy. Astron. Soc.* **515**, 1942 (2022), [arXiv:2203.07128](https://arxiv.org/abs/2203.07128) [astro-ph.CO].
 - [7] E. Abdalla *et al.*, Cosmology intertwined: A review of the particle physics, astrophysics, and cosmology associated with the cosmological tensions and anomalies, *JHEAp* **34**, 49 (2022), [arXiv:2203.06142](https://arxiv.org/abs/2203.06142) [astro-ph.CO].
 - [8] S.-F. Chen, M. M. Ivanov, O. H. E. Philcox, and L. Wenzl, Suppression without Thawing: Constraining Structure Formation and Dark Energy with Galaxy Clustering, [arXiv:2406.13388](https://arxiv.org/abs/2406.13388) [astro-ph.CO] (2024).
 - [9] T. Karim *et al.* (DESI), Measuring σ_8 using DESI Legacy Imaging Surveys Emission-Line Galaxies and Planck CMB Lensing and the Impact of Dust on Parameter Inferenc, [arXiv:2408.15909](https://arxiv.org/abs/2408.15909) [astro-ph.CO] (2024).
 - [10] W. Hu, D. J. Eisenstein, and M. Tegmark, Weighing neutrinos with galaxy surveys, *Phys. Rev. Lett.* **80**, 5255 (1998), [arXiv:astro-ph/9712057](https://arxiv.org/abs/astro-ph/9712057).
 - [11] J. Lesgourgues, L. Perotto, S. Pastor, and M. Piat, Probing neutrino masses with cmb lensing extraction, *Phys. Rev. D* **73**, 045021 (2006), [arXiv:astro-ph/0511735](https://arxiv.org/abs/astro-ph/0511735).

- [12] K. N. Abazajian *et al.* (CMB-S4), CMB-S4 Science Book, First Edition, [arXiv:1610.02743 \[astro-ph.CO\]](#) (2016).
- [13] P. Ade *et al.* (Simons Observatory), The Simons Observatory: Science goals and forecasts, *JCAP* **02**, 056, [arXiv:1808.07445 \[astro-ph.CO\]](#).
- [14] A. Font-Ribera, P. McDonald, N. Mostek, B. A. Reid, H.-J. Seo, and A. Slosar, DESI and other dark energy experiments in the era of neutrino mass measurements, *JCAP* **05**, 023, [arXiv:1308.4164 \[astro-ph.CO\]](#).
- [15] O. Doré *et al.*, WFIRST: The Essential Cosmology Space Observatory for the Coming Decade, [arXiv:1904.01174 \[astro-ph.CO\]](#) (2019).
- [16] M. Archidiacono, T. Brinckmann, J. Lesgourgues, and V. Poulin, Physical effects involved in the measurements of neutrino masses with future cosmological data, *JCAP* **02**, 052, [arXiv:1610.09852 \[astro-ph.CO\]](#).
- [17] T. M. C. Abbott *et al.* (DES), Dark Energy Survey Year 3 results: Constraints on extensions to Λ CDM with weak lensing and galaxy clustering, *Phys. Rev. D* **107**, 083504 (2023), [arXiv:2207.05766 \[astro-ph.CO\]](#).
- [18] A. Abate *et al.* (LSST Dark Energy Science), Large Synoptic Survey Telescope: Dark Energy Science Collaboration, [arXiv:1211.0310 \[astro-ph.CO\]](#) (2012).
- [19] M. Archidiacono *et al.* (Euclid), Euclid preparation. Sensitivity to neutrino parameters, [arXiv:2405.06047 \[astro-ph.CO\]](#) (2024).
- [20] A. B. Mantz *et al.*, Weighing the giants – IV. Cosmology and neutrino mass, *Mon. Not. Roy. Astron. Soc.* **446**, 2205 (2015), [arXiv:1407.4516 \[astro-ph.CO\]](#).
- [21] C. Dvorkin *et al.*, Neutrino Mass from Cosmology: Probing Physics Beyond the Standard Model, [arXiv:1903.03689 \[astro-ph.CO\]](#) (2019).
- [22] S. Ferraro, N. Sailer, A. Slosar, and M. White, Snowmass2021 Cosmic Frontier White Paper: Cosmology and Fundamental Physics from the three-dimensional Large Scale Structure, [arXiv:2203.07506 \[astro-ph.CO\]](#) (2022).
- [23] M. Gerbino *et al.*, Synergy between cosmological and laboratory searches in neutrino physics, *Phys. Dark Univ.* **42**, 101333 (2023), [arXiv:2203.07377 \[hep-ph\]](#).
- [24] N.-M. Nguyen, D. Huterer, and Y. Wen, Evidence for Suppression of Structure Growth in the Concordance Cosmological Model, *Phys. Rev. Lett.* **131**, 111001 (2023), [arXiv:2302.01331 \[astro-ph.CO\]](#).
- [25] A. G. Riess *et al.*, A 2.4% Determination of the Local Value of the Hubble Constant, *Astrophys. J.* **826**, 56 (2016), [arXiv:1604.01424 \[astro-ph.CO\]](#).
- [26] A. G. Riess, S. Casertano, W. Yuan, L. M. Macri, and D. Scolnic, Large Magellanic Cloud Cepheid Standards Provide a 1% Foundation for the Determination of the Hubble Constant and Stronger Evidence for Physics beyond Λ CDM, *Astrophys. J.* **876**, 85 (2019), [arXiv:1903.07603 \[astro-ph.CO\]](#).
- [27] A. G. Riess *et al.*, A Comprehensive Measurement of the Local Value of the Hubble Constant with 1 km s⁻¹ Mpc⁻¹ Uncertainty from the Hubble Space Telescope and the SHOES Team, *Astrophys. J. Lett.* **934**, L7 (2022), [arXiv:2112.04510 \[astro-ph.CO\]](#).
- [28] W. L. Freedman, B. F. Madore, I. S. Jang, T. J. Hoyt, A. J. Lee, and K. A. Owens, Status Report on the Chicago-Carnegie Hubble Program (CCHP): Three Independent Astrophysical Determinations of the Hubble Constant Using the James Webb Space Telescope, [arXiv:2408.06153 \[astro-ph.CO\]](#) (2024).
- [29] W. L. Freedman *et al.*, The Carnegie-Chicago Hubble Program. VIII. An Independent Determination of the Hubble Constant Based on the Tip of the Red Giant Branch, *Astrophys. J.* **882**, 34 (2019), [arXiv:1907.05922 \[astro-ph.CO\]](#).
- [30] W. L. Freedman, B. F. Madore, T. Hoyt, I. S. Jang, R. Beaton, M. G. Lee, A. Monson, J. Neeley, and J. Rich, Calibration of the Tip of the Red Giant Branch (TRGB), [arXiv:2002.01550 \[astro-ph.GA\]](#) (2020).
- [31] W. L. Freedman, Measurements of the Hubble Constant: Tensions in Perspective, *Astrophys. J.* **919**, 16 (2021), [arXiv:2106.15656 \[astro-ph.CO\]](#).
- [32] W. L. Freedman and B. F. Madore, Progress in direct measurements of the Hubble constant, *JCAP* **11**, 050, [arXiv:2309.05618 \[astro-ph.CO\]](#).
- [33] M. Kaplinghat, L. Knox, and Y.-S. Song, Determining neutrino mass from the CMB alone, *Phys. Rev. Lett.* **91**, 241301 (2003), [arXiv:astro-ph/0303344](#).
- [34] D. Brout *et al.*, The Pantheon+ Analysis: Cosmological Constraints, *Astrophys. J.* **938**, 110 (2022),

- [arXiv:2202.04077 \[astro-ph.CO\]](#).
- [35] D. Scolnic *et al.*, The Pantheon+ Analysis: The Full Data Set and Light-curve Release, *Astrophys. J.* **938**, 113 (2022), [arXiv:2112.03863 \[astro-ph.CO\]](#).
 - [36] T. M. C. Abbott *et al.* (DES), The Dark Energy Survey: Cosmology Results With ~ 1500 New High-redshift Type Ia Supernovae Using The Full 5-year Dataset, [arXiv:2401.02929 \[astro-ph.CO\]](#) (2024).
 - [37] D. Rubin *et al.*, Union Through UNITY: Cosmology with 2,000 SNe Using a Unified Bayesian Framework, [arXiv:2311.12098 \[astro-ph.CO\]](#) (2023).
 - [38] I. Etherington, Lx. on the definition of distance in general relativity, *The London, Edinburgh, and Dublin Philosophical Magazine and Journal of Science* **15**, 761 (1933).
 - [39] A. G. Adame *et al.* (DESI), DESI 2024 VI: Cosmological Constraints from the Measurements of Baryon Acoustic Oscillations, [arXiv:2404.03002 \[astro-ph.CO\]](#) (2024).
 - [40] A. G. Adame *et al.* (DESI), DESI 2024 IV: Baryon Acoustic Oscillations from the Lyman Alpha Forest, [arXiv:2404.03001 \[astro-ph.CO\]](#) (2024).
 - [41] A. G. Adame *et al.* (DESI), DESI 2024 III: Baryon Acoustic Oscillations from Galaxies and Quasars, [arXiv:2404.03000 \[astro-ph.CO\]](#) (2024).
 - [42] I. Esteban, M. C. Gonzalez-Garcia, M. Maltoni, T. Schwetz, and A. Zhou, The fate of hints: updated global analysis of three-flavor neutrino oscillations, *JHEP* **09**, 178, [arXiv:2007.14792 \[hep-ph\]](#).
 - [43] P. F. de Salas, D. V. Forero, S. Gariazzo, P. Martínez-Miravé, O. Mena, C. A. Ternes, M. Tórtola, and J. W. F. Valle, 2020 global reassessment of the neutrino oscillation picture, *JHEP* **02**, 071, [arXiv:2006.11237 \[hep-ph\]](#).
 - [44] S. Alam *et al.* (eBOSS), Completed SDSS-IV extended Baryon Oscillation Spectroscopic Survey: Cosmological implications from two decades of spectroscopic surveys at the Apache Point Observatory, *Phys. Rev. D* **103**, 083533 (2021), [arXiv:2007.08991 \[astro-ph.CO\]](#).
 - [45] J. E. Bautista *et al.* (eBOSS), The Completed SDSS-IV extended Baryon Oscillation Spectroscopic Survey: measurement of the BAO and growth rate of structure of the luminous red galaxy sample from the anisotropic correlation function between redshifts 0.6 and 1, *Mon. Not. Roy. Astron. Soc.* **500**, 736 (2020), [arXiv:2007.08993 \[astro-ph.CO\]](#).
 - [46] H. Gil-Marín *et al.* (eBOSS), The Completed SDSS-IV extended Baryon Oscillation Spectroscopic Survey: measurement of the BAO and growth rate of structure of the luminous red galaxy sample from the anisotropic power spectrum between redshifts 0.6 and 1.0, *Mon. Not. Roy. Astron. Soc.* **498**, 2492 (2020), [arXiv:2007.08994 \[astro-ph.CO\]](#).
 - [47] A. J. Ross, L. Samushia, C. Howlett, W. J. Percival, A. Burden, and M. Manera, The clustering of the SDSS DR7 main Galaxy sample – I. A 4 per cent distance measure at $z = 0.15$, *Mon. Not. Roy. Astron. Soc.* **449**, 835 (2015), [arXiv:1409.3242 \[astro-ph.CO\]](#).
 - [48] M. S. Madhavacheril *et al.* (ACT), The Atacama Cosmology Telescope: DR6 Gravitational Lensing Map and Cosmological Parameters, *Astrophys. J.* **962**, 113 (2024), [arXiv:2304.05203 \[astro-ph.CO\]](#).
 - [49] F. J. Qu *et al.* (ACT), The Atacama Cosmology Telescope: A Measurement of the DR6 CMB Lensing Power Spectrum and Its Implications for Structure Growth, *Astrophys. J.* **962**, 112 (2024), [arXiv:2304.05202 \[astro-ph.CO\]](#).
 - [50] Z. Hou *et al.*, Constraints on Cosmology from the Cosmic Microwave Background Power Spectrum of the 2500 deg² SPT-SZ Survey, *Astrophys. J.* **782**, 74 (2014), [arXiv:1212.6267 \[astro-ph.CO\]](#).
 - [51] G. Mangano, G. Miele, S. Pastor, T. Pinto, O. Pisanti, and P. D. Serpico, Relic neutrino decoupling including flavor oscillations, *Nucl. Phys. B* **729**, 221 (2005), [arXiv:hep-ph/0506164](#).
 - [52] M. Archidiacono, S. Hannestad, and J. Lesgourgues, What will it take to measure individual neutrino mass states using cosmology?, *JCAP* **09**, 021, [arXiv:2003.03354 \[astro-ph.CO\]](#).
 - [53] K. Akita and M. Yamaguchi, A precision calculation of relic neutrino decoupling, *JCAP* **08**, 012, [arXiv:2005.07047 \[hep-ph\]](#).
 - [54] J. Froustey, C. Pitrou, and M. C. Volpe, Neutrino decoupling including flavour oscillations and primordial nucleosynthesis, *JCAP* **12**, 015, [arXiv:2008.01074 \[hep-ph\]](#).
 - [55] J. J. Bennett, G. Buldgen, P. F. De Salas, M. Drewes, S. Gariazzo, S. Pastor, and Y. Y. Y. Wong, Towards a precision calculation of N_{eff} in the Standard Model II: Neutrino decoupling in the presence of flavour oscillations and finite-temperature QED, *JCAP* **04**, 073, [arXiv:2012.02726 \[hep-ph\]](#).
 - [56] S. Bashinsky and U. Seljak, Neutrino perturbations in CMB anisotropy and matter clustering, *Phys. Rev. D* **69**, 083002 (2004), [arXiv:astro-ph/0310198](#).

- [57] D. Baumann, D. Green, J. Meyers, and B. Wallisch, Phases of New Physics in the CMB, *JCAP* **01**, 007, [arXiv:1508.06342 \[astro-ph.CO\]](#).
- [58] M. Baryakhtar, O. Simon, and Z. J. Weiner, Varying-constant cosmology from hyperlight, coupled scalars, [arXiv:2405.10358 \[astro-ph.CO\]](#) (2024).
- [59] W. Hu and M. J. White, The Damping tail of CMB anisotropies, *Astrophys. J.* **479**, 568 (1997), [arXiv:astro-ph/9609079](#).
- [60] W. Hu and N. Sugiyama, Small scale cosmological perturbations: An Analytic approach, *Astrophys. J.* **471**, 542 (1996), [arXiv:astro-ph/9510117](#).
- [61] M. Cielo, M. Escudero, G. Mangano, and O. Pisanti, Neff in the Standard Model at NLO is 3.043, *Phys. Rev. D* **108**, L121301 (2023), [arXiv:2306.05460 \[hep-ph\]](#).
- [62] D. J. Eisenstein and W. Hu, Baryonic features in the matter transfer function, *Astrophys. J.* **496**, 605 (1998), [arXiv:astro-ph/9709112](#).
- [63] W. T. Hu, *Wandering in the Background: A CMB Explorer*, Other thesis (1995), [arXiv:astro-ph/9508126](#).
- [64] M. Zaldarriaga and D. D. Harari, Analytic approach to the polarization of the cosmic microwave background in flat and open universes, *Phys. Rev. D* **52**, 3276 (1995), [arXiv:astro-ph/9504085](#).
- [65] S. Weinberg, *Cosmology* (2008).
- [66] W. Hu and M. J. White, A CMB polarization primer, *New Astron.* **2**, 323 (1997), [arXiv:astro-ph/9706147](#).
- [67] S. Perlmutter *et al.* (Supernova Cosmology Project), Measurements of the cosmological parameters Omega and Lambda from the first 7 supernovae at $z \geq 0.35$, *Astrophys. J.* **483**, 565 (1997), [arXiv:astro-ph/9608192](#).
- [68] W. Hu and Z. Haiman, Redshifting rings of power, *Phys. Rev. D* **68**, 063004 (2003), [arXiv:astro-ph/0306053](#).
- [69] H.-J. Seo and D. J. Eisenstein, Probing dark energy with baryonic acoustic oscillations from future large galaxy redshift surveys, *Astrophys. J.* **598**, 720 (2003), [arXiv:astro-ph/0307460](#).
- [70] C. Blake and K. Glazebrook, Probing dark energy using baryonic oscillations in the galaxy power spectrum as a cosmological ruler, *Astrophys. J.* **594**, 665 (2003), [arXiv:astro-ph/0301632](#).
- [71] S. Cole *et al.* (2dFGRS), The 2dF Galaxy Redshift Survey: Power-spectrum analysis of the final dataset and cosmological implications, *Mon. Not. Roy. Astron. Soc.* **362**, 505 (2005), [arXiv:astro-ph/0501174](#).
- [72] D. J. Eisenstein, H.-j. Seo, E. Sirko, and D. Spergel, Improving Cosmological Distance Measurements by Reconstruction of the Baryon Acoustic Peak, *Astrophys. J.* **664**, 675 (2007), [arXiv:astro-ph/0604362](#).
- [73] D. W. Hogg, Distance measures in cosmology, [arXiv:astro-ph/9905116](#) (1999).
- [74] M. Baes, P. Camps, and D. Van De Putte, Analytical expressions and numerical evaluation of the luminosity distance in a flat cosmology, *Mon. Not. Roy. Astron. Soc.* **468**, 927 (2017), [arXiv:1702.08860 \[astro-ph.CO\]](#).
- [75] K. Thepsuriya and A. Lewis, Accuracy of cosmological parameters using the baryon acoustic scale, *JCAP* **01**, 034, [arXiv:1409.5066 \[astro-ph.CO\]](#).
- [76] N. Schöneberg, J. Lesgourgues, and D. C. Hooper, The BAO+BBN take on the Hubble tension, *JCAP* **10**, 029, [arXiv:1907.11594 \[astro-ph.CO\]](#).
- [77] W. Lin, X. Chen, and K. J. Mack, Early Universe Physics Insensitive and Uncalibrated Cosmic Standards: Constraints on Ω_m and Implications for the Hubble Tension, *Astrophys. J.* **920**, 159 (2021), [arXiv:2102.05701 \[astro-ph.CO\]](#).
- [78] D. M. Scolnic *et al.* (Pan-STARRS1), The Complete Light-curve Sample of Spectroscopically Confirmed SNe Ia from Pan-STARRS1 and Cosmological Constraints from the Combined Pantheon Sample, *Astrophys. J.* **859**, 101 (2018), [arXiv:1710.00845 \[astro-ph.CO\]](#).
- [79] T. M. Davis *et al.*, The Effect of Peculiar Velocities on Supernova Cosmology, *Astrophys. J.* **741**, 67 (2011), [arXiv:1012.2912 \[astro-ph.CO\]](#).
- [80] T. M. Davis, S. R. Hinton, C. Howlett, and J. Calcino, Can redshift errors bias measurements of the Hubble Constant?, *Mon. Not. Roy. Astron. Soc.* **490**, 2948 (2019), [arXiv:1907.12639 \[astro-ph.CO\]](#).
- [81] A. Carr, T. M. Davis, D. Scolnic, D. Scolnic, K. Said, D. Brout, E. R. Peterson, and R. Kessler, The Pantheon+ analysis: Improving the redshifts and peculiar velocities of Type Ia supernovae used in cosmological analyses, *Publ. Astron. Soc. Austral.* **39**, e046 (2022), [arXiv:2112.01471 \[astro-ph.CO\]](#).
- [82] J. R. Bond, G. Efstathiou, and J. Silk, Massive Neutrinos and the Large Scale Structure of the Universe, *Phys. Rev. Lett.* **45**, 1980 (1980).

- [83] A. Lewis and A. Challinor, Weak gravitational lensing of the CMB, *Phys. Rept.* **429**, 1 (2006), [arXiv:astro-ph/0601594](#).
- [84] D. N. Limber, The Analysis of Counts of the Extragalactic Nebulae in Terms of a Fluctuating Density Field. II, *Astrophys. J.* **119**, 655 (1954).
- [85] M. LoVerde and N. Afshordi, Extended Limber Approximation, *Phys. Rev. D* **78**, 123506 (2008), [arXiv:0809.5112 \[astro-ph\]](#).
- [86] J. M. Bardeen, J. R. Bond, N. Kaiser, and A. S. Szalay, The Statistics of Peaks of Gaussian Random Fields, *Astrophys. J.* **304**, 15 (1986).
- [87] J. Lesgourgues and S. Pastor, Massive neutrinos and cosmology, *Phys. Rept.* **429**, 307 (2006), [arXiv:astro-ph/0603494](#).
- [88] Z. Pan and L. Knox, Constraints on neutrino mass from Cosmic Microwave Background and Large Scale Structure, *Mon. Not. Roy. Astron. Soc.* **454**, 3200 (2015), [arXiv:1506.07493 \[astro-ph.CO\]](#).
- [89] U. Seljak, Gravitational lensing effect on cosmic microwave background anisotropies: A Power spectrum approach, *Astrophys. J.* **463**, 1 (1996), [arXiv:astro-ph/9505109](#).
- [90] M. Zaldarriaga and U. Seljak, Gravitational lensing effect on cosmic microwave background polarization, *Phys. Rev. D* **58**, 023003 (1998), [arXiv:astro-ph/9803150](#).
- [91] R. Stompor and G. Efstathiou, Gravitational lensing of cosmic microwave background anisotropies and cosmological parameters estimation, *Mon. Not. Roy. Astron. Soc.* **302**, 735 (1999), [arXiv:astro-ph/9805294](#).
- [92] K. M. Smith, W. Hu, and M. Kaplinghat, Cosmological Information from Lensed CMB Power Spectra, *Phys. Rev. D* **74**, 123002 (2006), [arXiv:astro-ph/0607315](#).
- [93] E. Calabrese, A. Slosar, A. Melchiorri, G. F. Smoot, and O. Zahn, Cosmic Microwave Weak lensing data as a test for the dark universe, *Phys. Rev. D* **77**, 123531 (2008), [arXiv:0803.2309 \[astro-ph\]](#).
- [94] E. Rosenberg, S. Gratton, and G. Efstathiou, CMB power spectra and cosmological parameters from Planck PR4 with CamSpec, *Mon. Not. Roy. Astron. Soc.* **517**, 4620 (2022), [arXiv:2205.10869 \[astro-ph.CO\]](#).
- [95] M. Tristram *et al.*, Cosmological parameters derived from the final Planck data release (PR4), *Astron. Astrophys.* **682**, A37 (2024), [arXiv:2309.10034 \[astro-ph.CO\]](#).
- [96] S. Dodelson, E. Gates, and A. Stebbins, Cold + hot dark matter and the cosmic microwave background, *Astrophys. J.* **467**, 10 (1996), [arXiv:astro-ph/9509147](#).
- [97] J. Lesgourgues and S. Pastor, Neutrino mass from Cosmology, *Adv. High Energy Phys.* **2012**, 608515 (2012), [arXiv:1212.6154 \[hep-ph\]](#).
- [98] K. Ichikawa, M. Fukugita, and M. Kawasaki, Constraining neutrino masses by CMB experiments alone, *Phys. Rev. D* **71**, 043001 (2005), [arXiv:astro-ph/0409768](#).
- [99] G. Hinshaw *et al.* (WMAP), Nine-Year Wilkinson Microwave Anisotropy Probe (WMAP) Observations: Cosmological Parameter Results, *Astrophys. J. Suppl.* **208**, 19 (2013), [arXiv:1212.5226 \[astro-ph.CO\]](#).
- [100] N. Craig, D. Green, J. Meyers, and S. Rajendran, No ν s is Good News, *JHEP* **09**, 097, [arXiv:2405.00836 \[astro-ph.CO\]](#).
- [101] D. Green and J. Meyers, The Cosmological Preference for Negative Neutrino Mass, [arXiv:2407.07878 \[astro-ph.CO\]](#) (2024).
- [102] I. J. Allali and A. Notari, Neutrino mass bounds from DESI 2024 are relaxed by Planck PR4 and cosmological supernovae, [arXiv:2406.14554 \[astro-ph.CO\]](#) (2024).
- [103] D. Naredo-Tuero, M. Escudero, E. Fernández-Martínez, X. Marcano, and V. Poulin, Living at the Edge: A Critical Look at the Cosmological Neutrino Mass Bound, [arXiv:2407.13831 \[astro-ph.CO\]](#) (2024).
- [104] W. Elbers, C. S. Frenk, A. Jenkins, B. Li, and S. Pascoli, Negative neutrino masses as a mirage of dark energy, [arXiv:2407.10965 \[astro-ph.CO\]](#) (2024).
- [105] J. Carron, M. Mirmelstein, and A. Lewis, CMB lensing from Planck PR4 maps, *JCAP* **09**, 039, [arXiv:2206.07773 \[astro-ph.CO\]](#).
- [106] J.-Q. Jiang, W. Giarè, S. Gariazzo, M. G. Dainotti, E. Di Valentino, O. Mena, D. Pedrotti, S. S. da Costa, and S. Vagnozzi, Neutrino cosmology after DESI: tightest mass upper limits, preference for the normal ordering, and tension with terrestrial observations, [arXiv:2407.18047 \[astro-ph.CO\]](#) (2024).
- [107] ACT Collaboration, [act.dr6.lenslike](#) (2024), commit hash 78dcd4a.
- [108] D. Blas, J. Lesgourgues, and T. Tram, The Cosmic Linear Anisotropy Solving System (CLASS) II: Approximation schemes, *JCAP* **07**, 034, [arXiv:1104.2933 \[astro-ph.CO\]](#).

- [109] J. Lesgourgues, The Cosmic Linear Anisotropy Solving System (CLASS) I: Overview, [arXiv:1104.2932 \[astro-ph.IM\]](#) (2011).
- [110] A. Mead, C. Heymans, L. Lombriser, J. Peacock, O. Steele, and H. Winther, Accurate halo-model matter power spectra with dark energy, massive neutrinos and modified gravitational forces, *Mon. Not. Roy. Astron. Soc.* **459**, 1468 (2016), [arXiv:1602.02154 \[astro-ph.CO\]](#).
- [111] A. Mead, S. Brieden, T. Tröster, and C. Heymans, HMcode-2020: Improved modelling of non-linear cosmological power spectra with baryonic feedback, [arXiv:2009.01858 \[astro-ph.CO\]](#) (2020).
- [112] D. Foreman-Mackey, D. W. Hogg, D. Lang, and J. Goodman, emcee: The MCMC Hammer, *Publ. Astron. Soc. Pac.* **125**, 306 (2013), [arXiv:1202.3665 \[astro-ph.IM\]](#).
- [113] D. W. Hogg and D. Foreman-Mackey, Data analysis recipes: Using Markov Chain Monte Carlo, *Astrophys. J. Suppl.* **236**, 11 (2018), [arXiv:1710.06068 \[astro-ph.IM\]](#).
- [114] D. Foreman-Mackey, W. Farr, M. Sinha, A. Archibald, D. Hogg, J. Sanders, J. Zuntz, P. Williams, A. Nelson, M. de Val-Borro, T. Erhardt, I. Pashchenko, and O. Pla, Emcee v3: A Python ensemble sampling toolkit for affine-invariant MCMC, *Journal of Open Source Software* **4**, 1864 (2019).
- [115] J. L. Bernal, T. L. Smith, K. K. Boddy, and M. Kamionkowski, Robustness of baryon acoustic oscillation constraints for early-Universe modifications of Λ CDM cosmology, *Phys. Rev. D* **102**, 123515 (2020), [arXiv:2004.07263 \[astro-ph.CO\]](#).
- [116] S. Li, A. G. Riess, S. Casertano, G. S. Anand, D. M. Scolnic, W. Yuan, L. Breuval, and C. D. Huang, Reconnaissance with JWST of the J-region Asymptotic Giant Branch in Distance Ladder Galaxies: From Irregular Luminosity Functions to Approximation of the Hubble Constant, *Astrophys. J.* **966**, 20 (2024), [arXiv:2401.04777 \[astro-ph.CO\]](#).
- [117] M. Dixon *et al.* (DES), Calibrating the Absolute Magnitude of Type Ia Supernovae in Nearby Galaxies using [OII] and Implications for H_0 , [arXiv:2408.01001 \[astro-ph.CO\]](#) (2024).
- [118] E. Aubourg *et al.* (BOSS), Cosmological implications of baryon acoustic oscillation measurements, *Phys. Rev. D* **92**, 123516 (2015), [arXiv:1411.1074 \[astro-ph.CO\]](#).
- [119] A. Pérez-Fernández *et al.* (DESI), Fiducial-Cosmology-dependent systematics for the DESI 2024 BAO Analysis, [arXiv:2406.06085 \[astro-ph.CO\]](#) (2024).
- [120] F. Ge *et al.* (SPT-3G), Cosmology From CMB Lensing and Delensed EE Power Spectra Using 2019-2020 SPT-3G Polarization Data, [arXiv:2411.06000 \[astro-ph.CO\]](#) (2024).
- [121] A. Amon and G. Efstathiou, A non-linear solution to the S_8 tension?, *Mon. Not. Roy. Astron. Soc.* **516**, 5355 (2022), [arXiv:2206.11794 \[astro-ph.CO\]](#).
- [122] C. Preston, A. Amon, and G. Efstathiou, A non-linear solution to the S_8 tension – II. Analysis of DES Year 3 cosmic shear, *Mon. Not. Roy. Astron. Soc.* **525**, 5554 (2023), [arXiv:2305.09827 \[astro-ph.CO\]](#).
- [123] S. Hannestad, Neutrino masses and the dark energy equation of state - Relaxing the cosmological neutrino mass bound, *Phys. Rev. Lett.* **95**, 221301 (2005), [arXiv:astro-ph/0505551](#).
- [124] R. Allison, P. Caucal, E. Calabrese, J. Dunkley, and T. Louis, Towards a cosmological neutrino mass detection, *Phys. Rev. D* **92**, 123535 (2015), [arXiv:1509.07471 \[astro-ph.CO\]](#).
- [125] V. Poulin, K. K. Boddy, S. Bird, and M. Kamionkowski, Implications of an extended dark energy cosmology with massive neutrinos for cosmological tensions, *Phys. Rev. D* **97**, 123504 (2018), [arXiv:1803.02474 \[astro-ph.CO\]](#).
- [126] S. Vagnozzi, S. Dhawan, M. Gerbino, K. Freese, A. Goobar, and O. Mena, Constraints on the sum of the neutrino masses in dynamical dark energy models with $w(z) \geq -1$ are tighter than those obtained in Λ CDM, *Phys. Rev. D* **98**, 083501 (2018), [arXiv:1801.08553 \[astro-ph.CO\]](#).
- [127] S. Roy Choudhury and S. Hannestad, Updated results on neutrino mass and mass hierarchy from cosmology with Planck 2018 likelihoods, *JCAP* **07**, 037, [arXiv:1907.12598 \[astro-ph.CO\]](#).
- [128] J. a. Rebouças, D. H. F. de Souza, K. Zhong, V. Miranda, and R. Rosenfeld, Investigating Late-Time Dark Energy and Massive Neutrinos in Light of DESI Y1 BAO, [arXiv:2408.14628 \[astro-ph.CO\]](#) (2024).
- [129] H. Shao, J. J. Givans, J. Dunkley, M. Madhavacheril, F. Qu, G. Farren, and B. Sherwin, Cosmological limits on the neutrino mass sum for beyond- Λ CDM models, [arXiv:2409.02295 \[astro-ph.CO\]](#) (2024).
- [130] C. Dvorkin *et al.*, The Physics of Light Relics, in *Snowmass 2021* (2022) [arXiv:2203.07943 \[hep-ph\]](#).
- [131] L. Hart and J. Chluba, Updated fundamental constant constraints from Planck 2018 data and possible relations to the Hubble tension, *Mon. Not. Roy. Astron. Soc.* **493**, 3255 (2020), [arXiv:1912.03986 \[astro-ph.CO\]](#).
- [132] T. Sekiguchi and T. Takahashi, Early recombination as a solution to the H_0 tension, *Phys. Rev. D* **103**, 083507 (2021), [arXiv:2007.03381 \[astro-ph.CO\]](#).

- [133] M. M. Ivanov, Y. Ali-Haïmoud, and J. Lesgourgues, H0 tension or T0 tension?, *Phys. Rev. D* **102**, 063515 (2020), [arXiv:2005.10656 \[astro-ph.CO\]](#).
- [134] D. J. Fixsen, E. S. Cheng, J. M. Gales, J. C. Mather, R. A. Shafer, and E. L. Wright, The Cosmic Microwave Background spectrum from the full COBE FIRAS data set, *Astrophys. J.* **473**, 576 (1996), [arXiv:astro-ph/9605054](#).
- [135] D. J. Fixsen, The Temperature of the Cosmic Microwave Background, *Astrophys. J.* **707**, 916 (2009), [arXiv:0911.1955 \[astro-ph.CO\]](#).
- [136] V. Poulin, T. L. Smith, T. Karwal, and M. Kamionkowski, Early Dark Energy Can Resolve The Hubble Tension, *Phys. Rev. Lett.* **122**, 221301 (2019), [arXiv:1811.04083 \[astro-ph.CO\]](#).
- [137] J. C. Hill, E. McDonough, M. W. Toomey, and S. Alexander, Early dark energy does not restore cosmological concordance, *Phys. Rev. D* **102**, 043507 (2020), [arXiv:2003.07355 \[astro-ph.CO\]](#).
- [138] A. Reeves, L. Herold, S. Vagnozzi, B. D. Sherwin, and E. G. M. Ferreira, Restoring cosmological concordance with early dark energy and massive neutrinos?, *Mon. Not. Roy. Astron. Soc.* **520**, 3688 (2023), [arXiv:2207.01501 \[astro-ph.CO\]](#).
- [139] A. R. Khalife, M. B. Zanjani, S. Galli, S. Günther, J. Lesgourgues, and K. Benabed, Review of Hubble tension solutions with new SH0ES and SPT-3G data, *JCAP* **04**, 059, [arXiv:2312.09814 \[astro-ph.CO\]](#).
- [140] P. A. R. Ade *et al.* (Planck), Planck 2013 results. XVI. Cosmological parameters, *Astron. Astrophys.* **571**, A16 (2014), [arXiv:1303.5076 \[astro-ph.CO\]](#).
- [141] M. Archidiacono, E. Castorina, D. Redigolo, and E. Salvioni, Unveiling dark fifth forces with linear cosmology, *JCAP* **10**, 074, [arXiv:2204.08484 \[astro-ph.CO\]](#).
- [142] S. Bottaro, E. Castorina, M. Costa, D. Redigolo, and E. Salvioni, Unveiling Dark Forces with Measurements of the Large Scale Structure of the Universe, *Phys. Rev. Lett.* **132**, 201002 (2024), [arXiv:2309.11496 \[astro-ph.CO\]](#).
- [143] S. Bottaro, E. Castorina, M. Costa, D. Redigolo, and E. Salvioni, From 100 kpc to 10 Gpc: Dark Matter self-interactions before and after DESI, [arXiv:2407.18252 \[astro-ph.CO\]](#) (2024).
- [144] R. Hlozek, D. Grin, D. J. E. Marsh, and P. G. Ferreira, A search for ultralight axions using precision cosmological data, *Phys. Rev. D* **91**, 103512 (2015), [arXiv:1410.2896 \[astro-ph.CO\]](#).
- [145] R. Hložek, D. J. E. Marsh, D. Grin, R. Allison, J. Dunkley, and E. Calabrese, Future CMB tests of dark matter: Ultralight axions and massive neutrinos, *Phys. Rev. D* **95**, 123511 (2017), [arXiv:1607.08208 \[astro-ph.CO\]](#).
- [146] R. Hlozek, D. J. E. Marsh, and D. Grin, Using the Full Power of the Cosmic Microwave Background to Probe Axion Dark Matter, *Mon. Not. Roy. Astron. Soc.* **476**, 3063 (2018), [arXiv:1708.05681 \[astro-ph.CO\]](#).
- [147] A. Laguë, J. R. Bond, R. Hložek, K. K. Rogers, D. J. E. Marsh, and D. Grin, Constraining ultralight axions with galaxy surveys, *JCAP* **01** (01), 049, [arXiv:2104.07802 \[astro-ph.CO\]](#).
- [148] K. K. Rogers, R. Hložek, A. Laguë, M. M. Ivanov, O. H. E. Philcox, G. Cabass, K. Akitsu, and D. J. E. Marsh, Ultra-light axions and the S_8 tension: joint constraints from the cosmic microwave background and galaxy clustering, *JCAP* **06**, 023, [arXiv:2301.08361 \[astro-ph.CO\]](#).
- [149] W. Giarè, E. Di Valentino, A. Melchiorri, and O. Mena, New cosmological bounds on hot relics: axions and neutrinos, *Mon. Not. Roy. Astron. Soc.* **505**, 2703 (2021), [arXiv:2011.14704 \[astro-ph.CO\]](#).
- [150] R. Z. Ferreira, A. Notari, and F. Rompineve, Dine-Fischler-Srednicki-Zhitnitsky axion in the CMB, *Phys. Rev. D* **103**, 063524 (2021), [arXiv:2012.06566 \[hep-ph\]](#).
- [151] F. D’Eramo, E. Di Valentino, W. Giarè, F. Hajkarim, A. Melchiorri, O. Mena, F. Renzi, and S. Yun, Cosmological bound on the QCD axion mass, redux, *JCAP* **09**, 022, [arXiv:2205.07849 \[astro-ph.CO\]](#).
- [152] A. Notari, F. Rompineve, and G. Villadoro, Improved Hot Dark Matter Bound on the QCD Axion, *Phys. Rev. Lett.* **131**, 011004 (2023), [arXiv:2211.03799 \[hep-ph\]](#).
- [153] F. Bianchini, G. G. di Cortona, and M. Valli, The QCD Axion: Some Like It Hot, [arXiv:2310.08169 \[hep-ph\]](#) (2023).
- [154] S. Wang, L. Hui, M. May, and Z. Haiman, Is Modified Gravity Required by Observations? An Empirical Consistency Test of Dark Energy Models, *Phys. Rev. D* **76**, 063503 (2007), [arXiv:0705.0165 \[astro-ph\]](#).
- [155] E. J. Ruiz and D. Huterer, Testing the dark energy consistency with geometry and growth, *Phys. Rev. D* **91**, 063009 (2015), [arXiv:1410.5832 \[astro-ph.CO\]](#).
- [156] J. L. Bernal, L. Verde, and A. J. Cuesta, Parameter splitting in dark energy: is dark energy the same in the background and in the cosmic structures?, *JCAP* **02**, 059, [arXiv:1511.03049 \[astro-ph.CO\]](#).
- [157] W. Lin and M. Ishak, Cosmological discordances: A new measure, marginalization effects, and applica-

- tion to geometry versus growth current data sets, *Phys. Rev. D* **96**, 023532 (2017), [arXiv:1705.05303 \[astro-ph.CO\]](#).
- [158] J. Muir *et al.* (DES), DES Y1 results: Splitting growth and geometry to test Λ CDM, *Phys. Rev. D* **103**, 023528 (2021), [arXiv:2010.05924 \[astro-ph.CO\]](#).
- [159] U. Andrade, D. Anbajagane, R. von Marttens, D. Huterer, and J. Alcaniz, A test of the standard cosmological model with geometry and growth, *JCAP* **11**, 014, [arXiv:2107.07538 \[astro-ph.CO\]](#).
- [160] K. Zhong, E. Saraivanov, V. Miranda, J. Xu, T. Eifler, and E. Krause, Growth and geometry split in light of the DES-Y3 survey, *Phys. Rev. D* **107**, 123529 (2023), [arXiv:2301.03694 \[astro-ph.CO\]](#).
- [161] Y. Mellier *et al.* (Euclid), Euclid. I. Overview of the Euclid mission, [arXiv:2405.13491 \[astro-ph.CO\]](#) (2024).
- [162] T. Eifler *et al.*, Cosmology with the Roman Space Telescope – multiprobe strategies, *Mon. Not. Roy. Astron. Soc.* **507**, 1746 (2021), [arXiv:2004.05271 \[astro-ph.CO\]](#).
- [163] A. Aghamousa *et al.* (DESI), The DESI Experiment Part I: Science, Targeting, and Survey Design, [arXiv:1611.00036 \[astro-ph.IM\]](#) (2016).
- [164] M. Rigault *et al.*, ZTF SN Ia DR2: Overview, [arXiv:2409.04346 \[astro-ph.CO\]](#) (2024).
- [165] R. Mandelbaum *et al.* (LSST Dark Energy Science), The LSST Dark Energy Science Collaboration (DESC) Science Requirements Document, [arXiv:1809.01669 \[astro-ph.CO\]](#) (2018).
- [166] D. Foreman-Mackey, corner.py: Scatterplot matrices in python, *Journal of Open Source Software* **1**, 24 (2016).
- [167] C. R. Harris *et al.*, Array programming with NumPy, *Nature* **585**, 357 (2020), [arXiv:2006.10256 \[cs.MS\]](#).
- [168] P. Virtanen *et al.*, SciPy 1.0–Fundamental Algorithms for Scientific Computing in Python, *Nature Meth.* **17**, 261 (2020), [arXiv:1907.10121 \[cs.MS\]](#).
- [169] J. D. Hunter, Matplotlib: A 2D Graphics Environment, *Comput. Sci. Eng.* **9**, 90 (2007).
- [170] S. Hoyer and J. Hamman, xarray: N-D labeled arrays and datasets in Python, *Journal of Open Research Software* **5**, 10.5334/jors.148 (2017).
- [171] R. Kumar, C. Carroll, A. Hartikainen, and O. Martin, Arviz a unified library for exploratory analysis of bayesian models in python, *Journal of Open Source Software* **4**, 1143 (2019).
- [172] A. Meurer *et al.*, SymPy: symbolic computing in Python, *PeerJ Comput. Sci.* **3**, e103 (2017).
- [173] E. van der Velden, CMasher: Scientific colormaps for making accessible, informative and ‘cmashing’ plots, *The Journal of Open Source Software* **5**, 2004 (2020), [arXiv:2003.01069 \[eess.IV\]](#).
- [174] K. Karchev, Analytic auto-differentiable Λ CDM cosmography, *JCAP* **07**, 065, [arXiv:2212.01937 \[astro-ph.IM\]](#).
- [175] V. Poulin, T. L. Smith, R. Calderón, and T. Simon, On the implications of the ‘cosmic calibration tension’ beyond H_0 and the synergy between early- and late-time new physics, [arXiv:2407.18292 \[astro-ph.CO\]](#) (2024).